

# Traceable Calibration of Openand Closed-Path Ammonia Analyzers Using the VSL RGM System and Its Impact on Livestock Emission Uncertainty

quantiAGREMI deliverable report TNO



www.tno.nl +31 88 866 50 65 info@tno.nl

TNO 2024 R12917 – 17 November 2025 Traceable Calibration of Open- and Closed-Path Ammonia Analyzers Using the VSL RGM System and Its Impact on Livestock Emission Uncertainty

#### quantiAGREMI deliverable report TNO

Author(s) J. Zhang, P.C.P. Bronsveld, A. Hensen, H. van Mansom, W.C.M. van

den Bulk, I. Velzeboer

Classification report TNO Public
Title TNO Public
Report text TNO Public
Appendices TNO Public

Number of pages 78 (excl. front and back cover)

Number of appendices 3

Sponsor Euramet
Programme number 21GRD10
Project name quantiAGREMI
Project number 060.49719

All rights reserved

No part of this publication may be reproduced and/or published by print, photoprint, microfilm or any other means without the previous written consent of TNO.

© 2025 TNO

# **Contents**

1	Introduction	4
1.1	Challenges in NH₃ analyzer calibration	4
1.2	TNO mobile remote farm measurements (Task 2.1)	
1.3	Outline of the report	6
2	Laboratory calibration (Task 2.2)	8
2.1	Calibration set-up and method (A2.2.1)	
2.2	Open-path NH₃ analyzer mobile HT calibration results (A2.2.5, A2.2.6)	
2.3	Open-path NH₃ analyzer flux HT calibration results	16
3	Field calibration (Task 2.3)	21
3.1	Campaign design (A2.3.2)	21
3.2	Minimum test protocol for the field calibration of the TNO HT8700	
3.3	Mobile HT field calibration results (A2.3.6)	
3.4	In-field calibration of UKCEH and vTI closed-path NH₃ analyzers	30
4	Remote estimates of farm emissions (input A.2.3.6)	34
4.1	Tracer Dispersion Method (TDM) application	
4.2	In-situ calibration and uncertainty analysis of CH4 and N2O measurements	
4.3	In-situ calibration and uncertainty analysis of NH₃ measurements	
4.4	Remote measurements uncertainty calculations (A.2.3.7)	49
5	Summary (input A2.2.7 & A2.3.8)	52
5.1	Input for D3 (A.2.2.7): calibration results	
5.2	Input for D4 (A.2.3.8): TDM uncertainties	56
6	Recommendations for NH3 analyzer calibration and emission estimation	
6.1	Open-path analyzer (HT8700) calibration	
6.2	Closed-path analyzer (QCL) calibration	
6.3	VSL RGM system adaptation	
6.4	Reducing TDM uncertainty in livestock farm emission measurements	59
7	References	60
8	Acknowledgement	63
Appe	ndices	
	ndix A: TNO Tasks in quantiAGREMI	64
Appe	ndix B: CH4, N2O and NH3 Plume Transects	66
Appe	ndix C: Net NH3 plume and its uncertainty	73

) TNO Public 3/78

# 1 Introduction

In work package 2 of the quantiAGREMI project <sup>1</sup> TNO committed itself to tasks A2.1, A.2.2 and A2.3, the details of these tasks are given in Appendix A.

In these tasks, TNO has installed, calibrated and tested a set-up for mobile remote measurements of ammonia emissions from livestock, in addition to its mobile set-up for estimates of methane and nitrous oxide emissions. In this report, TNO describes the detailed results of this work. The key conclusions of Chapters 2, 3 and 4 are input to deliverable reports D2, D3 and D4, respectively, of the quantiAGREMI project.

# 1.1 Challenges in NH<sub>3</sub> analyzer calibration

Ammonia (NH<sub>3</sub>) is a reactive and highly variable atmospheric species that plays a central role in nitrogen deposition, secondary aerosol formation, and air-quality management (Nair & Yu, 2020; Fehsenfeld et al., 2002). Accurate measurement of NH<sub>3</sub> remains technically challenging because the molecule readily adsorbs onto instrument surfaces, exhibits strong humidity-dependent behavior, and is often present at low concentrations near instrument detection limits (Pogány et al., 2016; Pollack et al., 2019; Twigg et al., 2022). These challenges place exceptional importance on robust, traceable calibration procedures for both open-path and closed-path NH<sub>3</sub> analyzers (Macé et al., 2022; Pogány et al., 2016; Norman et al., 2008).

Closed-path analyzers enable the use of controlled calibration gases, such as permeation-tube standards, dynamic dilution systems, and certified cylinders, and therefore allow laboratory-based multi-point calibrations with well-defined uncertainty. However, they are sensitive to inlet losses, memory effects, and environmental conditions (Lemes et al., 2023; Pollack, et al., 2019). Open-path analyzers avoid inlet artifacts but cannot be calibrated through direct gas injection; instead, they rely on indirect methods including co-located reference instruments, controlled releases, or comparative field tests (Lemes et al., 2023; Macé et al., 2022), or converted the open-path system into a close-path one during calibration phase (Wang et al, 2021).

Despite substantial progress, multiple literatures indicate that calibration practices remain highly heterogeneous, with limited standardization across platforms (Nair & Yu, 2020; Twigg et al., 2022; Pogány, et al., 2016). Common issues include traceability at low concentrations, humidity corrections, inlet loss quantification, and uncertainty reporting (Pogány et al., 2016; Pollack et al., 2019; Macé et al., 2022). A clear synthesis of current calibration approaches, challenges, and gaps is therefore essential to guide instrument deployment, ensure data comparability, and support future improvements in NH<sub>3</sub> monitoring networks.

This report focuses on the results of the calibration of the open-path NH<sub>3</sub> gas analyzer HT8700E from Healthy Photon<sup>2</sup> with the Reference Gas Mixture (RGM) system developed in quantiAGREMI by Van Swinden Laboratory (VSL), the National Metrology Institute of the Netherlands (Pogány et al., 2025). The RGM can deliver air with controlled concentration levels of NH<sub>3</sub> and controlled humidity levels to a measurement unit through an inlet line. To calibrate the open-path HT8700E, the path of the laser beam needed to be enclosed in a glass cell to

) TNO Public 4/78

<sup>&</sup>lt;sup>1</sup> https://www.uknml.com/our-programmes/metpart-quantiagremi/

<sup>&</sup>lt;sup>2</sup> Open-path NH3 Analyzer-Healthy Photon Co., Ltd.

offer a controlled concentration. Besides the calibration of the HT8700E for mobile applications, also a similar HT system for measuring  $NH_3$  fluxes, owned by TNO, was tested in the lab for comparison.

During the flux measurement campaign of quantiAGREMI work package 3, in September-October 2024 at a dairy farm in the Netherlands, mobile measurements transects were driven with the TNO measurement truck and the HT8700E system mounted. Before and after these drives, the HT8700E was calibrated in-field with the RGM-system. Additionally, a HT8700E from the UK Centre for Ecology & Hydrology (UKCEH) and two closed-path TILDAS Compact Single Laser Ammonia Analyzers from Aerodyne<sup>3</sup>, owned by UKCEH and Johann Heinrich von Thünen Institute (vTI) were calibrated in-field during this campaign.

# 1.2 TNO mobile remote farm measurements (Task 2.1)

The Netherlands hosts approximately 18 million livestock animals, making agricultural emissions a major contributor to ammonia and methane levels in the atmosphere. These emissions negatively impact biodiversity in nearby nature reserves and contribute to climate change (Chen et al., 2025; Van der Zee, et al., 2022). Remote measurement methods offer the potential to assess total farm emissions, including those from non-standard sources on the farm terrain such as manure storage and ventilation leaks, without requiring direct access to the farm premises. Additionally, remote measurements provide a fast extra reference method in cases where in-barn measurements, the standard, are difficult to apply, such as strongly naturally vented barns.

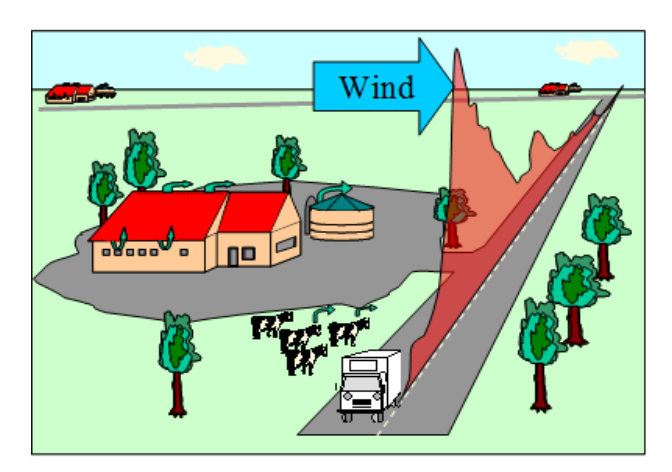


Figure 1.1: Schematic representation of a transect drive conducted at a livestock farm during remote mobile measurements. The  $CH_4$  and  $NH_3$  concentrations measured during multiple transects are used to estimate the corresponding emission rates of the farm.

For these reasons, TNO developed a remote mobile measurement technique that enables fast methane (CH<sub>4</sub>) and ammonia (NH<sub>3</sub>) emission estimates of livestock barns. The method makes use of a truck with trailer that makes mobile transect drives through the "emission plume" from the barn, which arises because the wind blowing over and through the barn picks up the substances emitted from it (Figure 1.1). As a reference, to later on eliminate the effects of turbulence and dispersion in the calculations, a gas bottle of nitrous oxide (N<sub>2</sub>O) with a known emission rate in g s<sup>-1</sup> is placed in front of the barn of which the emission rate will be estimated.

) TNO Public 5/78

<sup>&</sup>lt;sup>3</sup> https://aerodyne.com/wp-content/uploads/NH3.pdf

During these drives, ambient air is drawn in through an inlet on top of the mobile truck and transported via intake lines to a Tunable Infrared Laser Direct Absorption Spectroscopy (TILDAS) Dual Laser Tracer Gas Analyzer from Aerodyne<sup>4</sup>. The instrument measures methane (CH<sub>4</sub>) and nitrous oxide (N<sub>2</sub>O) concentrations at a frequency of 1 Hz within an optical absorption cell. This configuration, in which the sampled air continuously flows through an enclosed measurement cell, is referred to as a 'closed-path' system.



Figure 1.2: The HT8700E ammonia measurement instrument from Healthy Photon mounted on top of the truck trailer under a specially designed metal hood for rain protection.

Also closed-path mobile NH<sub>3</sub> measurements were tested at the beginning of the quantiAGREMI project, using the mid-infrared laser absorption spectroscopy system from MIRO Analytical <sup>5</sup>. The use of a closed-path system is, however, challenging for this application: the "stickiness" of ammonia causes the measured concentration signal to be smeared out in time, due to adsorption and desorption in the inlet lines and the optical cell of the instrument. For this reason, an open-path ammonia measurement instrument, the HT8700E was placed on the roof of the truck, which resolved this problem and resulted in real-time ammonia measurements at a frequency of 10 Hz and a concentration detection limit and resolution of 0.3 ppb.

The  $CH_4$ ,  $NH_3$  and  $N_2O$  concentrations measured during these back-and-forth transects were used to estimate the corresponding emission rates of the dairy farm using the Tracer Dispersion Method (TDM) (Hensen et al., 2009). In the TDM, by assuming the same dispersion for all three gases and knowing the emission rate of the  $N_2O$  tracer, farm emission rates of  $CH_4$  and  $NH_3$  can be calculated by taking the ratios of their measured concentrations and those of the  $N_2O$  tracer. In chapter 4, the use of the TDM-method for the estimation of farm emissions and the associated uncertainties in the calculated values will be discussed in more depth.

# 1.3 Outline of the report

The following research questions will be addressed in this report, followed by a short chapter summarizing the conclusions as input for deliverables D3 and D4 of quantiAGREMI:

Lab calibration of the HT8700E (Chapter 2)

) TNO Public 6/78

<sup>&</sup>lt;sup>4</sup> Dual.pdf

<sup>&</sup>lt;sup>5</sup> <u>Home - MIRO Analytical</u>

- Is the VSL RGM system well-suited for calibration of the newly developed open-path ammonia instrument HT8700E?
- Are the results of the calibration repeatable?
- Does it matter whether an upward or a downward series of concentrations is used?
- Is the calibration result influenced by other ambient factors, such as relative humidity and/or temperature?

#### Field calibration of the HT8700E and NH₃ instruments from partners (Chapter 3)

- Is there a difference in the RGM calibration results in the lab and in the field?
- Are the calibration results different before and after a mobile drive of plume transects?
- Are the measured concentration values temperature dependent?
- Can the RGM also be used for the calibration of other NH<sub>3</sub> measurement instruments in the field?

#### TDM emission estimates from mobile measurements (Chapter 4)

- What is the uncertainty in the NH<sub>3</sub> and CH<sub>4</sub> emission estimates of a dairy farm based on remote mobile measurements using TDM?
- What is the effect of the new NH<sub>3</sub> calibration results on these emission estimates?
- How do choices made during the mobile drive, such as tracer flow, tracer placement, measurement distance and number of transects, affect the emission estimates? How much do these contribute to the uncertainty in the emission estimates?
- Are there external parameters during the mobile drives that have a relevant effect on the
  emission estimates, such as the weather conditions (wind speed and direction, humidity
  level, temperature) or background concentration levels? How much do these contribute
  to the uncertainty in the emission estimates?

) TNO Public 7/78

# 2 Laboratory calibration (Task 2.2)

# 2.1 Calibration set-up and method (A2.2.1)

The first lab calibration of the HT8700E from the truck trailer (after this referred to as **"mobile HT"**) with the high dilution RGM system from VSL (after this referred to as the **"RGM"**) was performed in the TNO lab in Petten on September 19, 2024.

For this test, the mobile HT was mounted horizontally on a table, with the laser path enclosed by a glass cell that was fixed airtight in between the body of the HT and the mirror holder. On one end of the glass cell, close to the body, an inlet line from the RGM was connected to the glass cell, and on the other end of the glass cell an outlet line was connected to the pump. The RGM provided a range of different NH<sub>3</sub> concentrations and humidity levels in air and the flow of the air/NH<sub>3</sub> mixture from the RGM through the cell was kept constant. The pressure in the glass cell was monitored by the built-in sensor of the HT.

A broad range of concentration and humidity settings of the RGM was tested in a few days to get a first-order estimate of the linearity, repeatability and zero reading of the  $NH_3$  measurements of the HT. Based on the results of these elaborate tests, a minimum calibration protocol for an application in the field was designed by selecting a minimum range of concentration and humidity settings.

After lab calibration of the mobile HT, also the HT8700E system that is normally used by TNO for NH<sub>3</sub> flux measurements (after this referred to as the "flux HT") was calibrated with the RGM, using the same set-up described above, but with the HT mounted vertically. This flux HT was used for almost a year in Dutch Loobos forest for stationary (flux) measurements, next to the mini-DOAS NH<sub>3</sub> instrument from RIVM. A preliminary field comparison between

#### The Reference Gas Mixture (RGM) system from VSL

The dynamic dilution system for the generation of ammonia reference gas from VSL is based on the dilution using thermal mass flow controllers (MFCs) in two consecutive steps of gravimetrically prepared  $NH_3$  standards. For the comparison, an  $NH_3$  reference mixture was prepared in a 10 L AcuLife IV treated cylinder at 130 bars of pressure. The gas mixture was analysed at VSL, both prior and after the comparison. For data analysis, the average determined amount fraction  $NH_3$  was used (102.43  $\mu$ mol·mol·1).

The dynamic dilution system is based on two thermal MFCs in the first dilution stage to dilute the NH<sub>3</sub> reference mixture up to 400 times with air at a maximum flow rate of 4 L/min. An MFC was placed at the start of the second dilution stage to sample a portion of this reference gas and dilute it with dry air and with air that was humidified by passing through a wash bottle filled with milli-Q water. This allows to dilute the dynamically generated calibration gas another 800 times. Zero air from a 50 L cylinder was used in this comparison. All MFCs are of the type of EL Flow Prestige by Bronkhorst B.V. The pressure controllers are of the type of EL-PRESS by Bronkhorst B.V. and have an operating range of 2 bar (a). The software was developed at VSL in LabView and allows control of the MFCs based on their calibration that was performed at VSL, registration of MFC performance and automatic generation of predefined gas mixtures.

The NH<sub>3</sub> gas mixture can be generated in dry or wet air with a relative expanded uncertainty (k=2) around 2.7%.

) TNO Public 8/78

the HT and the mini-DOAS was made based on these data. The lab calibration with the RGM is to validate whether it is similar to its field calibration results or not.

When all lab calibrations were finished, the RGM was placed in an aluminum travel box for the field calibration measurements. The field calibrations are discussed in the next chapter. All calibration settings, indoor and outdoor are shown in Figure 2.1.



Figure 2.1: From left to right, a) VSL calibration set up at TNO laboratory to do indoor calibration of TNO mobile HT and flux HT. Note that a closed-glass cell with 3.7 L volume is applied in both HTs during the calibration period; b) VSL-TNO mobile HT outdoor calibration in TNO; c) UKCEH HT field calibration using RGM at a Dutch dairy farm during the field campaign in October 2024.

### 2.1.1 Settings used during lab calibration

The settings used for the calibration runs are given in Table 2.1. For each HT at least 5 levels of concentrations (including zero) were decided as a minimum for the regression analysis. Also, because of the different applications, different settings were used for the mobile HT and the flux HT.

During mobile drives, the mobile HT may encounter  $NH_3$  concentrations up to 1 ppm, e.g. very close to or inside a dairy farm, but also values in the 10 ppb range, when further away from the source. The flux HT is mainly used at nature areas for lower  $NH_3$  concentration measurement, therefore a range of 0 to 200 ppb was selected for the it.

The chosen relative humidity (RH) range should be representative for outdoor measurements in the Netherlands. The KNMI website  $^6$  gives an annual average for the Netherlands of > 75%. In historical meteorological measurement data, diurnal and seasonal RH variations in the ranging from 30% to 100% were observed between 1990 and 2022. So ideally, three RH values of 30% (low), 60% (median) and 90% (highest) were used. However, the RGM settings were limited to 0-55% because of its limited flow rate in the wet air.

) TNO Public 9/78

<sup>&</sup>lt;sup>6</sup> Netherlands: relative humidity 2022 | Statista

Table 2.1: Experiment matrix of the RGM settings during lab calibration of the two HT's. " $\checkmark$ " means conducted calibration settings. VSL raw reading in ppb; HT raw reading in  $\mu$ g/m³, the unit of HT was then converted into ppb based on the ideal gas law using the environmental temperature and air pressure.

	NH <sub>3</sub> NH <sub>3</sub>			Re	elative hu	midity ran	ge	
	concentration (ppb)	concentration (µg/m³)	0 - 10%	10-20%	20-30%	30-40%	40-50%	50-60%
Mobile HT	0	0			✓		✓	✓
	29	20					✓	✓
	72	50			✓		✓	✓
	143	100					✓	✓
	285	200	✓		✓		✓	✓
	710	503						✓
	1262	895	✓		✓			✓
Flux HT	0	0	✓			✓		<b>√</b>
	20	14	✓			✓		✓
	50	35	✓			✓		✓
	100	71	✓			✓		✓
	200	141	✓			✓		✓

# 2.2 Open-path NH₃ analyzer mobile HT calibration results (A2.2.5, A2.2.6)

Laboratory calibration of the mobile HT system was conducted from 21 to 23 September 2024. The calibration protocol aimed to establish four stable relative humidity (RH) conditions; however, initial equipment constraints resulted in moderately unstable RH plateaus at approximately 7%, 25%, 47%, and 50%. For each RH condition, multiple  $\rm NH_3$  concentration levels were evaluated in steps of at least 3 hours, while maintaining a constant flow rate of  $\rm 3.5 \ L \ min^{-1}$ .

At the highest RH condition ( $\sim$ 50%), the full set of NH $_3$  concentrations (0, 29, 72, 143, 285, 710, and 1262 ppb) was examined in both increasing and decreasing sequences. Subsets of these concentration levels were subsequently repeated at the remaining RH conditions. No measurements were obtained under fully dry conditions, as VSL data logging ceased before this range was reached. Throughout the calibration period, laboratory temperature remained stable between 20 and 24  $^{\circ}$ C.

## 2.2.1 Zero calibration at various relative humidity

In Figure 2.2 the zero calibration at two humidity levels is given. Two continuous time periods were selected during which the HT readings were stable. Within these periods, RH varied from 25% to 50%, but no significant change in HT concentrations is observed. The zero offset remained stable at  $0.36 \pm 0.1$  ppb (Mean  $\pm$  SD).

) TNO Public 10/78

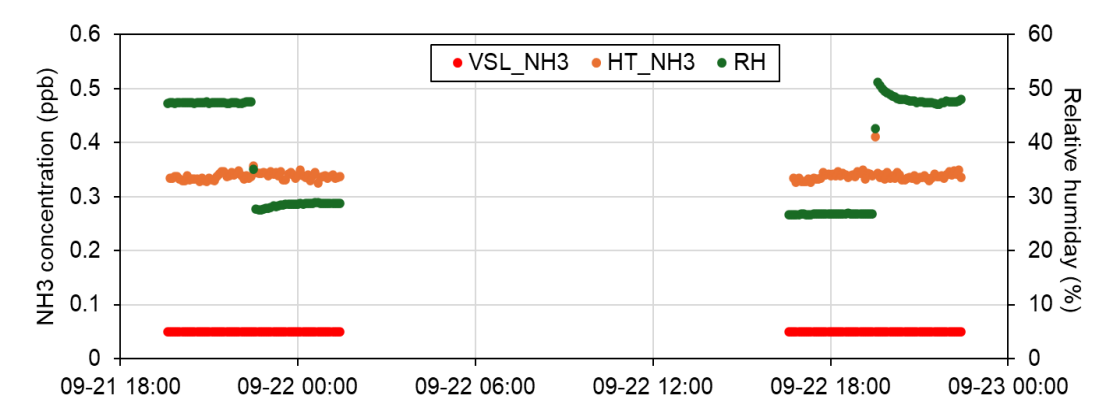


Figure 2.2: Zero calibration of mobile HT at the indoor lab settings. X-axis is month-date and UTC time.

### 2.2.2 Regression analysis

During HT calibration, the manufacturer's 3.7 L glass cell with 1500 cm² surface area was used. At the calibration, VSL flow rate was set at 3.5 L/min constantly, the residence time is approximately 1 minute if it starts from zero. If it is *a well-mixed volume*, the concentration approaches steady state exponentially, however, the cell is not a leak-free system strictly speaking. Also, when add humid air into the cell, ammonia can be absorbed not only by the moisture on the cell surfaces but also potentially react with the water vapor. To ensure that reasonable calibration data were selected only from stable periods, a two-step filtering approach was tested based on both VSL and HT signal and also environmental conditions (e.g. RH).

#### A. Simple filter: stability detection using rolling coefficient of variation

A 30-minute rolling coefficient of variation (CV) was calculated for the VSL and HT signals, as well as environmental parameters (RH), using six consecutive data points per window. Indoor calibration temperature changes were relatively small and therefore not considered as extra filtering factor. Stability criteria were defined as: VSL CV  $\leq$  1%, RH CV  $\leq$  3%, and HT CV  $\leq$  3%, reflecting the different noise levels of the signals.

#### B. Complex filter: tail part & detrend

To account for HT system lag (due to the large cell volume and surface area) at the start of each stable period, a buffer of 15 minutes (3 data points) was applied at the beginning. After initial filtering, only the last 1 hour of each stable period (12 data points per period) was retained as the final stable block. Furthermore, only blocks with no significant upward or downward trend in HT  $\rm NH_3$  or RH were kept; any block showing measurable drift was discarded. The stability thresholds were set so that HT  $\rm NH_3$  concentration does not drift more than 1 ppb per hour and RH does not change more than 1.5% per hour.

This approach ensures that calibration is based on the most stable and representative measurements, minimizing the influence of transient or drifting fluctuations. A subsequent t-test comparing the slopes and intercepts of the simple (A method above) and final-cleaned (B method) datasets showed no significant differences between the two methods (p  $\geq$  0.05), indicating that using the simpler filtering approach is sufficient in this case. Below 200 ppb, there seems to be no RH impact on the linear regression anymore. The results for the mobile HT lab calibration were shown in Figure 2.3 and Table 2.2.

) TNO Public 11/78

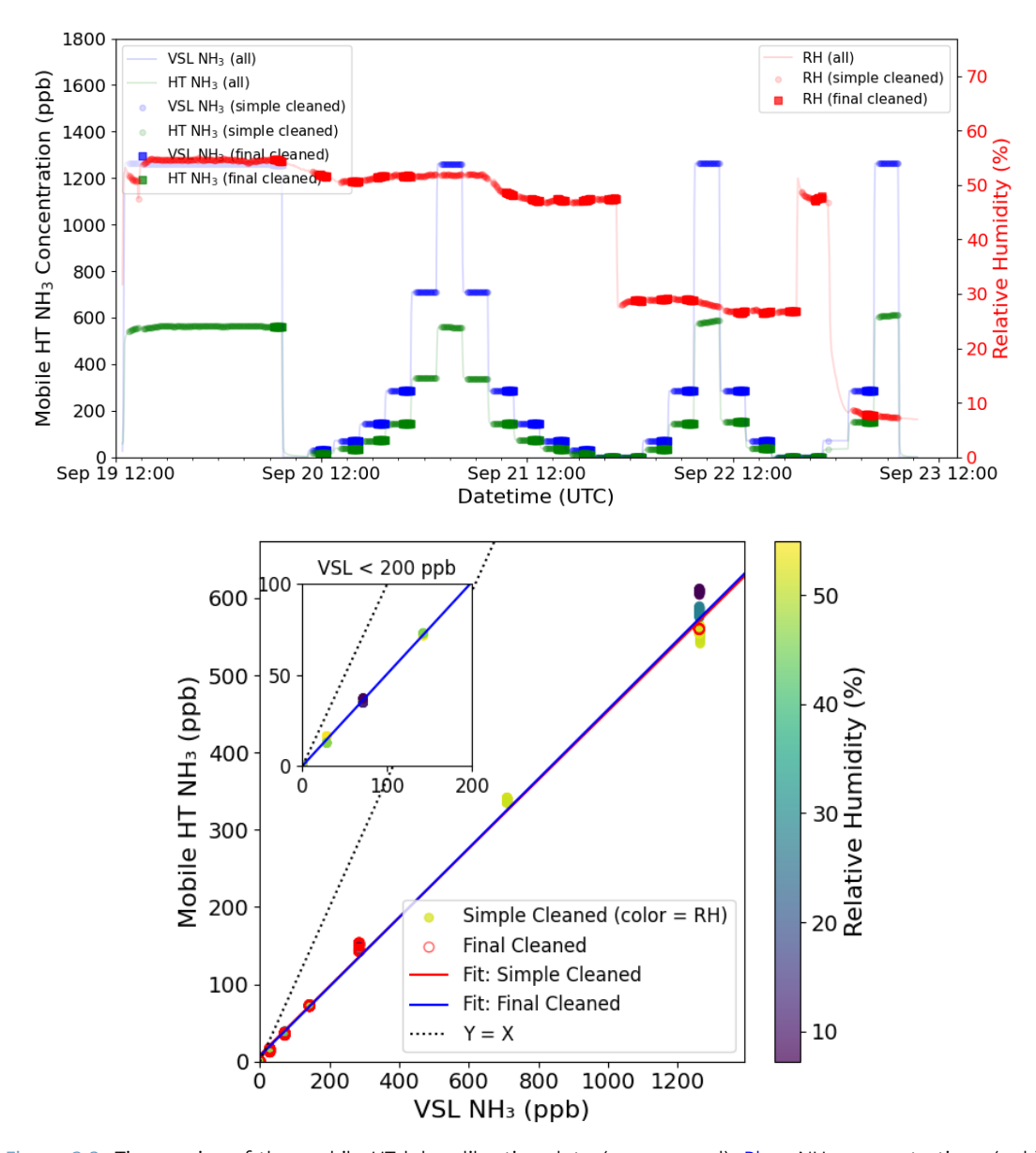


Figure 2.3: Time series of the mobile HT lab calibration data (upper panel): Blue:  $NH_3$  concentrations (ppb) offered by the RGM; Green: corresponding  $NH_3$  concentrations (ppb) measured by the mobile HT; Red: RH-values offered by the RGM. "Simple cleaned" refers to data processed only with rolling-CV-based outlier removal and large-variation filtering. "Final cleaned" refers to the last 1 hour of detrended data. The lower panel shows linear regressions of such methods. The regression equation for the VSL < 200 ppb range is shown in the zoomin plot, based on the simple cleaned data set.

) TNO Public 12/78

Table 2.2: Mobile HT indoor calibration results: linear regressions using 2 different filter methor	ods and the low
concentration range result ( VSL < 200 ppb)	

Parameters	All RH (stable)	All RH (stable + detrend)	Mixed RH (VSL < 200 ppb)
Slope	0.445	0.449	0.505
Intercept	8.55	7.14	0.16
Std. error of slope	0.001	0.002	0.002
Std. error of intercept	0.59	0.70	0.12
R <sup>2</sup>	0.998	0.996	0.999
Number of data	846	216	144

# 2.2.3 Effect of relative humidity on measured NH₃ in the closed calibration cell

In an ideal calibration cell, the concentration response to a step change would follow a simple Continuous Stirred-Tank Reactor (CSTR) model, where the outlet concentration approaches the inlet value exponentially with a single time constant ( $\tau$  = V/Q) (Núñez, 2013). In practice, NH<sub>3</sub> interacts strongly with surfaces and water films: during step-up/rising, adsorption suppresses the measured concentration, while during step-down/falling, slow release due to desorption elevates it, creating hysteresis.

At moderate RH ( $\sim$ 28%), thin water films strongly absorb and later release NH<sub>3</sub>, giving the largest difference between rising and falling phases (Figure 2.4). At higher RH ( $\sim$ 50%), thicker films reduce the overall measured concentration even further, but the hysteresis gap narrows because the surfaces are closer to saturation. Thus, RH both lowers apparent NH<sub>3</sub> levels and shifts the balance of hysteresis, with the strongest asymmetry observed at intermediate humidity.

An example, when VSL supplied a constant concentration of 285 ppb NH<sub>3</sub> to the HT calibration cell under different RH conditions, the following results were observed. As it is showed in Figure 2.4, HT measures only about half of the provided reference concentration.

- a) At RH = 8%, the measured maximum was about 152 ppb.
- b) At RH = 27 29%, the measured concentration dropped further, to 146 150 ppb, depending on whether the measurement was during the rising or falling phase (falling phase consistently higher).
- c) At RH = 48 52%, the measured concentration fell to 143 145 ppb, again with the falling phase slightly higher than the rising phase.

As expected, RH not only lowers the apparent NH<sub>3</sub> concentration in the cell but also enhances hysteresis between rising and falling phases, but it is not linearly.

) TNO Public 13/78

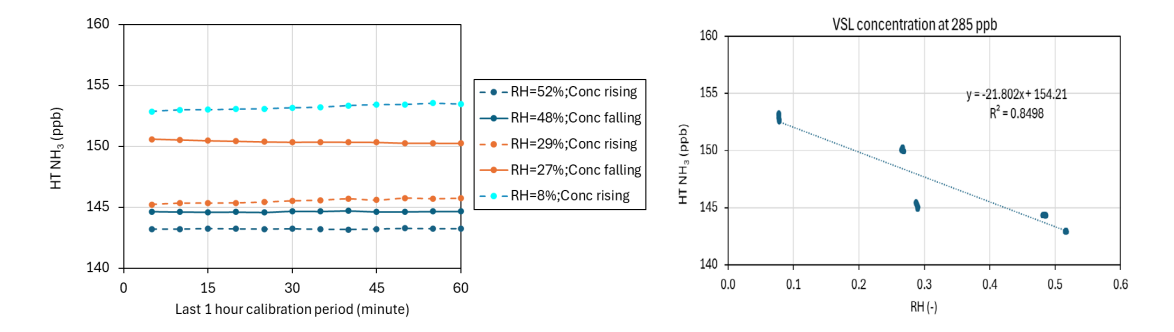


Figure 2.4: Comparison of HT-measured NH<sub>3</sub> concentrations at different RH ranges for the same VSL-fed concentration (285 ppb) during the mobile HT lab calibration phase in the last 1 hour of each calibration stage, showing both the rising and falling limbs. The 2<sup>nd</sup> panel illustrates the correlation between RH and HT-measured concentration at this concentration level (Note that RH is presented as a unitless ratio here instead of as a percentage).

At higher setpoints, the same RH effect is visible under steady-state conditions. For example, when VSL supplied 1267 ppb reference NH3, three distinct sets of HT values were observed despite nearly identical ambient temperatures (22–24°C) (Figure 2.5). The key difference was relative humidity, with mean  $\pm$  SD values of 7.0  $\pm$  0.06%, 28.0  $\pm$  0.08%, 52.0  $\pm$  0.08%, and 55.0  $\pm$  0.15%. The HT-measured concentrations were strongly and negatively correlated with RH: the higher the humidity, the lower the measured NH3 concentration (R² = 0.988). This steady-state result suggests that RH is the dominant factor controlling the apparent NH3 response in the calibration cell. At high relative humidity, changes in the measured NH3 may partly arise from spectroscopic interference by H2O, which both absorbs near the HT operating wavelength (9.06  $\mu$ m) and contributes to pressure broadening of the NH3 absorption line (Miller et al., 2014).

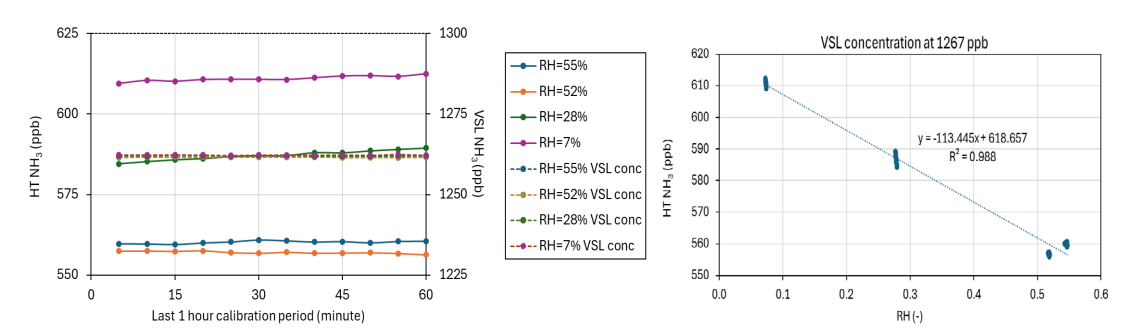


Figure 2.5: Comparison of HT-measured  $NH_3$  concentrations at different RH ranges for the same VSL-fed concentration (1267 ppb) during the mobile HT lab last 1 hour calibration stage per block, showing both the rising and falling limbs. The  $2^{nd}$  panel illustrates the correlation between RH and HT-measured concentration at this concentration level (Note that RH is presented as a unitless ratio here instead of as a percentage).

When VSL = 71 ppb, a relatively low NH $_3$  concentration value, measured HT NH $_3$  concentration has no significant correlation with RH anymore (Figure 2.6). It showed that when RH at ~28%, the falling value is still higher than the rising phase, but the difference disappears when RH at 50%. It seems that the RH impact on low NH $_3$  concentrations are less pronounced. Which suggests a simple calibration equation can be built (without RH) when the VSL concentration is below 200 ppb.

) TNO Public 14/78

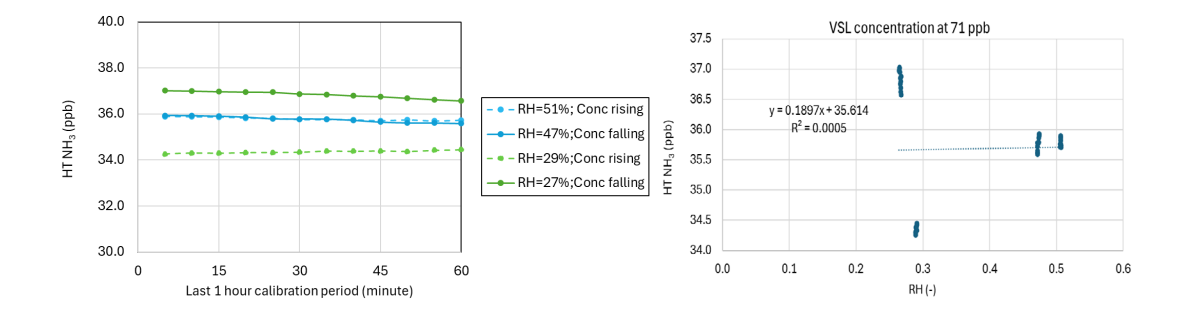


Figure 2.6: Comparison of HT-measured  $NH_3$  concentrations at different RH ranges for the same VSL-fed concentration (71 ppb) during the mobile HT lab calibration last 1 hour of each stage, showing both the rising and falling limbs. The  $2^{nd}$  panel illustrates the correlation between RH and HT-measured concentration at this concentration level (Note that RH is presented as a unitless ratio here instead of as a percentage).

Based on the observations, a conditional calibration approach is adopted:

At low concentrations (VSL < 200 ppb), there was no statistically significant relationship between measured HT values and relative humidity (example: VSL = 71 ppb), so a simple RH-independent linear calibration was used for this range.

At higher concentrations (VSL  $\geq$  200 ppb), HT response showed a strong negative dependence on RH and therefore RH was included as an additional predictor in the calibration model. The calibration equations were fitted by ordinary least squares and validated by residual analysis and cross-validation; inclusion of the RH term for the higher concentration range removed the RH bias and improved predictive performance. Where practical, controlling the calibration cell RH (or pre-conditioning surfaces) is recommended to reduce uncertainty further. The following two equations were determined:

1) For VSL < 200 ppb: a RH-independent calibration obtained as below:

$$HT_{Calib} = \frac{HT_{raw} - 0.16}{0.505}$$
 Equation 2.1

2) For VSL ≥ 200 ppb: a RH-dependent calibration equation obtained as below:

Assuming that relative humidity (RH) affects both the measured  $NH_3$  slope and intercept, the linear regression analysis indicated that all three components (HT, RH, and HT×RH) had p-values < 0.05. This result demonstrates that RH significantly influences both the slope and the offset, with an excellent model fit ( $R^2 = 0.999$ ).

$$Predicted VSL_{NH_3} = a + b \cdot HT + c \cdot RH + d \cdot (HT \times RH)$$

$$HT_{Calib} = \frac{HT_{raw} + 0.60 \cdot RH + 31.89}{2.09 + 0.005 \cdot RH}$$
Equation 2.2

It should be noted that the HT system is an open-path instrument and does not use a glass cell during normal operation. Therefore, the RH-dependent effects observed in the closed-cell tests at reference concentrations >200 ppb do not necessarily occur in the field. Consequently, high-concentration corrections should not be applied to field data unless they can be validated under representative open-path conditions (e.g., by comparison with the RIVM open-path Mini-DOAS). To avoid bias, only concentrations < 200 ppb were used for the final lab calibration, resulting in an offset of 0.16 ppb and a slope of 0.505, with no difference between rising and falling phases.

) TNO Public 15/78

# 2.3 Open-path NH₃ analyzer flux HT calibration results

The lab calibration of the flux HT was performed on September 24-26, 2024. Each calibration point was maintained for 1.5 hours, with a constant total flow rate of 3 L min<sup>-1</sup> directed to the flux HT. The NH<sub>3</sub> concentration levels of the RGM were set at 0, 20, 50, 100, and 200 ppb. Relative humidity (RH) was adjusted to 3 nominal levels: 0-5%, 30-35%, and 50-60%. Higher values were not possible due to limitations of the RGM.

### 2.3.1 Zero calibration at various relative humidity

Zero calibration results (Figure 2.7) showed that there is relative constant offset of 31 ppb for all relative humidity ranges. Although under higher RH range the offset seems slightly higher than in the dry condition (32 vs 29 ppb), but the difference is not significant. Such a large offset could be induced during bumpy road transport, or additional mechanical forces could shift the laser bin position, leading to significant offset drift.

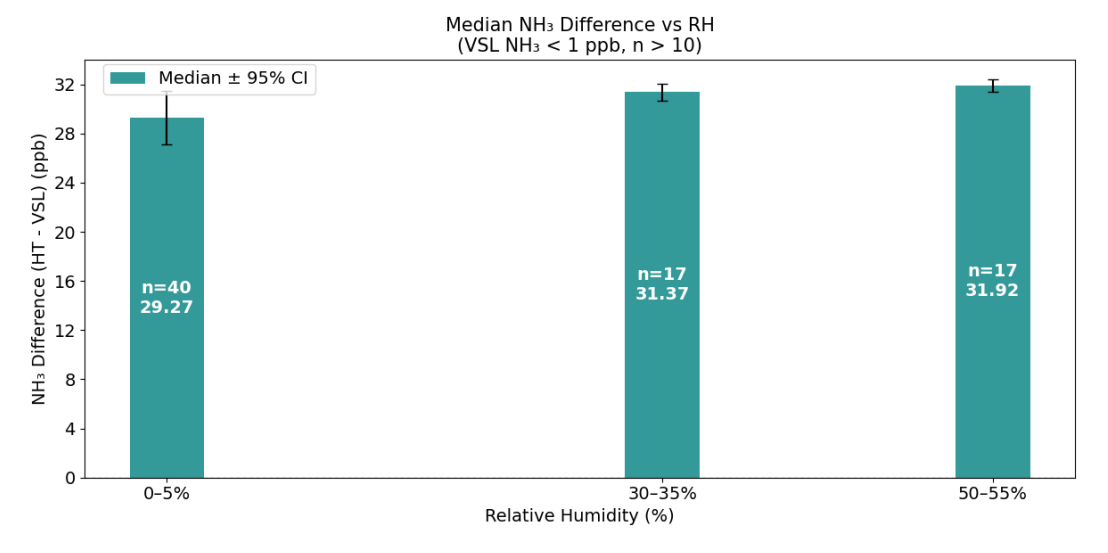


Figure 2.7: Flux HT zero calibration at each RH bin (n > 10, VSL's RGM concentration < 1 ppb), median NH $_3$  differences are shown at the centre of each bin, suggest no difference of zero offset value under different RH ranges.

## 2.3.2 Regression analysis

A similar data filtering approach was applied; however, due to the shorter calibration period, the final cleaned data were defined using the last 30-minute window instead of the 1-hour window used for the mobile HT. Overall, the simple filtering approach was also found to be sufficient in this case.

In all, the TNO flux HT system demonstrates a very linear response for all humidity levels, showed in Figure 2.8. The R<sup>2</sup> of the fit on all data is 1.0, which is also the case for all humidity levels separately. However, there is a clear offset in the data of about 31 ppb.

Some decrease in slope occurs when RH is increased (Table 2.3). This is in line with what is observed in Figure 2.8 at higher humidity, the stabilization time increases, which also seems

) TNO Public 16/78

to affect the highest measured concentrations the most, leading to a downward trend in the slope of 0.980 to 0.919 for increasing humidity.

The observed stabilization effect (longer time needed to reach equilibrium NH₃ concentration under higher RH) is due to the fact that with the laser path enclosed in a glass cell, it functions effectively as a closed-path system. After stabilization, with all tubing and glass cell surface in equilibrium, all measured concentration values (at least up to 200 ppb) that were measured in a humid environment, approach the values measured in a dry environment. Therefore it is hard to derive the RH impact.

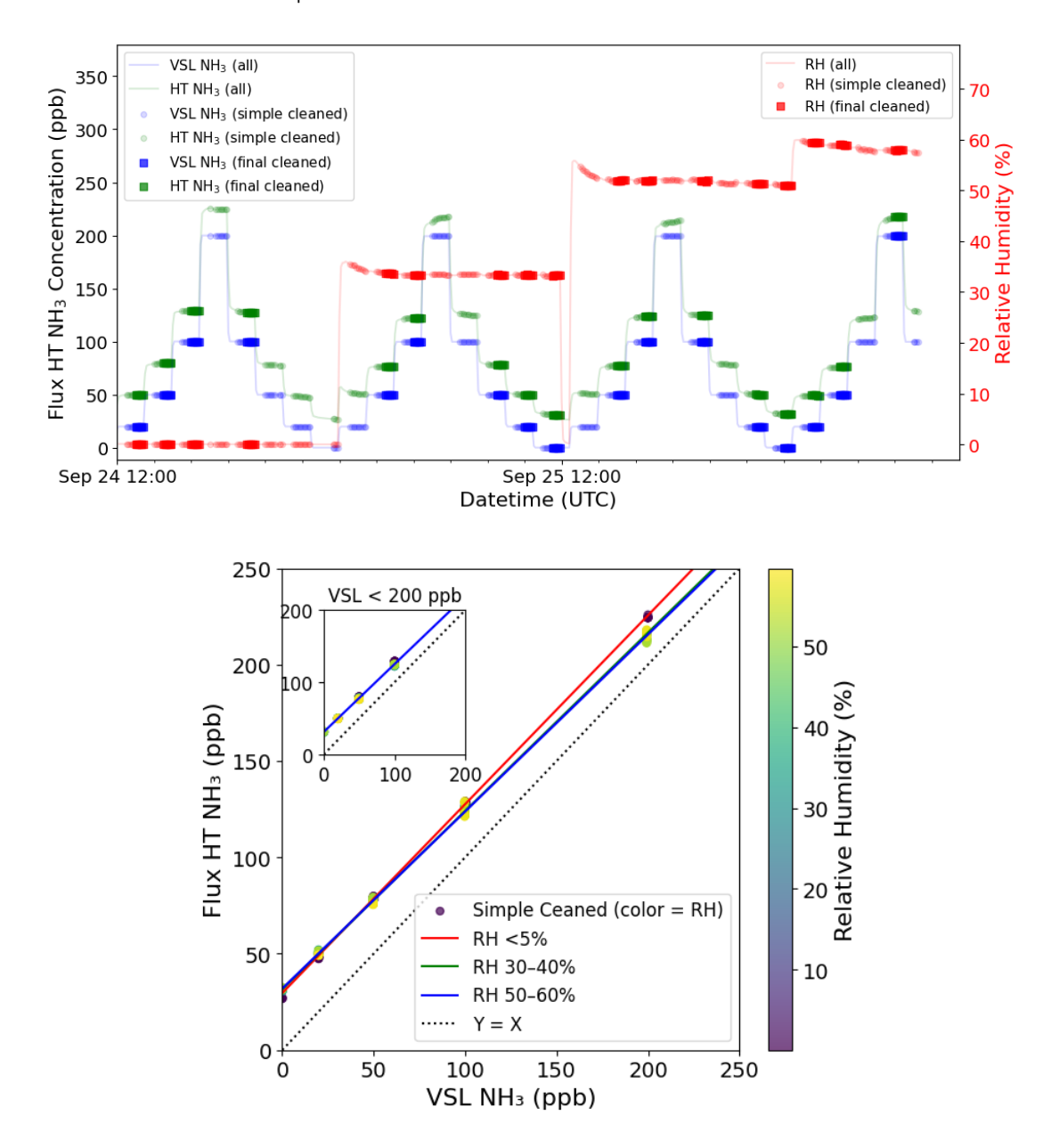


Figure 2.8: Time series of the flux HT laboratory calibration data (upper panel). Blue:  $NH_3$  concentrations (ppb) supplied by the RGM. Green: corresponding  $NH_3$  concentrations (ppb) measured by the flux HT. Red: RH values supplied by the RGM. "Simple cleaned" refers to data processed only with rolling-CV outlier removal and large-variation filtering. "Final cleaned" refers to the final 30 minutes of detrended data. The lower panel shows linear regressions based on the simple-cleaned data set for three RH levels. A zoom-in plot displays the regression equation for the VSL < 200 ppb range based on the simple cleaned data set.

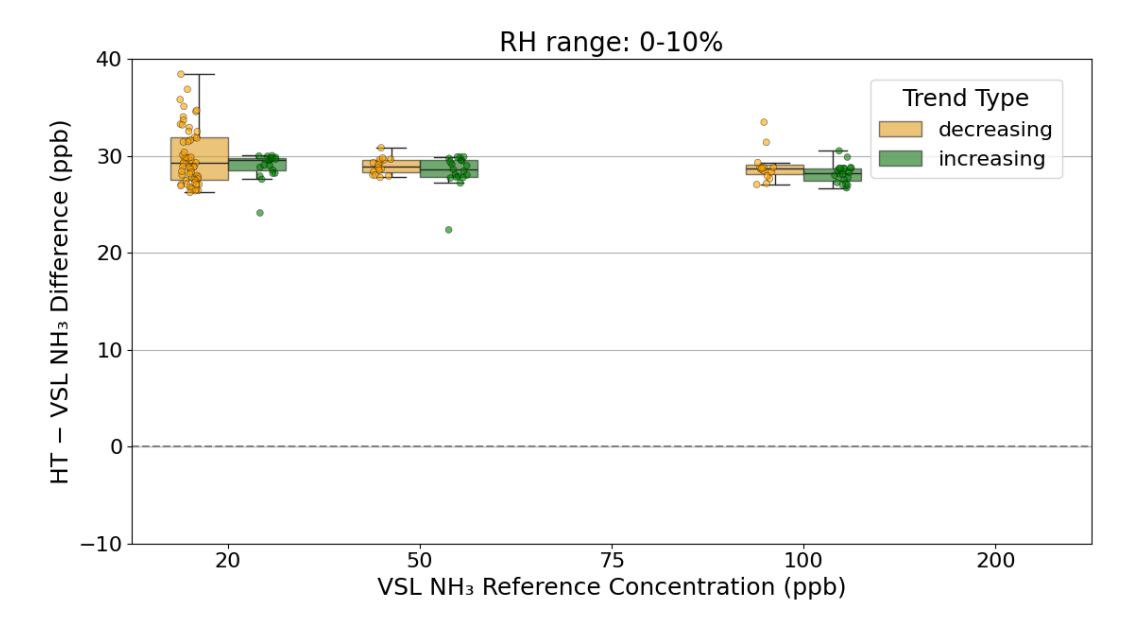
) TNO Public 17/78

Table 2.3: Flux HT indoor calibration:	linear regressions fo	or different relative	humidity settings by	y comparing
with the VSL system.	-			

Parameters	All RH	RH<5%	RH = 30-40%	RH = 50-60%	Mixed RH (< 200 ppb)
Slope	0.934	0.980	0.925	0.919	0.940
Intercept	31.34	29.55	31.53	31.90	31.05
Std. error of slope	0.002	0.002	0.002	0.002	0.003
Std. error of intercept	0.19	0.19	0.19	0.20	0.22
R <sup>2</sup>	0.999	1.000	1.000	0.999	0.999
Number of data	326	83	95	148	102

# 2.3.3 Effect of increasing and decreasing step changes in concentration

The current calibration protocol includes both rising and falling concentration phases. Under dry conditions, no significant difference was observed between the rising and falling phases in  $\Delta NH_3$  (HT – VSL). However, at higher relative humidity levels (30%–60% RH), the flux HT calibration cell exhibited an "adsorbing surface" effect toward incoming ammonia. During the rising phase, some  $NH_3$  was initially adsorbed by the system, leading to lower  $\Delta NH_3$  values compared to the falling phase, during which the previously adsorbed ammonia was released. Results of the HT's offset under different RH classes during concentration increasing and decreasing phases are presented in Figure 2.9 It was also observed during the mobile HT calibration period (Figure 2.4 to Figure 2.6).



) TNO Public 18/78

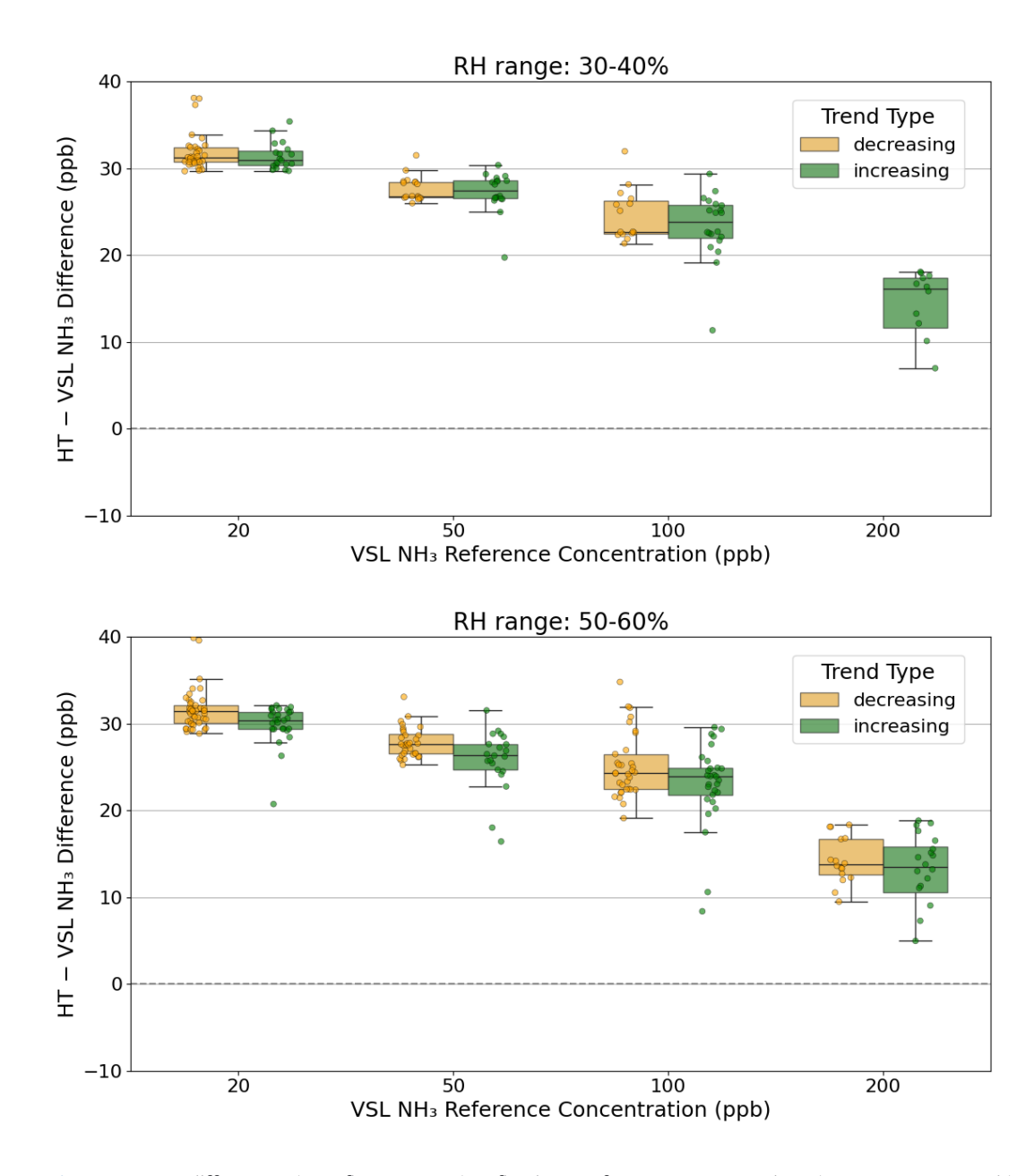


Figure 2.9:  $NH_3$  differences (TNO flux HT – VSL) at fixed VSL reference concentrations (20, 50, 100, 200 ppb) for three RH ranges (0–10%, 30–40%, 50–60%). Boxplots show the distribution of  $NH_3$  differences: the box represents the interquartile range (25th–75th percentile), the horizontal line inside the box is the median, and whiskers indicate the range excluding outliers. Individual dots represent single measurements. Green represents increasing and orange decreasing concentration steps.

Based on the observed "adsorbing surface" effect in the HT calibration cell at higher relative humidity levels (30%–60%), it is recommended to modify the calibration protocol to improve accuracy. Specifically, rising and falling concentration phases should be analyzed separately to account for the lag caused by ammonia adsorption and subsequent release. Extending the stabilization time at each concentration step, particularly under higher RH conditions, will help the system reach equilibrium and reduce transient adsorption and desorption effects.

Additionally, pre-conditioning the calibration cell with a slightly acidified coating before the calibration sequence can saturate the surface and reduce adsorption during the rising phase.

) TNO Public 19/78

For RH levels above 30%, it may be preferable to rely primarily on data from the falling phase, which reflects more stable NH<sub>3</sub> concentrations if the calibration period is short. Finally, incorporating RH-dependent correction factors or separate calibration equations that account for adsorption/desorption behaviors during both increasing and decreasing concentration steps can further improve calibration accuracy under varying environmental RH conditions, especially when using a large glass calibration cell.

) TNO Public 20/78

# 3 Field calibration (Task 2.3)

# 3.1 Campaign design (A2.3.2)

In work package 2, two measurement campaigns were organized: one at a dairy farm in Finland and one at a pig farm in the Netherlands. For practical reasons, however, for the field tests of the remote measurements TNO joined (and hosted) the measurement campaign of WP3 at a dairy farm in the Netherlands in the period of September 2 – October 12, 2024 (6 weeks).

The goal of this campaign was to test different sensing methods of quantiAGREMI partners that are to be used outside of the stable, such as eddy-covariance measurements to determine NH<sub>3</sub> fluxes, passive samplers, and soil sampling. An overview of the tested equipment and a schematic of its placement is given in Figure 3.1.

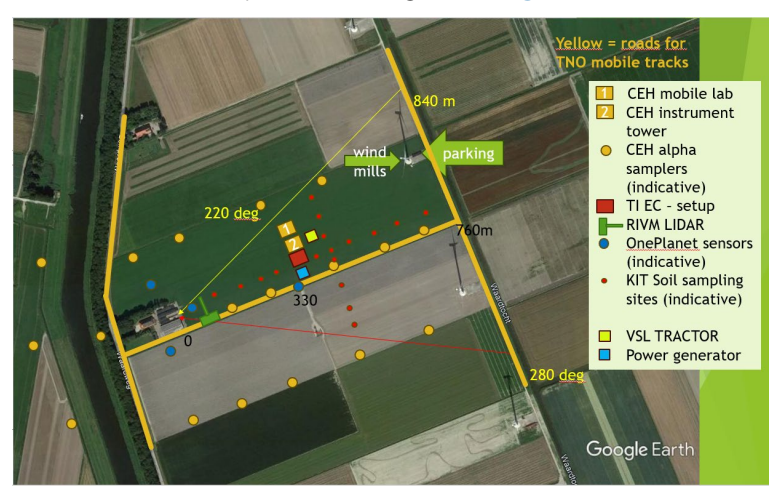


Figure 3.1: Placement of the equipment of the WP3 campaign at a dairy farm in the Netherlands.

Beside the stationary set-ups placed in the surroundings of the farm, TNO has in parallel performed several mobile drives to test the mobile open-path NH<sub>3</sub> instrument, placed on the truck, after calibration with the field NH<sub>3</sub> calibration set-up (A2.3.5)

On October 2-3, the VSL RGM system was placed in a box at the farm site of the campaign. Here, calibration of the open-path  $NH_3$  system was performed with a minimal calibration protocol and the TNO mobile HT8700 mounted on the truck. The goal of this test was to find out if any practical adaptations may be needed for application of the RGM in real-world conditions.

Additionally, after calibration of the mobile HT, it was attempted to calibrate the HT8700E system of UKCEH and the two closed-path NH<sub>3</sub> Aerodyne<sup>7</sup> instruments of UKCEH and vTI with the VSL RGM system in a calibration range of 0 to 150 ppb.

) TNO Public 21/78

<sup>&</sup>lt;sup>7</sup>TILDAS Compact Single Laser Ammonia Analyzers (closed-path), mainly used for concentration and flux measurements next to livestock sources or at nature areas.

The flux tower from UKCEH, with their HT8700E instrument and a 3D anemometer, for stationary  $NH_3$  concentrations and eddy covariance fluxes, was placed approximately 350 meters from the dairy farm, together with the two Aerodyne instruments. Although these calibrations were not mandatory for TNO, the results provide a valuable comparison to evaluate the VSL system for different open-path and closed-path  $NH_3$  instruments.



Figure 3.2: a) VSL RGM system set-up at the TNO Petten laser lab on Sept. 19. b) The RGM system tested at the campaign site on October  $2^{nd}$  before the start of the  $1^{st}$  remote measurement at the dairy farm. c) The RGM system outside the TNO Petten lab to calibrate TNO mobile HT on Oct. 4-6 after the  $1^{st}$  remote measurement, but before the  $2^{nd}$  remote measurement at the farm started on October  $11^{th}$ , 2024.

# 3.2 Minimum test protocol for the field calibration of the TNO HT8700

Calibration of the TNO mobile HT8700 measurements with the RGM system was performed before and after the remote mobile emission measurements at the dairy farm:

- Pre-calibration took place at the campaign site on October 2, 2024, from 09:45 to 13:10 UTC. During this session, strong winds caused notable leakage at both ends of the HT calibration cell. Due to time constraints prior to the plume measurements, only three concentration levels of 0, 50, and 200 ppb, were completed under dry conditions (R<sub>H</sub> = 0%).
- **Post-calibration** was performed at TNO Petten, outside the Petten laser lab, from October 4, 11:30 UTC, to October 5, 13:45 UTC, also under dry conditions. Concentrations levels of 20, 50, 100, 200, approximately 500, and 750 ppb were used for this.
- Temperature drift test under dry conditions (RH = 0%) was conducted at TNO Petten from October 5, 13:00 UTC to October 6, 13:00 UTC. During this 24-hour period, a fixed NH $_3$  concentration of 50 ppb was maintained to evaluate the impact of temperature drift on the HT measurements.

The full range of field-calibrated concentrations and corresponding RH values are summarized below in Table 3.1.

TNO Public 22/78

Table 3.1: Field calibration settings for TNO mobile HT calibrations. The values in ppb were converted to
μg/m³ according to the ideal gas law (Physical Chemistry, 1961) using the actual temperature and air
pressure as measured by the HT system.

Field	VSL system	VSL converted NH <sub>3</sub>		Relative humidity range of the cal. gas				
calibration settings	provided NH <sub>3</sub> concentration (ppb)	concentration (µg/m³)		10-20%	20-30%	30-40%	40-50%	50-60%
Mobile HT	0	0	✓					
(Meas. site)	50	36	✓					
	200	142	✓					
Mobile HT	0	0		•	•	✓	3	
(TNO Petten)	(TNO Petten) 20		✓			✓		
	50	36	✓			✓		
	100	73	✓			✓		
	200	146	✓			✓		
	496	360	✓			✓		
	750	542	✓			✓		

# 3.3 Mobile HT field calibration results (A2.3.6)

The mobile HT was pre-calibrated at the farm site, just before the start of the remote mobile measurements of the farm emissions. The NH<sub>3</sub> concentration measurements are given in Figure 3.3. Owing to time constraints in the field, only one zero-concentration calibration (30 min) was conducted, followed by calibration levels of 100 ppb and 200 ppb NH<sub>3</sub>, each held for 1 h. Strong winds during the measurements likely intensified the observed cell leakage problem. However, the available data are too limited to provide reliable results under such field conditions, as the green line in Figure 3.3 continues to increase or decrease and does not reach a stable level.

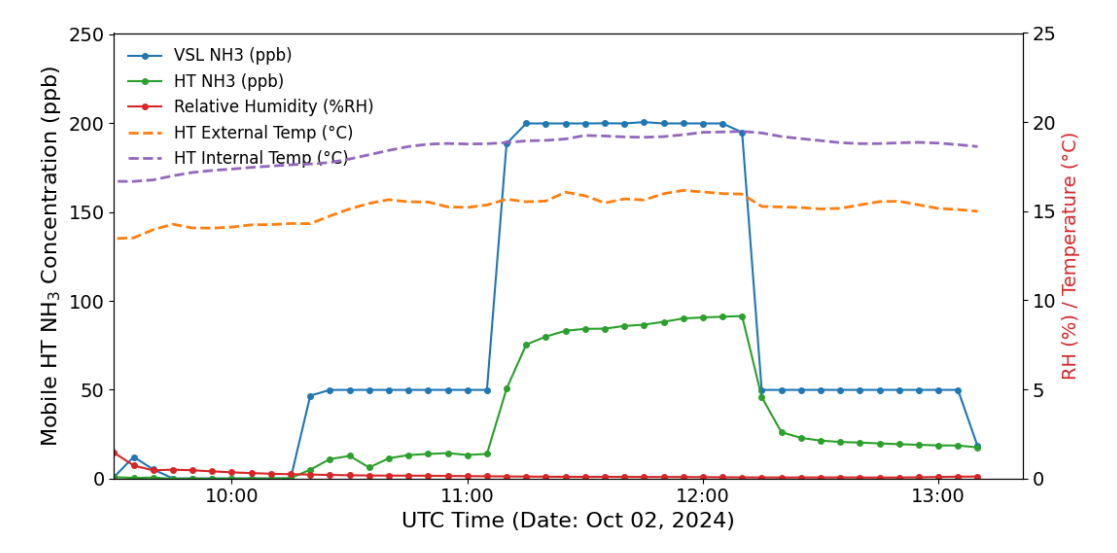


Figure 3.3: Results of mobile HT pre-calibration at the farm site on October 2, 2024. Blue: NH<sub>3</sub> concentrations offered to the system by the VSL RGM. Green: NH<sub>3</sub> concentrations measured by the HT8700 system by the

) TNO Public 23/78

VSL RGM. Red: relative humidity settings of the VSL RGM system. Orange and purple: HT measured external and internal temperatures respectively.

The post-calibration at TNO Petten was substantially longer, from October 4 to October 7. First, for 48 hours, a set of varying concentration values was offered to the HT system under dry and semi-dry RH conditions. This was followed by an additional 24 hours temperature dependence check at a fixed concentration and a fixed RH value, as there are multiple field studies that have demonstrated the temperature drift can significantly impact he concentrations measured by the HT (Swart et al., 2023). The post-calibration results are given in Figure 3.4.

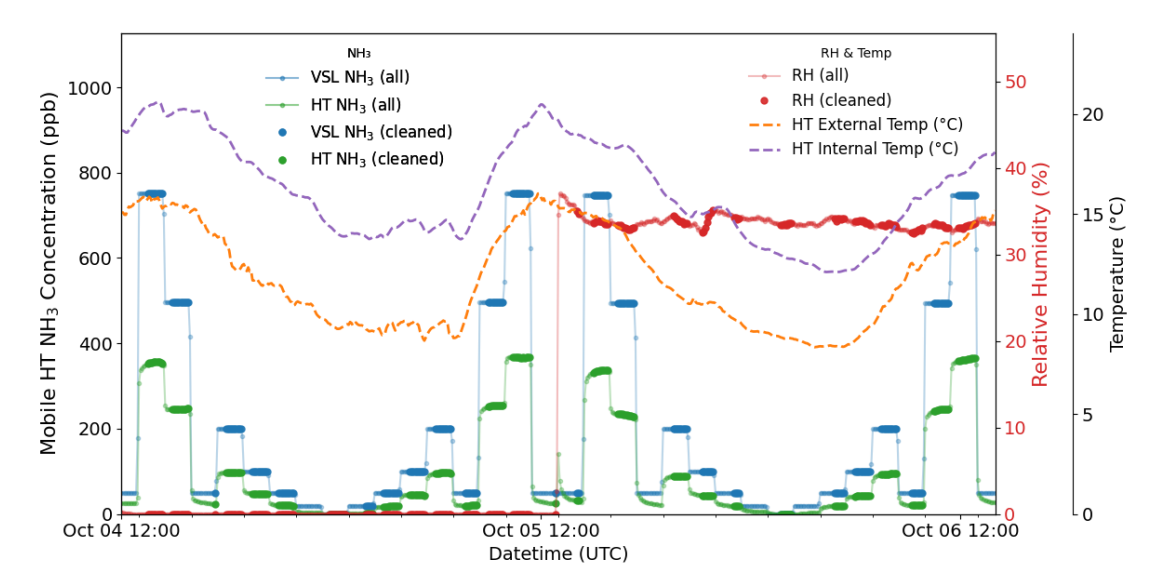


Figure 3.4: Results of **post-calibration** at **dry** ( $R_H < 10\%$ ) **and semi-dry conditions** ( $R_H \approx 33\%$ ) at the TNO Petten site on October 4-6, 2024. **Blue:** NH<sub>3</sub> concentrations offered to the system by the VSL RGM. **Green:** NH<sub>3</sub> concentrations measured by the HT8700 system by the VSL RGM. **Red:** relative humidity settings of the VSL RGM system. "Clean" means 'simple clean' dataset using the same method as mentioned before.

### 3.3.1 Regression analysis

The linear regression results for the **pre-calibration** are shown in Figure 3.5 without any quality filter (as after even applying a simple rolling CV, there were not enough data points left to do a meaningful regression). Full equilibration could not be achieved in such a short time. The resulting slope was slightly lower than the laboratory calibration results obtained under similar dry RH conditions, which were based on only two concentration levels.

) TNO Public 24/78

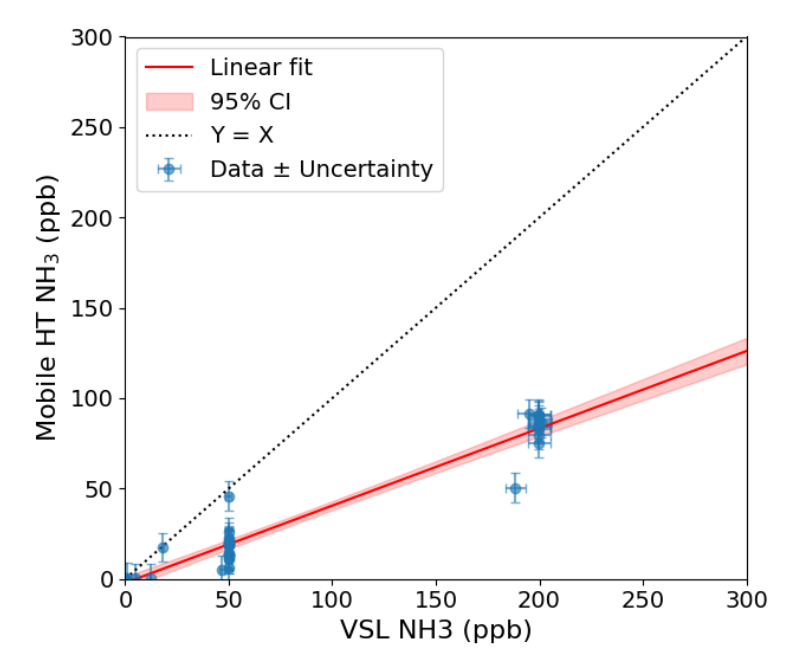


Figure 3.5: Linear regression plot of the pre-calibration results under dry conditions in the farm site. The regression on all data points without filtering.

The linear regression results for the post-calibration under all, dry and semi-dry conditions are given in Figure 3.6.

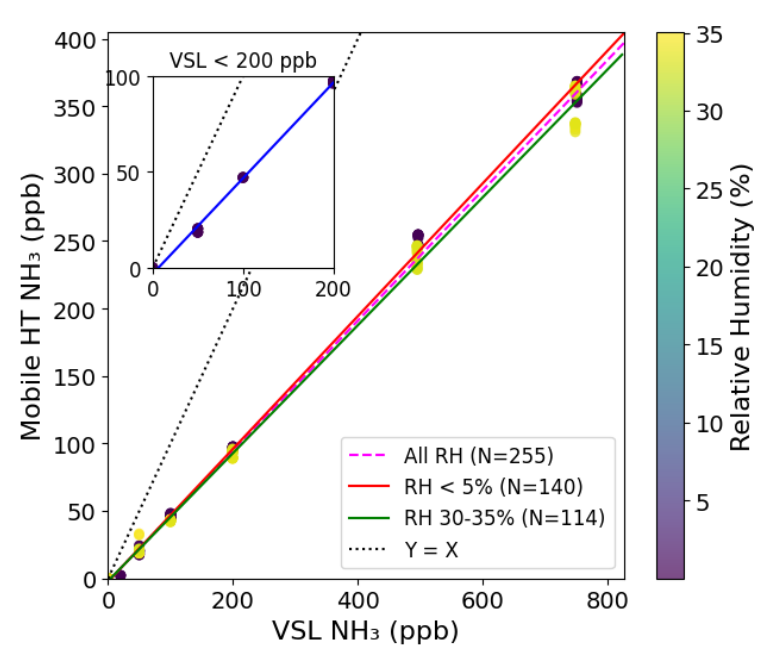


Figure 3.6: Linear regression plot of the mobile HT post-calibration results under dry conditions ( $R_H < 5\%$ ) and semi-dry conditions ( $R_H \approx 33\%$ ), the regression on all data points after simple filtered measured concentration values in the main plot; zoom in plot are only after the detrend filter and when VSL no more than 200 ppb.

A comparison of the pre- and post-field calibration results under dry conditions shows almost no shift in offset (-2.20 ppb pre-field and -2.35 ppb post-field), which is much smaller than the offset difference observed between the laboratory and field calibrations (0.16 ppb in the

) TNO Public 25/78

Number of data

laboratory calibration). The slope values remained consistent across all calibrations: the post-field slope was 0.492, closely matching the laboratory value of 0.505. In short, the primary difference between the laboratory and field calibrations under similar dry conditions is a shift in the offset, while the slope remains largely unchanged.

The complete linear regression results for these field calibrations at various RH ranges are summarized in Table 3.2.

Parameters	R <sub>H</sub> = 0% dry pre- calibration at the farm site	R <sub>H</sub> = 0% dry post- calibration at TNO Petten	R <sub>H</sub> ≈ 33% Semi-dry post- calibration at TNO Petten	R <sub>H</sub> = 0% dry post- calibration VSL<200 ppb
Slope	0.428	0.492	0.474	0.499
Intercept	-2.20	-2.35	-1.93	-3.23
Std. error of slope	0.016	0.002	0.003	0.004
Std. error of intercept	1.75	0.64	1.11	0.55
R <sup>2</sup>	0.946	0.997	0.996	0.997

140

114

36

Table 3.2: Linear regressions for different relative humidity settings, with concentration range from 0-200 ppb for pre-calibration, and 0 to 750 ppb for post-calibration.

# 3.3.2 Temperature dependence of mobile HT (post campaign check)

The outdoor calibration series of the mobile HT was followed by an additional 24 hours temperature dependence check at a fixed concentration level of 50 ppb and dry conditions (RH  $\approx$  0). A drift in the measured concentration values was observed, which seems related to temperature (Figure 3.7.).

To compensate for this, we implemented a combined correction approach: First, a linear regression was applied using the reference NH $_3$  measurements provided by VSL in the lab when VSL < 200 ppb in HT<sub>Calib</sub> =  $\frac{\mathrm{HT_{raw}}\cdot0.16}{0.505}$  (Equation 2.1).

A second-order polynomial correction was applied using the HT's internal or water-cooling temperature sensors, which closely track ambient air temperature. This correction, following the initial first-order adjustment, significantly improved NH<sub>3</sub> measurement accuracy under varying environmental conditions. The final calibration equation for the mobile HT is as follows:

$$NH_3^{cal} = \frac{(-0.16 + NH_3^{raw})}{0.505} * [1 - (-0.00267 * T_w^2 + 0.141 * T_w - 2.047)]$$
 Equation 3.1

$$NH_3^{cal} = \frac{(-0.16 + NH_3^{raw})}{0.505} * [1 - (-0.002 * T_{in}^2 + 0.113 * T_{in} - 1.423)]$$
 Equation 3.2

Where,

•  $NH_3^{cal}$  is the final calibrated ammonia concentration of the mobile HT (in ppb);

) TNO Public 26/78

- $NH_3^{raw}$  is the raw concentration of the mobile HT (in ppb);
- $T_w$  is the water circular temperature recorded by HT (in °C);
- $T_{in}$  is the inner temperature recorded by HT instrument (in °C).

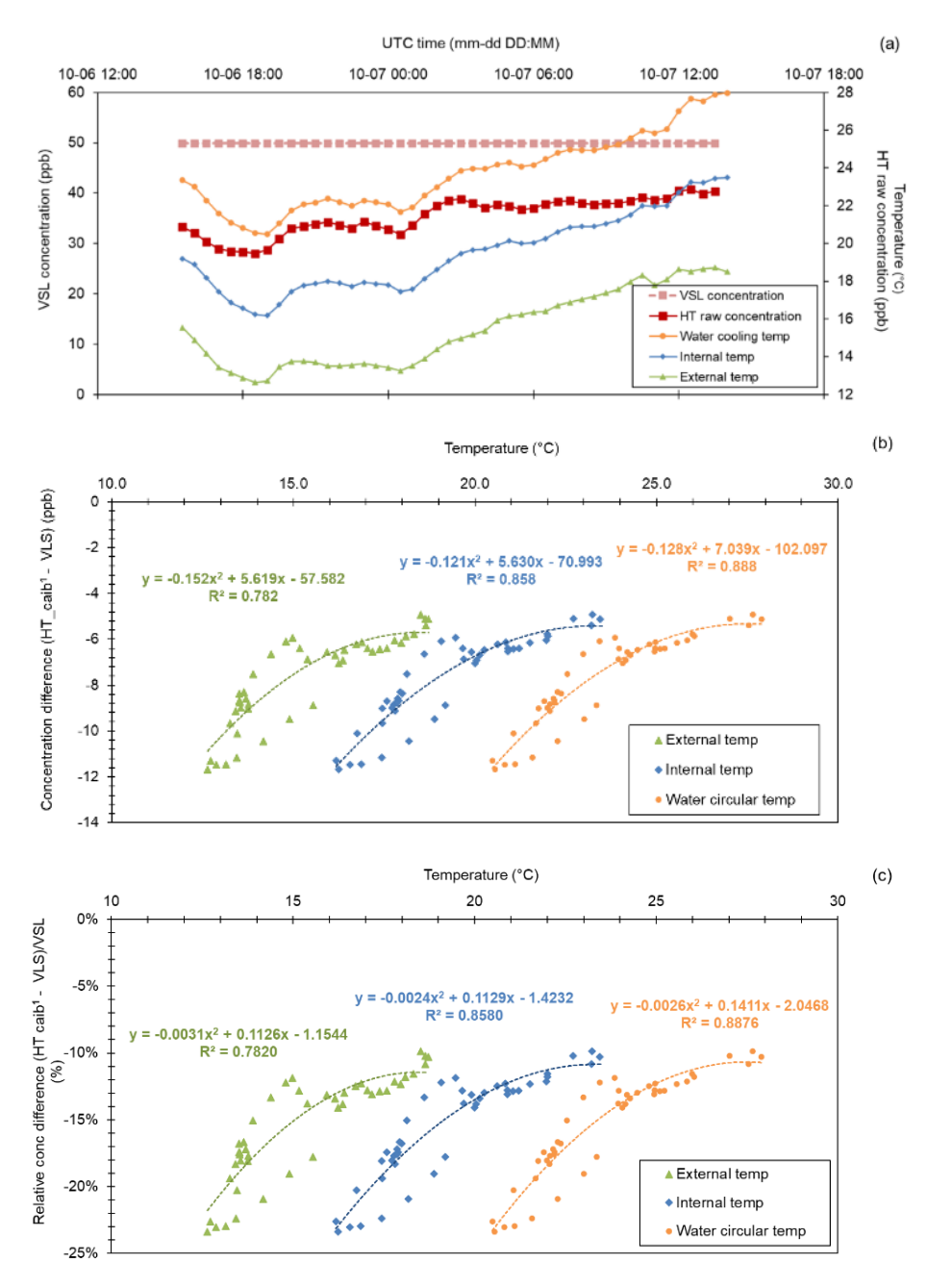


Figure 3.7: Results of the temperature check in dry conditions after the outdoor calibration run. During this check, (a) Difference between HT and VSL measured NH<sub>3</sub> concentrations (HT - VSL) plotted against various temperature parameters: internal HT temperature, external HT temperature, and water cooling pump temperature. (b) Correlation analysis of (HT calib¹ - VSL) vs. the three temperature variables. Pearson correlation coefficients (R²) are calculated to assess the goodness of fit. Note that HT calib¹ is obtained by applying the low-concentration range (VSL<200 ppb) lab calibration equation. T-test outcome indicate that a 2<sup>nd</sup> polynomial fit is needed.

TNO Public 27/78

We observed that the HT-measured internal temperature tracked changes in the external ambient air temperature; however, the correlation was nonlinear. Specifically, when the external temperature was either rising or falling, the internal temperature exhibited a polynomial trend. Moreover, the relationship between internal and ambient air temperature exhibited a distinctive hysteresis-like loop: during periods of falling external temperature, the HT's internal temperature remained several degrees higher than during the corresponding rising phase of the external temperature, reflecting a typical thermal lag effect (Figure 3.8). Both the internal sensor and the water-cooling temperature sensor monitor conditions adjacent to the laser chamber, but at different positions. Therefore, the internal temperature showed a strong linear correlation with the circular water temperature, with a consistent offset of approximately 6 °C.

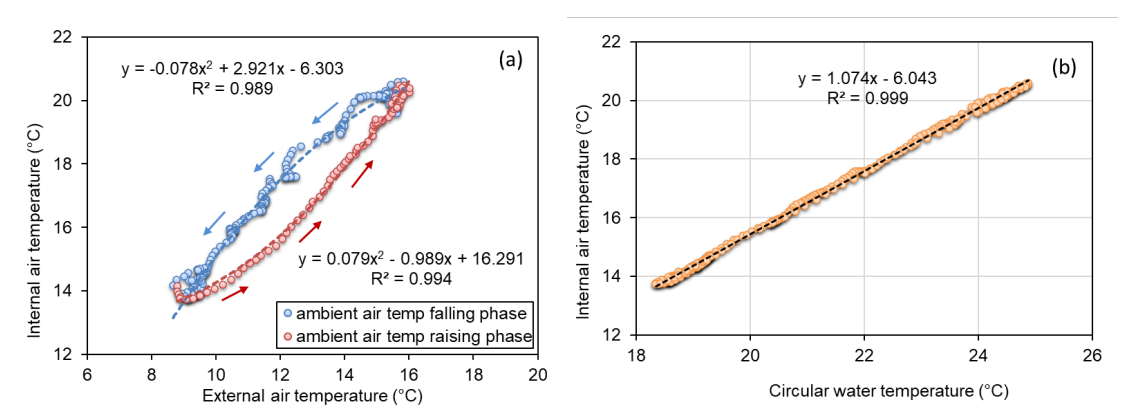


Figure 3.8: (a) The relationship between external temperature and internal temperature of the HT system exhibits hysteresis: A polynomial regression shows different behaviors when the temperature is rising versus falling. This indicates thermal lag or insulation effects, where internal temperature responds nonlinearly to external temperature depending on the direction of change. (b) The circular water pump temperature is linearly correlated with the internal HT temperature, suggesting effective heat transfer and a stable thermal regulation path via the cooling system. A strong linear fit  $(R^2 > 0.9)$  confirms this relationship.

During the mobile HT outdoor calibration, the ambient, internal, and water-circulation temperatures of the HT varied noticeably. Among these, the water-circulation temperature showed the strongest influence on both the calibration slope and offset, exceeding the effects of internal or external temperatures. After applying the temperature correction (Equation 3.3) to each VSL calibration level, the corrected calibration lines aligned much more closely with the indoor calibration results (*c.f.* Figure 3.9). In particular, the offset differences were substantially reduced, while changes in slope remained minimal. The comparison results are shown in Table 3.3.

TNO Public 28/78

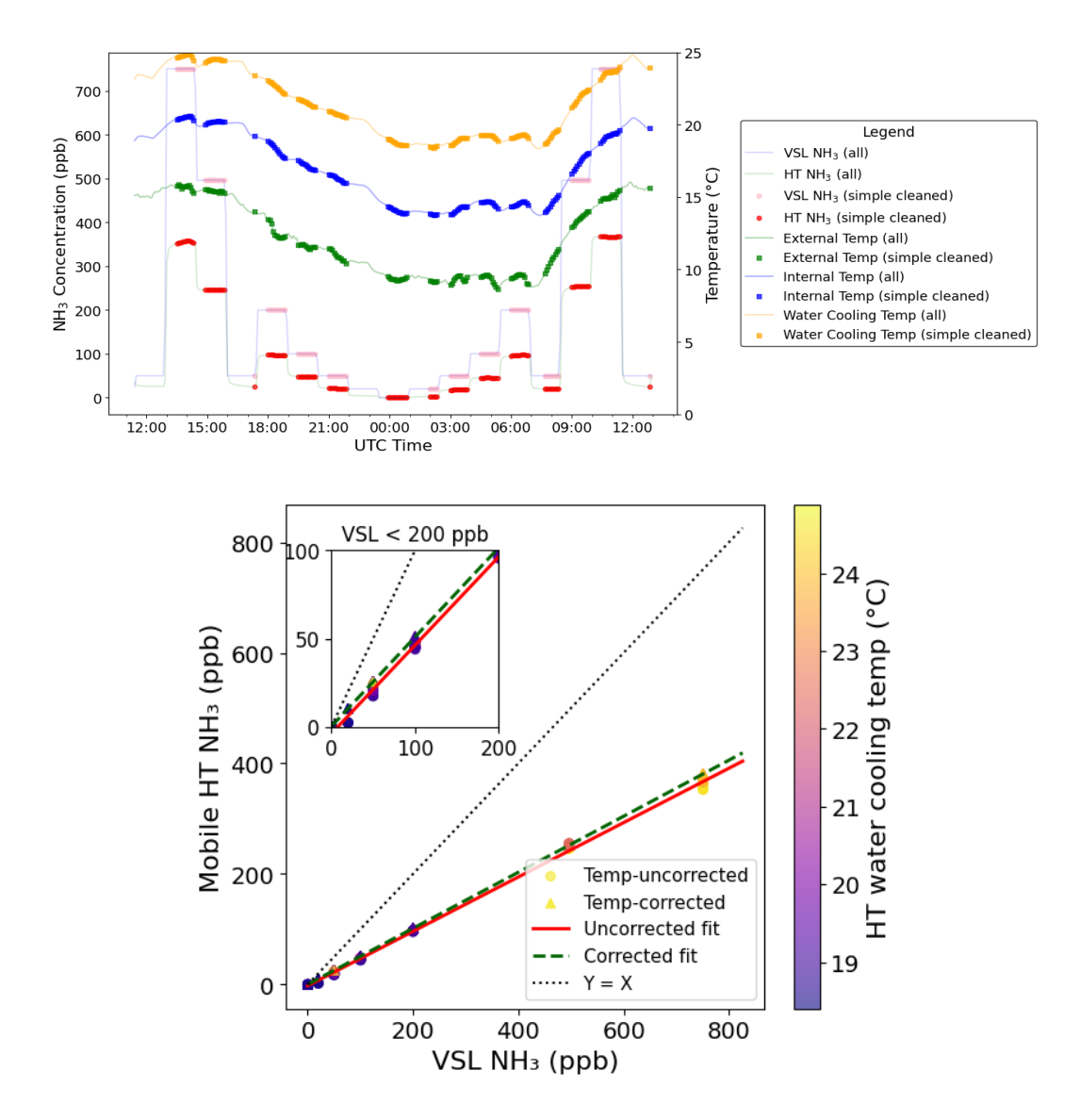


Figure 3.9: Time series of dry-period Mobile HT NH<sub>3</sub> over 24 h with external (in green), internal (in blue), and water circular temperatures(in orange) (upper plot) and temperature-corrected vs. uncorrected regression lines (lower plot), which suggests that the temperature correction is quite robust under the full range of correction despite it is only calibrated under 50 ppb level.

Table 3.3: Results of the regression analysis of the data in Figure 3.9, for the outdoor test at dry condition with and without temperature correction were compared.

	Slope	Std. error slope	Offset	Std. error offset	R²	N
Uncorrected (RGM < 800 ppb)	0.492	0.002	-2.35	0.64	0.998	140
Temperature-corrected (RGM < 800 ppb)	0.507	0.000	0.18	0.00	1.000	140
Uncorrected (RGM < 200 ppb)	0.502	0.003	-3.92	0.37	0.996	94
Temperature corrected (RGM < 200 ppb)	0.507	0.004	0.16	0.00	1.000	94

) TNO Public 29/78

### 3.3.3 Zero calibration in the field at dry condition

Results showed that after 24 hours of zero calibration under field conditions in Petten (Figure 3.10), the temperature varied from 18 to 24 °C, but the HT readings, after applying the fixed-slope correction, displayed no meaningful temperature-dependent offset drift.

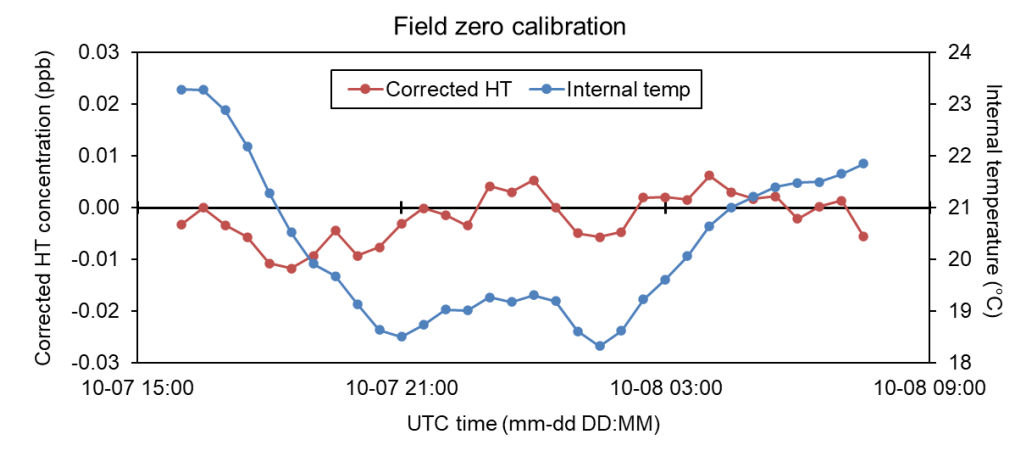


Figure 3.10: Field zero calibration results indicate that the ambient (& HT internal and water cooling) temperatures does not significantly influence the zero offset. This suggests that the HT instrument maintains thermal stability in its baseline response, and no temperature correction is needed for zero calibration under field conditions.

# 3.4 In-field calibration of UKCEH and vTI closedpath NH₃ analyzers

### 3.4.1 UKCEH open-path HT field calibration

The UKCEH-flux HT calibration was conducted overnight, from 09:00 UTC on October 3 to 09:00 UTC on October 4. Calibration concentrations were applied in the following sequence: 100 ppb, 50 ppb, 25 ppb, 10 ppb, 5 ppb, and zero, under both dry and 20–30% RH conditions. Each calibration step lasted either 60 minutes (at dry) or 90 minutes (at semi-dry). Its time lines results are shown in Figure 3.11. Due to the short field calibration period with the large glass cell, it was difficult to achieve stable conditions across all levels. To address this, a simple filtering method was applied: data were excluded when the 20-minute rolling CV of HT exceeded 3%. The remaining stable data were then used to build calibration equations under both semi-dry and dry conditions showing in Figure 3.12.

) TNO Public 30/78

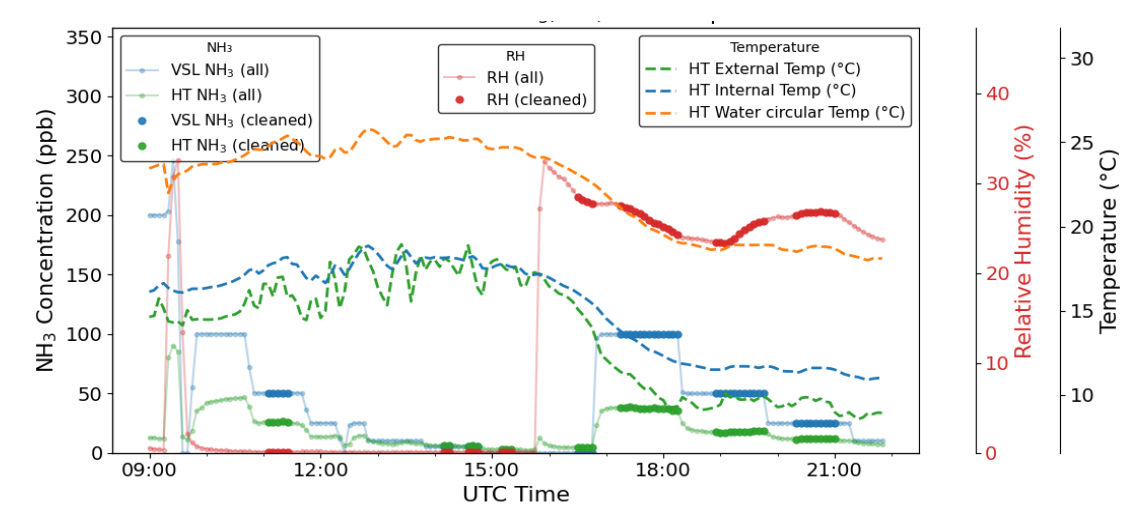


Figure 3.11: Time line of ammonia concentrations during UKCEH HT field calibration by VSL system at the dairy farm site on Oct 2, 2024 and simple cleaned stable data set was later used for calibration.

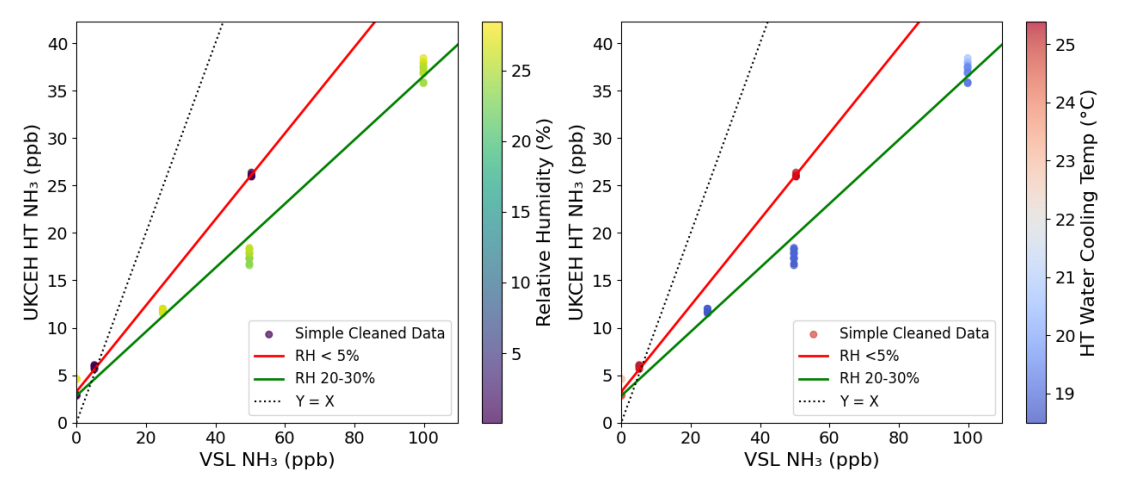


Figure 3.12: UKCEH HT field calibration results. Left: simple cleaned data points under both different RH conditions; right: same data points under different water cooling temperature of HT.

The external temperature sensor of the UKCEH HT exhibits more frequent fluctuations than the internal sensor, suggesting that it may be less stable or reliable compared to the TNO HT's temperature performance. The water cooling system temperature was constantly about 7.5 °C higher than its inner one, which is similar to TNO mobile HT.

Since the calibration was performed under field conditions, temperature effects were anticipated. Unlike the TNO mobile HT, no temperature-drifting checks were conducted for the UKCEH HT, hence no temperature correction has yet been applied. However, the temperature data show that during the dry calibration period, the HT water-circulation temperature was higher than during the semi-dry conditions (Figure 3.12). Based on the TNO HT performance, when the water-circulation temperature exceeds 22 °C, temperature-induced drift is minimal in Figure 3.7. This suggests that the regression line obtained under dry and warmer conditions is less affected by temperature and could serve as an initial check of the instrument's slope and offset. The summarized results of UKCEH HT field calibrations (together with vTI QCL and UKCEH QCL) are listed in Table 3.4.

) TNO Public 31/78

### 3.4.2 Two closed-path QCL field calibrations

In the field on October 2, 2024, two closed-path TILDAS QCL NH₃ analyzers were calibrated using the VSL RGM system. Although both analyzers were identical in type, they were owned and operated separately by the UKCEH and vTI teams.

The QCL analyzer required a total sample flow of  $13.0 \, L \, min^{-1}$  for the UKCEH instrument and  $11.6 \, L \, min^{-1}$  for the vTI instrument. However, after two-step dry-air dilution, the VSL system could supply only about  $4 \, L \, min^{-1}$ . To increase the available flow, a second line (originally designated for wet air) was connected, and the relative humidity was set to zero, allowing the VSL to provide up to  $8 \, L \, min^{-1}$  if needed. To simplify calibration calculations, the total flow was achieved by mixing  $6.5 \, L \, min^{-1}$  of calibrated gas from the VSL with  $6.5 \, L \, min^{-1}$  of ambient air for the UKCEH QCL, and  $5.8 \, L \, min^{-1}$  of each for the vTI instrument.

Ambient air was continuously monitored by the RIVM mini-DOAS open-path analyzer, calibrated against the high-accuracy VSL standard. The mini-DOAS has a reported random error of  $\sim$ 1.4% and an absolute uncertainty of  $\sim$ 0.2  $\mu$ g m<sup>-3</sup> (Sintermann et al., 2016).

The UKCEH QCL was calibrated in two sessions: 13:30-14:15 UTC with an incorrect VSL flow, followed by 14:15-15:00 UTC with the correct setup. During this time, the wind was from the north at 6-8 m s<sup>-1</sup>, and ambient NH<sub>3</sub> measured by the mini-DOAS was  $2.56 \pm 0.2$  ppb. The vTI QCL was subsequently calibrated from 15:00-15:40 UTC, with ambient NH<sub>3</sub> at  $2.16 \pm 0.2$  ppb, representing a near-zero 'clean' background.

QCL and VSL data were resampled to 5 s intervals, and stable, trend-free QCL periods were identified using a 12-sample (1 min) rolling filter with CV < 1 % and slope < 0.05 ppb/sample, followed by linear regression. Mini-DOAS data, originally at 2 min intervals, were also resampled to 5 s, and the final reference NH $_3$  concentration at each time step was obtained by averaging VSL and mini-DOAS values.

The time series and linear calibration results of UKCEH-QCL and vTI-QCL analyzers are presented in Figure 3.13 and Figure 3.14.

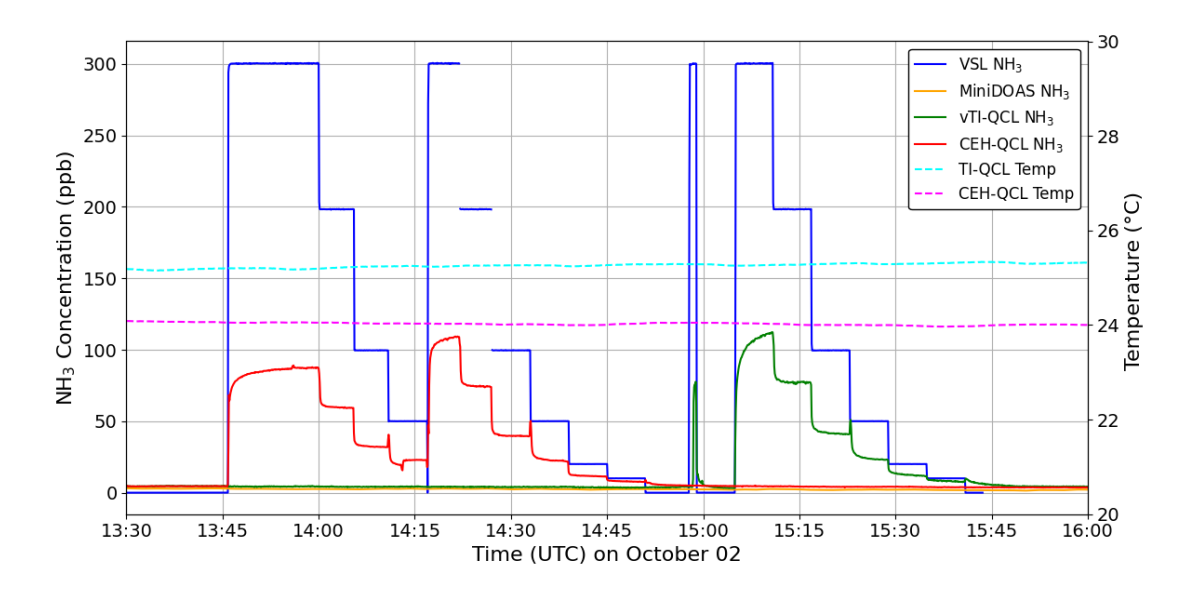


Figure 3.13: Field calibration time series of UKCEH (solid red line) and vTI QCLs (solid green line) using a mixed NH<sub>3</sub> stream combining VSL output (solid blue line) and ambient air measured by mini-DOAS (solid yellow line) at dry conditions.

) TNO Public 32/78

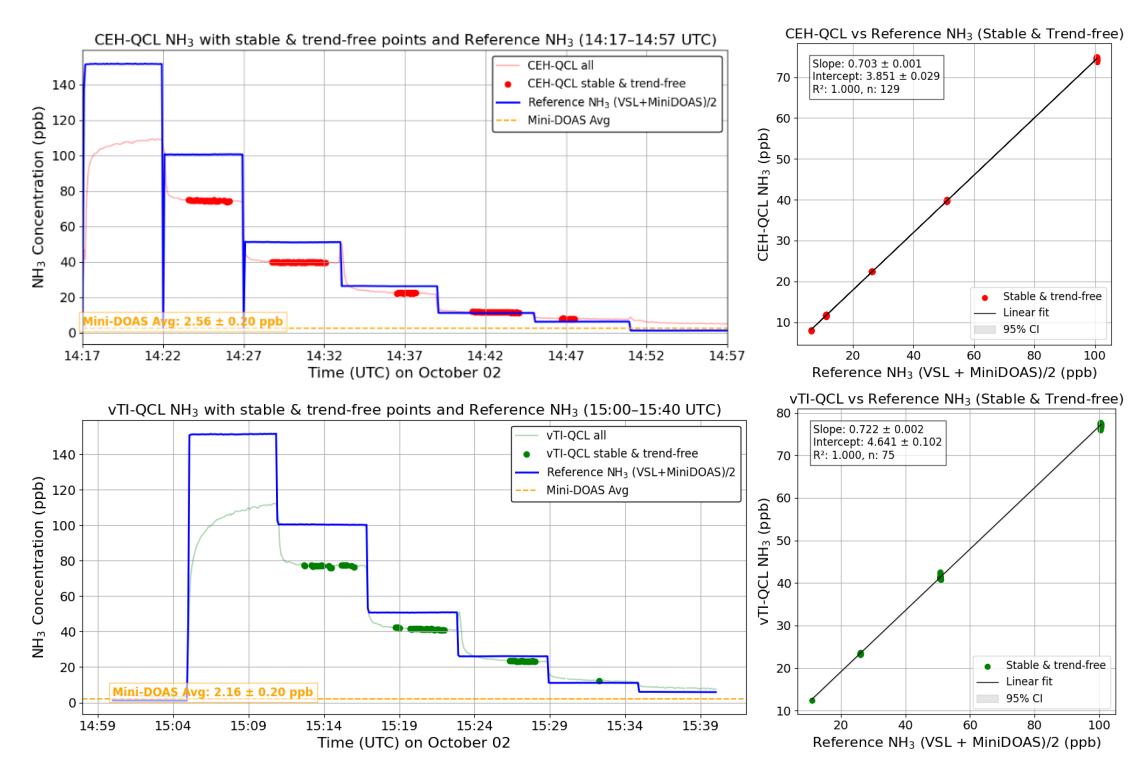


Figure 3.14: Upper plots: UKCEH QCL calibration; lower plots: vTI QCL calibration, both using filtered stable data. Input gases were mixed VSL gas and ambient air, with the mixed gas used for linear correlation. Stable periods were identified using a rolling 12-sample window (≈1 min), filtering data with CV <1% and slope magnitude <0.05 ppb/sample.

# 3.4.3 Summary regression results of partners

The calibrations of the three instruments from the project partners are summarized in Table 3.4. Both QCL systems exhibited approximately 30% underestimation, while the UKCEH HT showed a larger underestimation of around 50%, similar to the TNO mobile HT. These discrepancies may stem from improper factory calibration. Since the measured absolute concentrations of both instrument types rely on HITRAN parameters, further verification by the manufacturers may be warranted.

Table 3.4. CEH QCL, CEH-HT and TI-QCL at Dutch dairy farm field calibrations: linear regressions for different relative humidity settings.

Field instrument	TI-QCL	UKCEH-QCL	UKCEH-HT	
Parameters	RH = 0%	RH = 0%	RH = 0% RH = 20 - 30	
Slope	0.722	0.703	0.454	0.337
Intercept	4.64	3.85	3.27	2.83
Std. error of slope	0.002	0.001	0.004	0.007
Std. error of intercept	0.102	0.029	0.12	0.46
R <sup>2</sup>	1.000	1.000	0.999	0.986
Number of data	75	129	13	37

) TNO Public 33/78

# 4 Remote estimates of farm emissions (input A.2.3.6)

# 4.1 Tracer Dispersion Method (TDM) application

During the Dutch dairy farm quantiAGREMI campaign, the Tracer Dispersion Method (TDM) was employed to quantify ammonia ( $NH_3$ ) and methane ( $CH_4$ ) emissions from a dairy farm on two non-consecutive days: October  $2^{nd}$  and October  $11^{th}$ .

The Tracer Dispersion Method (TDM) involves releasing a tracer gas at a known emission rate to determine the emission strength of a target source. Various previous studies have examined such method and provided its robustness and uncertainty (Hensen et al., 2009; Vechi et al., 2022). In this study, nitrous oxide ( $N_2O$ ) was used as the tracer due to its low atmospheric background concentrations and chemical inertness. Furthermore,  $N_2O$  shares similar inlet and instrument response characteristics with methane ( $CH_4$ ), enabling direct comparability of dispersion behavior.

The location of the  $N_2O$  release cylinder was selected based on real-time wind direction, proximity to the emission source, and site accessibility, ensuring that the dispersion patterns of the tracer resembled those of the actual source emissions. The tracer release rate was adjusted dynamically depending on wind speed, site geometry, and the distance between the source and the mobile measurement path. The aim was to generate tracer plumes with a signal-to-noise ratio (SNR) greater than 3, typically corresponding to a plume centerline increase of 3–30 ppb in  $N_2O$  concentration.

To apply such method, certain stable meteorological conditions can ensure accurate emission estimates. Specifically, wind speeds should range between 2 and 12 m s<sup>-1</sup>, with a consistent wind direction and the availability of a clear measurement transect oriented perpendicular to the wind. Wind speeds below 2 m s<sup>-1</sup> can result in poorly defined plumes and increased uncertainty, while speeds above 12 m s<sup>-1</sup> may cause excessive dilution, reducing the ability to detect low emissions. In areas with complex terrain or nearby obstacles, longer measurement distances are necessary to adequately capture the representative plume. Further there must be no other sources of emissions in the measurement path.  $N_2O$  can only be used as a tracer gas if there are no other significant sources of  $N_2O$  present.

When using a tracer, the emission rate of the target gas can be estimated directly from the measured concentration ratios using the equation below:

$$Q_{\text{source}} = Q_{\text{tracer}} \cdot \frac{M_{\text{source}}}{M_{\text{tracer}}} \cdot \frac{\int s_{\text{source}}}{\int s_{\text{tracer}}}$$
 Equation 4.1

Where.

- $Q_{\text{source}}$  is the emission rate of the source gas (in g/s);
- $Q_{\text{tracer}}$  is the known emission rate of the tracer gas (in g/s);
- $M_{\text{source}}$ ,  $M_{\text{tracer}}$  are molar masses of the source and tracer gas (in g/mol);

) TNO Public 34/78

•  $\int s_{\text{source}}$ ,  $\int s_{\text{tracer}}$  are integrated concentrations of source and tracer plumes (in ppb).

On each measurement day, two tracer gas cylinders were deployed near the dairy farm (see field settings in Figure 4.1). The mobile van equipped with the  $NH_3$  and  $CH_4/N_2O$  gas analyzers, drove transects along nearby roads based on prevailing wind conditions:

- On October 2<sup>nd</sup>, driving occurred on the northwest (NW) side of the farm between 13:45–14:30 and 14:35–15:15 UTC.
- On October 11<sup>th</sup>, due to a shift in wind direction, the van drove on the southwest (SW) side between 10:30–11:30 and 12:00–13:35 UTC.

The road-to-barn distances were approximately 150 meters on October 2<sup>nd</sup> and 800 meters on October 11<sup>th</sup>. Tracer release rates were adjusted accordingly:

- On October 2<sup>nd</sup>, the tracer was released at 0.1 g/s.
- On October 11<sup>th</sup>, a higher release rate of 0.5 g/s was applied to compensate for greater source-receptor distance.

Meteorological conditions were continuously monitored throughout the tracer release periods:

- On October  $2^{nd}$ , wind direction was  $50.1^{\circ} \pm 6.3^{\circ}$  with a wind speed of  $6.9 \pm 0.9$  m/s.
- On October 11<sup>th</sup>, wind direction shifted to 259.2°  $\pm$  11.9°, and wind speed decreased to 4.1  $\pm$  0.7 m/s.

Relative humidity (RH) was measured using the TNO Vaisala instrument, located approximately 350 meters west of the farm, in the middle of the grass field. During the October  $2^{\rm nd}$  measurement period, RH ranged from 68.8% to 75.5%, with a mean  $\pm$  standard deviation of 71.9%  $\pm$  1.5%. On October 11<sup>th</sup>, RH ranged from 50.7% to 64.8%, with a mean  $\pm$  standard deviation of 55.3%  $\pm$  2.2%.

External air temperature ranged from  $14.3^{\circ}$ C to  $15.2^{\circ}$ C on October  $2^{nd}$ , and from  $13.5^{\circ}$ C to  $15.7^{\circ}$ C on October  $11^{th}$ , showing similarly mild but slightly broader temperature variation on the second measurement day.

These meteorological parameters, especially wind speed, direction, humidity, and temperature, strongly influenced tracer plume dispersion and gas detectability. On October  $11^{\rm th}$ , due to the longer source-to-receptor distance (~800 m) and probable NH $_3$  deposition under wetter and moderate turbulent conditions, CH $_4$  and N $_2$ O plumes were clearly detectable during the tracer release, whereas NH $_3$  concentrations remained near background levels with a very high signal-to-noise ratio. Therefore, the NH $_3$  farm emission results from October  $11^{\rm th}$  are not presented in this report.

) TNO Public 35/78

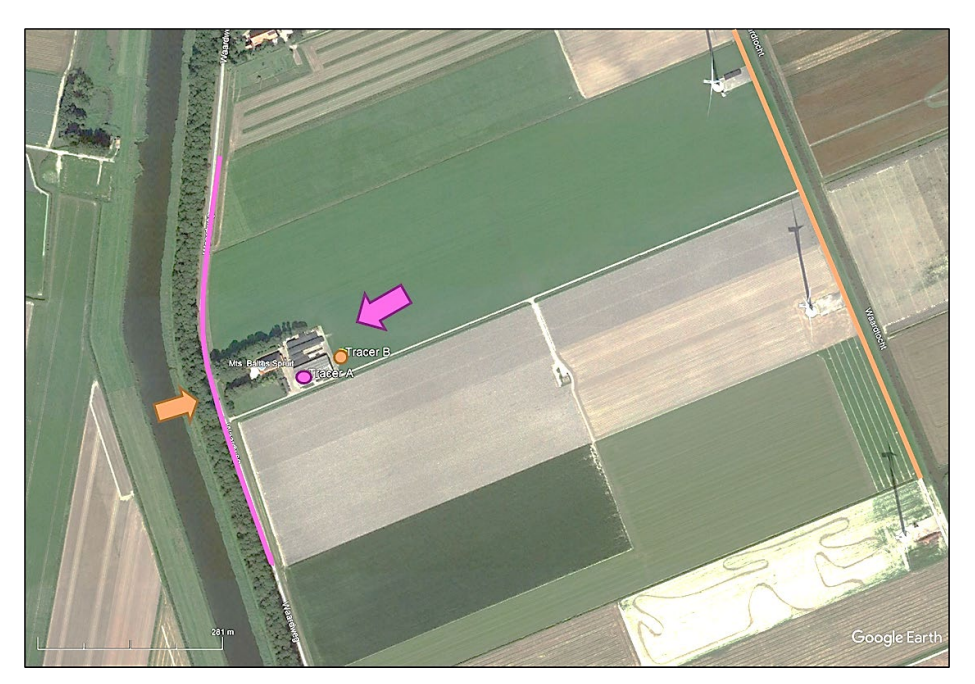


Figure 4.1. On Oct  $2^{nd}$  the plume measurements were along the right hand side road of the farm (in purple line with purple dot for placing  $N_2O$  tracer) due to the NW wind. On Oct  $11^{th}$ , the measurements were conducted in the left side of the road (in orange line with orange dot for placing  $N_2O$  tracer) due to the SW wind.

# 4.2 In-situ calibration and uncertainty analysis of CH<sub>4</sub> and N<sub>2</sub>O measurements

#### 4.2.1 Field calibration of QCL-TILDAS

To support emission uncertainty estimation, all gas measurement instruments were calibrated on-site under field conditions.

For the measurement of methane (CH<sub>4</sub>) and nitrous oxide (N<sub>2</sub>O), a Tunable Infrared Laser Direct Absorption Spectroscopy (QCL-TILDAS) dual-laser analyzer (Aerodyne Research, Inc., Billerica, USA)<sup>8</sup> was used. This closed-path system provides a reported precision of 2.4 ppb for CH<sub>4</sub> and 0.1 ppb for N<sub>2</sub>O.

The QCL was calibrated at both the start and end of the second measurement day (October  $11^{th}$ ) using calibration gases traceable to ICOS-certified standards measured at the Cabauw tower in the Netherlands. Two calibration gas bags were used, one with high and one with low concentrations of CH<sub>4</sub> and N<sub>2</sub>O, to enable linear calibration over a defined range. During the first campaign day (October  $2^{nd}$ ), no calibration was performed. Since the QCL remained unused and stationary in Petten between the two campaigns, the calibration data from October  $11^{th}$  is assumed to be valid for both measurement periods.

Each calibration session involved manual switching of the inlet between the high and low concentration gas bags every 30–40 seconds, over a total duration of approximately 4 minutes (Figure 4.2). To eliminate the influence of unstable transition phases, the first 20 seconds after each switch were excluded. Only the final 10–20 seconds of each stable phase were used in the calibration analysis.

<sup>8</sup> <u>Dual.pdf</u>

) TNO Public 36/78

In total, six calibration episodes were recorded for each concentration level, yielding twelve calibration points. These were further screened as such: any episode whose average concentration deviated by more than two standard deviations from the overall mean was treated as an outlier and excluded from regression analysis.

The remaining data were used for linear regression calibration and linear regressions results of  $CH_4$  and  $N_2O$  are shown in Figure 4.3. While using two concentration levels satisfies the minimum requirement for offset and slope estimation, it introduces some limitations:

- a) For CH<sub>4</sub>, the concentrations were 2359.8 ppb and 2050.9 ppb, which allows for calibration of both slope and offset. However, since only two concentration levels were used, the uncertainty in the regression fit could not be meaningfully assessed (Figure 4.3a).
- b) For N<sub>2</sub>O, the two standard concentrations were 339.1 ppb and 340.2 ppb, a difference of only 1 ppb, which is close to the instrument's noise level. As such, these calibrations were primarily used to assess offset stability rather than slope (Figure 4.3b and Figure 4.3c).

For improved calibration robustness in future campaigns, it is recommended to employ at least three distinct concentration levels, ideally covering a wider range of expected ambient values.

TNO Public 37/78

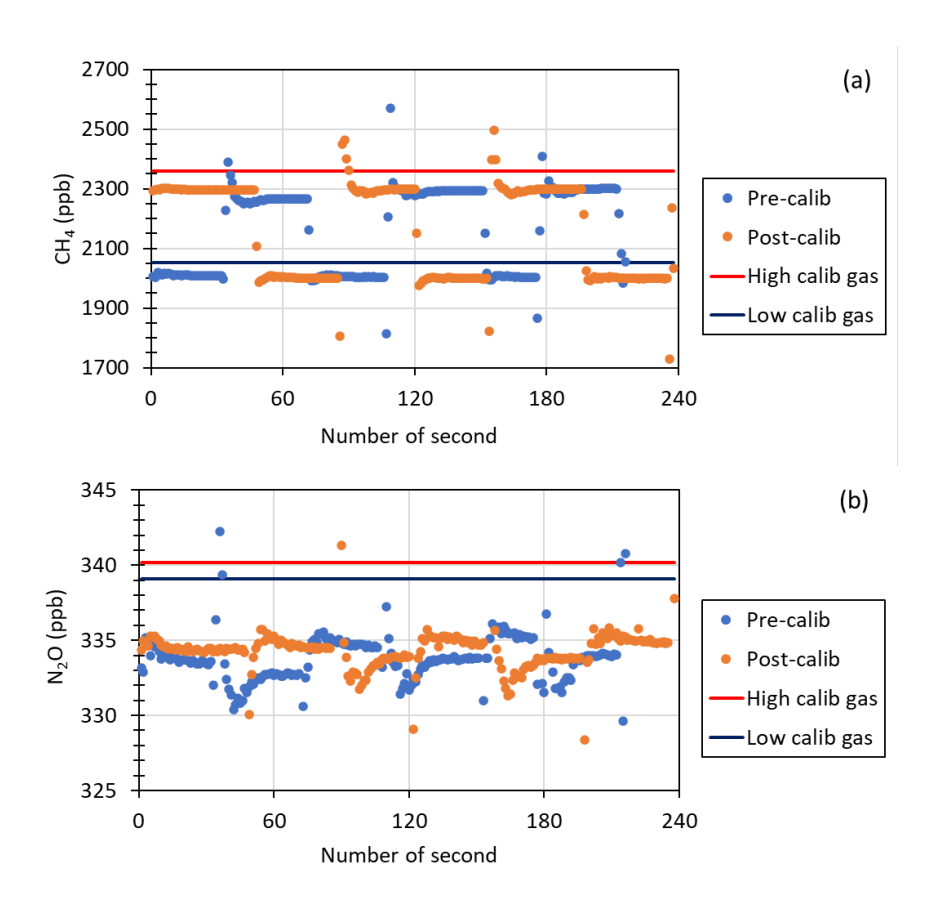


Figure 4.2. Calibration of the CH<sub>4</sub> and  $N_2O$  measured by TNO QCL: using two standard calibration gases to calibrate measured CH<sub>4</sub> and  $N_2O$  concentrations before and after the field tracer plume remote measurement in Oct  $11^{th}$ .

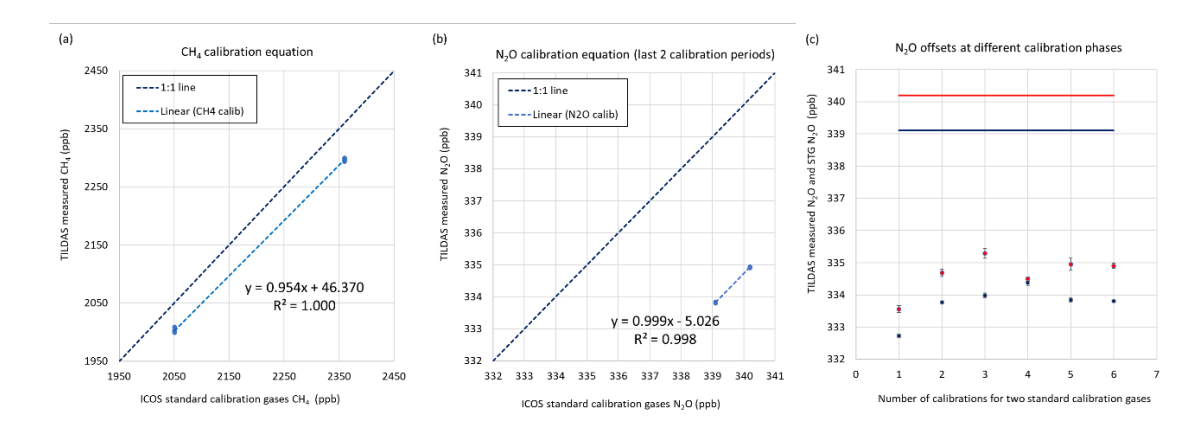


Figure 4.3. CH<sub>4</sub> QCL calibration results in (a), and  $N_2O$  calibration results in (b), the  $N_2O$  calibration gas concentration level are too close (only 1 ppb difference), the offset of it is consistent when equilibrium were reached in the last calibration episodes showing in (c).

) TNO Public 38/78

# 4.2.2 Uncertainty estimates for the CH₄ and N₂O concentrations

There are several sources of errors for measured  $CH_4$  and  $N_2O$  which can end up into the final estimated  $CH_4$  and  $NH_3$  emission values:

First of all, these are the uncertainties in the concentration of the standard gas cylinders from Cabauw Integrated Carbon Observation System (ICOS). The ICOS calibration gases are traceable to World Meteorological Organization – Global Atmosphere Watch (WMO-GAW) reference scales, such as the standards maintained by the National Oceanic and Atmospheric Administration (NOAA). The uncertainty for CH<sub>4</sub> reported in Sasakawa et al. (2025) is a scale-link uncertainty on the order of a few ppb, likely the standard uncertainty is less than 3 ppb. For  $N_2O$ , according to Jordan & Damak (2024), the standard uncertainty is less than 0.11 ppb. These uncertainties are extremely low and can be considered negligible for most ambient monitoring applications. But they still contribute directly to the final uncertainty budget of the QC-TILDAS analyzer when used for calibration.

Secondly, errors can be introduced when applying the calibration gas to the QC-TILDAS, such as leaks or pressure variations, moisture contamination, temperature or pressure drift. These can introduce 0.1% - 0.5% uncertainty if not properly controlled (e.g. with good flow control and pre-conditioning), like  $\pm$  0.5 ppb.

Thirdly, when applying a calibration function to the acquired data (a linear regression fit is applied), the calibration curve fit has its own uncertainty. To calculate residuals and uncertainty equations in below are used:

$$\sigma_{res} = \sqrt{\frac{1}{n-2} \sum r_i^2}$$
 Equation 4.2   
  $r_i = Y_i - \widehat{Y}_i$  Equation 4.3   
  $\widehat{Y}_i = a \cdot X_i + b$  Equation 4.4

#### Where.

- $\sigma_{res}$  is calibration fit uncertainty;
- $r_i$  is the residuals, which is the difference between what the instrument measured and what the regression model predicted;
- ullet Y is the mean value of CH4 measured by the TILDAS during calibration episode i,
- $\widehat{Y}_i$  is the predicted value of CH<sub>4</sub> from your linear regression model (i.e., the model's estimate based on the known gas concentration for that episode);
- $X_i$  is known CH<sub>4</sub> concentration of the calibration gas (in ppb);
- a is slope (sensitivity) for CH<sub>4</sub> is 0.954 and for N<sub>2</sub>O is 0.999;
- b is intercept (offset) as for CH<sub>4</sub> is 46.37 and for N<sub>2</sub>O is -5.03.

The root-sum-of-squares (RSS) method is applied here, combing independent uncertainty components into a single overall estimate, according to the Joint Committee for Guides in Metrology (2008).

) TNO Public 39/78

For CH<sub>4</sub>, the uncertainties are as follows: calibration gas  $\pm$  3 ppb, handling/systematic effects were estimated as  $\pm$  0.5 ppb, and the TILDAS calibration fit uncertainty were  $\pm$  3.2 ppb. This results in a total absolute uncertainty for CH<sub>4</sub> ( $\sigma_{total_{CH4}}$ ) of approximately 4.4 ppb at the average calibration concentration (2136 ppb for CH<sub>4</sub>). Similarly, the total absolute uncertainty for N<sub>2</sub>O ( $\sigma_{total_{N2O}}$ ) is estimated to be **1.5 ppb** at the average calibration concentration (334 ppb for N<sub>2</sub>O). These correspond to relative uncertainties of approximately 0.2% to 0.4% for CH<sub>4</sub> and N<sub>2</sub>O, respectively, indicating that the calibration-related errors are relatively small. During plume measurement periods, concentrations often exceed the calibrated levels, resulting in a decrease in relative error (%) as concentration increases.

For individual plumes, the relative error of N<sub>2</sub>O can be estimated using the equation below:

$$\sigma_{S_{N_2O}} = \frac{\sqrt{n} \cdot \sigma_{abs}}{S_{N_2O}}$$
 Equation 4.5

Where:

- *n* is the number of time points (e.g., 25-30 second)
- $\sigma_{abs}$  is the absolute instrument error per point (1.5 ppb as calculated above)
- $S_{N20}$  is the integrated  $N_2O$  signal after baseline subtraction (in ppb)

Based on 21 plumes measured on October 2, the relative uncertainty of integrated  $N_2O$  signal ranged from 4% to 14%, with an average of 7%  $\pm$  2%. For CH<sub>4</sub>, relative uncertainties were significantly lower, ranging from 1% to 2%, with a mean of 1.0%  $\pm$  0.3%. These uncertainties were used in the propagation of total NH<sub>3</sub> emission errors using standard root-sum-square methods later.

# 4.3 In-situ calibration and uncertainty analysis of NH₃ measurements

## 4.3.1 Evaluating the field calibration results

For  $NH_3$  concentration measurements, TNO's mobile open-path HT  $NH_3$  gas analyzer was employed. This instrument underwent two on-site calibrations using the VSL system: once on October  $2^{nd}$  (the first measurement day), and again on October  $8^{th}$  prior to the second measurement campaign in Petten using the closed-glass calibration cell under changing temperature.

Despite the actual measurement campaigns occurred at higher relative humidity levels ( $\sim 50-75\%$ ) but the measured NH<sub>3</sub> concentrations were rather low ( $\sim 50$  ppb downwind of the farm with 200 m distance), and outside the plume, NH<sub>3</sub> was about 2 ppb at the background level measured by RIVM mini-DOAS.

Important to be noted that the HT system is an open-path instrument and does not use a glass cell during normal operation. Therefore, the RH-dependent effects observed in the closed-cell tests at concentrations ≥200 ppb does not necessarily occur in the field.

Consequently, high-concentration corrections should not be applied to field data unless they can be validated under representative open-path conditions.

Moreover, the lab calibration results have demonstrated that under low concentration range (< 200 ppb), HT measured NH<sub>3</sub> is independent from RH. (*ref.* Chapter 2.2.2; Figure 2.4)

) TNO Public 40/78

Therefore, a few main sources of uncertainty in HT measurements: a) instrumental noise; b) linear calibration introduced uncertainty; 3) ambient temperature dependence drift. Additionally, there may be a small, unknown uncertainty at high relative humidity (RH) levels, which could not be validated using the current VSL calibration protocol and the closed glass cell of the HT. However, based on previous collaborative studies between TNO and RIVM during long-term field campaigns, the impact of RH on the HT open-path analyzer was found to be negligible (Swart et al., 2023; Melman; et al., 2025).

In this study, we have applied the calibration coefficients derived in the lab under low concentration range, which yielded slope as  $0.505 \pm 0.002$  and intercept as  $0.16 \pm 0.12$  ppb. Temperature correction was applied using a second-order polynomial fit.

The HT analyzer's temperature sensitivity correction has been shown in **Equation 3.3** and **Equation 3.4**.

Figure 4.4 presents the raw and calibrated NH<sub>3</sub> concentrations for October 2<sup>nd</sup>. These figures illustrate the variations in the HT's internal temperature and the water-cooling pump temperature during the measurement periods. The HT water circular temperature was used for calibration as it showed the highest R<sup>2</sup> value (0.888) to NH<sub>3</sub> concentration drift.

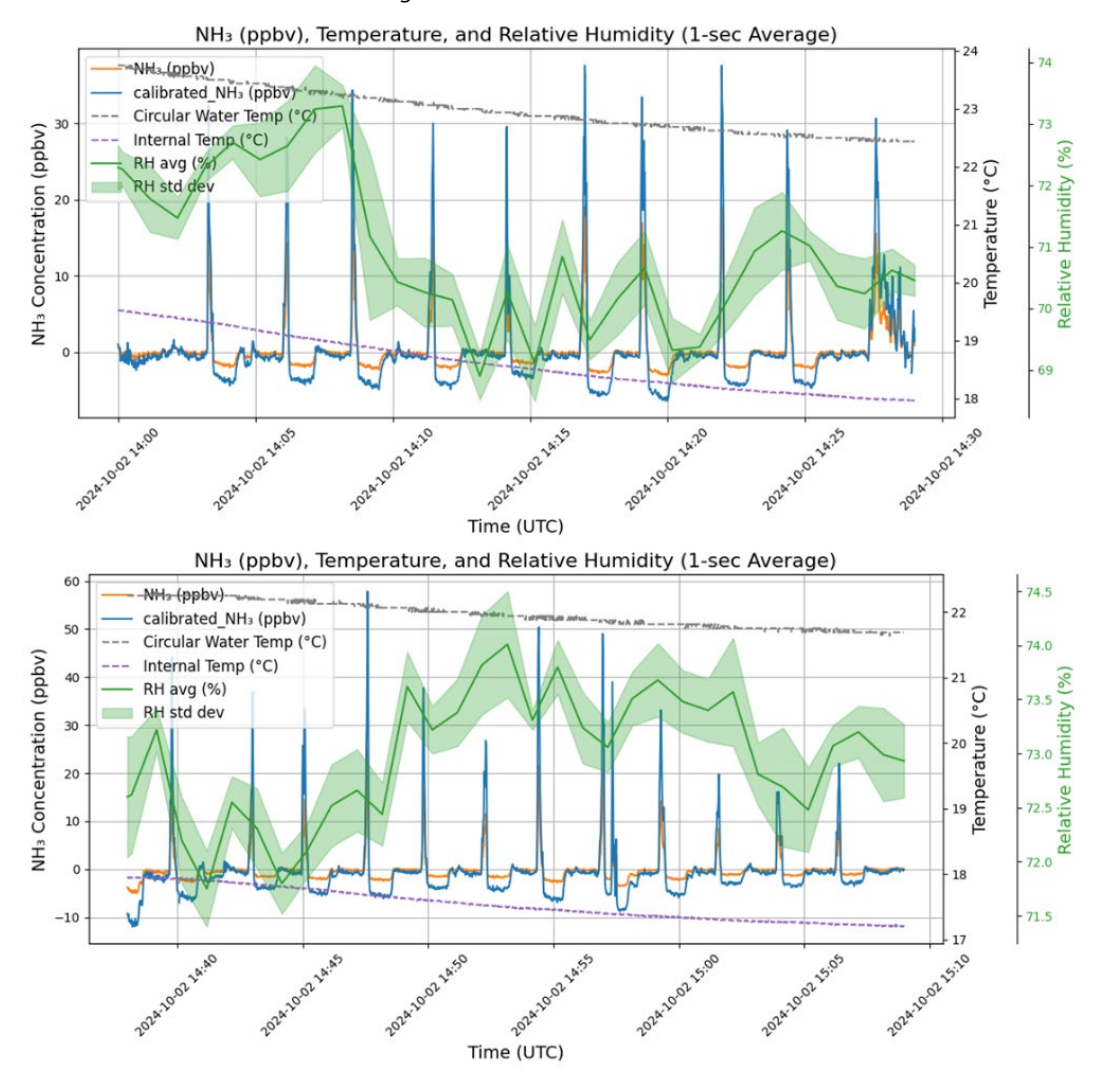


Figure 4.4: Raw  $NH_3$  data without baseline correction showing the artificial impact, along with calibration results for all tracer release periods in Oct  $2^{nd}$ , 2024.

) TNO Public 41/78

#### 4.3.2 Artificial drifted baseline correction

Besides the calibration corrections, an additional processing step was required due to a known artefact introduced by the instrument's internal software, it inadvertently introduced non-physical features in the  $NH_3$  signal when it is close to zero.

Specifically, this algorithm created an artificial baseline plateau (slightly elevated) prior to plume detection, and a negative dip immediately following the plume peak, as the algorithm compensated for the earlier offset.

These artefacts distorted the true baseline and could bias integrated concentration estimates. Therefore, before performing any plume integration for emission estimation, we identified and removed this baseline distortion. An additional correction was applied to the second half of the plume's falling limb using an average offset value, estimated from the 60 seconds of data recorded after the signal dropped below zero per individual plume. The true background was then re-established using smoothed pre- and post-plume concentrations. This correction ensured that the final NH<sub>3</sub> plume estimates represented actual atmospheric enhancements rather than software-induced signal modifications. After the baseline correction, the calibration equation was applied for all the measurement periodical data at least (Figure 4.5).

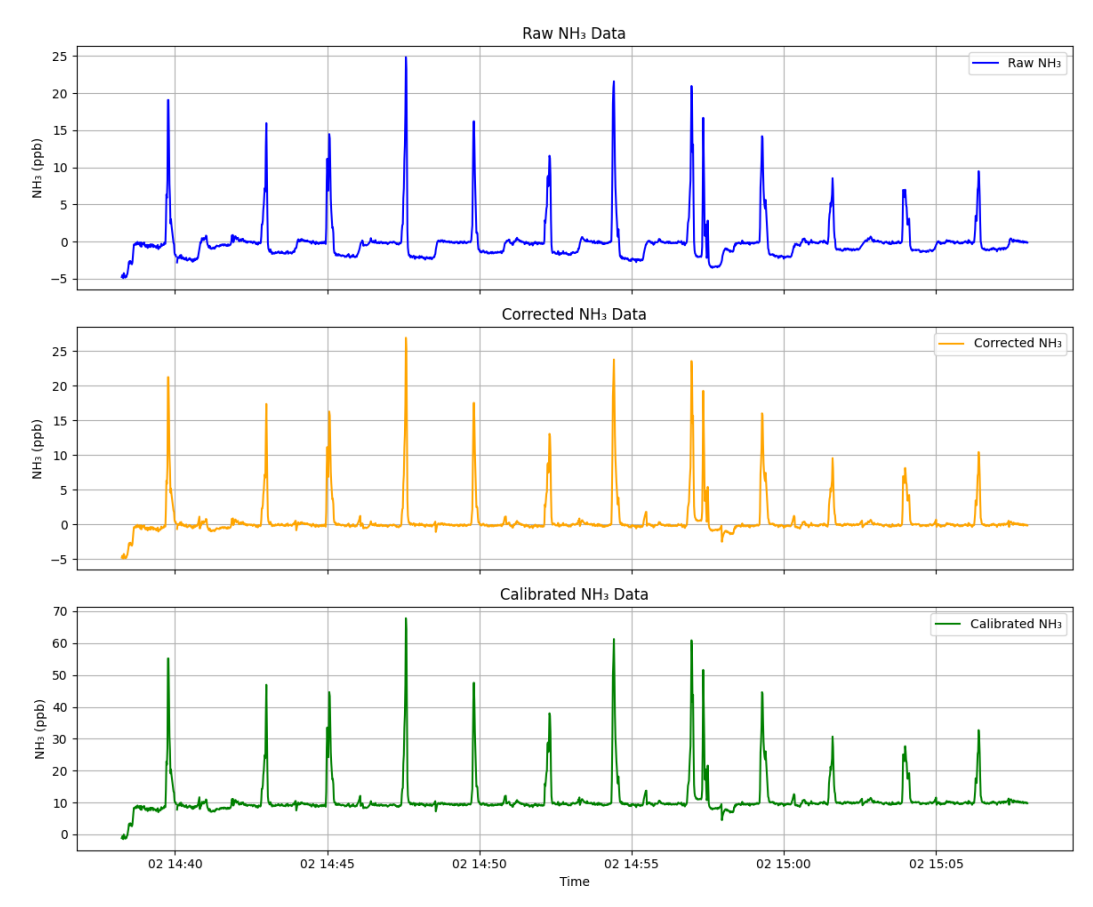


Figure 4.5. Results showing the baseline correction followed by calibration of NH<sub>3</sub> data, prepared for plume model analysis during the October 2<sup>nd</sup> tracer release Period 1.

) TNO Public 42/78

## 4.3.3 Error propagation for calibrated NH₃ concentrations

In this study, the calibrated ammonia concentration  $NH_3^{cal}$  was computed using the following calibration equation has been shown in Equation 3.3 or Equation 3.4., which can be rewritten as below:

$$NH_3^{cal} = \frac{b + NH_3^{raw}}{m} * (0.0026 * T_w^2 - 0.1411 * T_w - 1.0468)$$
 Equation 4.6

Where:

- $NH_3^{raw}$  is the raw HT analyzer measured concentration (in ppb);
- $T_w$  is the circular water temperature of HT (in °C);
- **m** and **b** are the calibration slope and intercept, respectively.

The total uncertainty in  $NH_3^{cal}$  arises from two main types of errors:

a) Random errors arise from short-term fluctuations in the measurements and are propagated as:

$$\sigma_{random} = \sqrt{\sigma_x^2 + (\sigma_m \cdot NH_3^{raw})^2 + \sigma_b^2 + (\sigma_{T_w} \cdot (0.0052T_w - 0.1411))^2} \quad \text{Equation 4.7}$$

Where,

- $\sigma_x$ ,  $\sigma_m$ ,  $\sigma_b$ ,  $\sigma_{T_w}$  are uncertainties from HT signal noise, slope, intercept and water circular temperature.
- b) *Systematic errors* arise from calibration biases, reference instrument uncertainty, and polynomial calibration accuracy.

*Note that:* Relative humidity was considered, but lab calibration showed no effect below 200 ppb, which is above the maximum measured concentration; therefore RH does not contribute to systematic error.

$$\sigma_{systematic} = \sqrt{(0.027 \cdot NH_3^{cal})^2 + (poly RSE)^2}$$
 Equation 4.8

Where:

- 2.7% VSL reference instrument uncertainty (0.027  $\times$  NH<sub>3</sub><sup>cal</sup>)
- Polynomial RSE represents systematic deviations from the polynomial calibration

Error propagation can be evaluated according to the law of propagation of uncertainty (Joint Committee for Guides in Metrology, 2008, sec. 5.1.2).

The total propagated uncertainty  $\sigma_{total}$  in the calibrated measurement is the combination of random and systematic errors:

$$\sigma_{total} = \sigma_{random} + \sigma_{systematic}$$
 Equation 4.9

An example of the measured  $NH_3$  plume error estimation and distribution is shown in Figure 4.6 for the first measured  $NH_3$  plume on Oct  $2^{nd}$ . After calibration, the integral of the total plume is 223 ppb, and the cumulative error within the plume window is 12 ppb, corresponding to a relative error of 5.4%. The majority of this error, approximately 95%, originates from the instrument's signal noise, while the remaining error components contribute less than 5% collectively.

) TNO Public 43/78

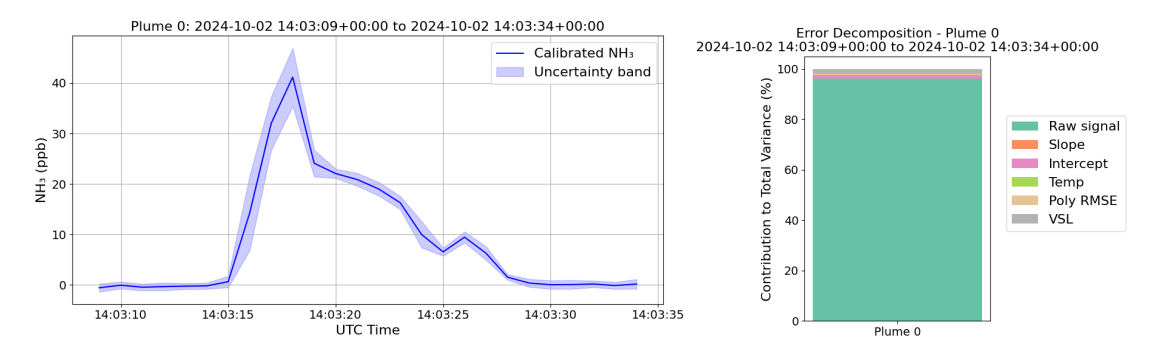


Figure 4.6: Time series of 1<sup>st</sup> calibrated NH<sub>3</sub> concentration total plume on Oct 2<sup>nd</sup> in the left; and its error decomposition in the right.

## 4.3.4 NH<sub>3</sub> plume analysis with uncertainty propagation

In the tracer method plume model application, we estimate the net NH₃ plume concentration and its uncertainty by integrating the calibrated concentration above the baseline over a given time window. The baseline is defined by a linear regression between the start and end points of the plume. The following steps are taken:

#### 1. Right-Half offset correction

Each plume is centered on the NH<sub>3</sub> peak, and a correction is applied to account for baseline drift. The right half of the plume, from the peak to the end, is analyzed to compute the average of any negative values ( $Neg_{avg}$ ). This average is then added to all points in the right half to correct the baseline and ensure non-negative plume values. Mathematically, the corrected NH<sub>3</sub> signal is given by  $NH_{3corrected} = NH_{3raw} + (Neg_{avg})$ .

#### 2. Calibration with Temperature Correction and Error Propagation

The raw NH<sub>3</sub> signal is calibrated by the VSL instrument using the slope and intercept of the calibration, and then corrected for the effect of water circular temperature drift impact (see section 4.3.3). Random uncertainties are propagated using partial derivatives with respect to the raw signal, slope, intercept, and temperature, while systematic uncertainties from polynomial fit RMSE and VSL fraction are combined to calculate the total uncertainty.

#### 3. Plume Baseline and Net Plume

For each plume, a linear baseline is constructed between the start and end points, and the net plume signal is obtained by subtracting this baseline from the calibrated NH<sub>3</sub> signal. Integrals of the calibrated plume, baseline, and net plume are then computed to quantify the total and net NH<sub>3</sub> contributions.

#### 4. Baseline Uncertainty Methods

A weighted propagation method is used, where each baseline point uncertainty is calculated as a weighted combination of the start and end uncertainties, and the total baseline uncertainty is the root sum square of all point uncertainties. The net plume uncertainty combines the integral and baseline uncertainties.

#### 5. Error Decomposition

The total variance/error for each plume is decomposed into contributions from the raw signal, slope, intercept, temperature, polynomial RMSE, VSL, and baseline. Each component's percentage contribution is calculated and visualized using stacked bar charts to illustrate the relative importance of different uncertainty sources.

) TNO Public 44/78

For example, the net plume integral is 228 ppb is shown in Figure 4.7. It slightly reduced due to a negative baseline, with an uncertainty of 12.8 ppb, corresponding to a relative error of 5.6%. Among the uncertainty sources, signal noise contributes 88%, the baseline contributes 7%, and all other components contribute less than 5% in total. This demonstrates that signal noise is the dominant source of error, while other factors play a minor role.

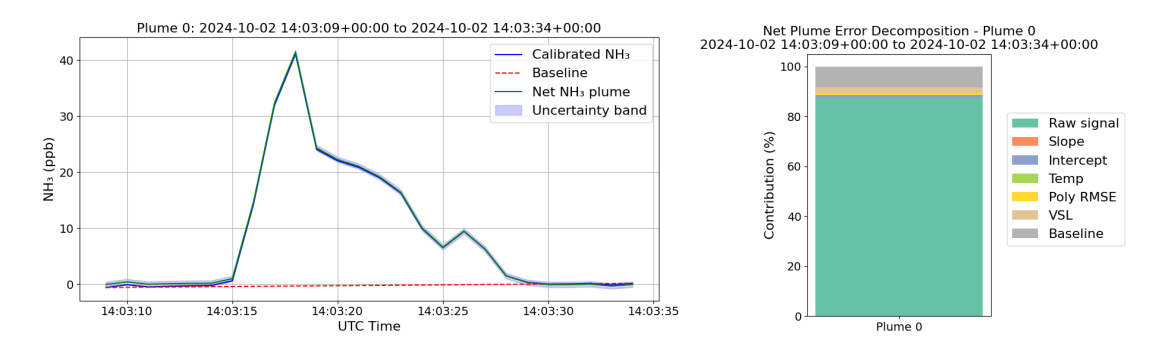


Figure 4.7: Time series of  $1^{st}$  calibrated Net NH<sub>3</sub> concentration plume after removing background on Oct  $2^{nd}$  in the left; and its error decomposition in the right.

The estimated total error and relative error (%) per integral net NH $_3$  plume are listed in Table 4.1. On average, the total error per net plume is related to both the cumulative duration of the plume window and the background level. Among all measured plumes (N = 21), the absolute error per plume averages 14.3  $\pm$  0.6 ppb (Mean  $\pm$  SE), and the relative error per plume averages 5.5%  $\pm$  0.3%. Also net plume time-line and error decomposition analysis stack bars are in list in the Appendix C.

) TNO Public 45/78

Table 4.1: NH<sub>3</sub> concentration error estimation for measured NH<sub>3</sub> net plume time windows on October 2<sup>nd</sup>, 2024.

Plume	Start time	End time	Duration	Total calibrated	Total baseline	Integrated net_NH₃	Net_plume_uncertaint I	Baseline_uncertaint	Cumulative	Relative
No.	(UTC)	(UTC)	(s)	NH₃ (ppb)	(ppb)	(ppb)	y (ppb)	y (ppb)	uncertainty (ppb)	error (%)
1	14:03:09	14:03:34	25	223.3	-4.6	227.9	12.7	3.7	16.4	7.2%
2	14:05:56	14:06:21	25	225.3	-21.6	246.9	11.2	2.0	13.2	5.3%
3	14:08:24	14:08:49	25	281.7	-1.4	283.1	15.5	2.9	18.4	6.5%
4	14:11:14	14:11:39	25	252.4	-14.8	267.2	9.4	2.7	12.1	4.5%
5	14:13:56	14:14:26	30	192.5	-10.1	202.6	13.6	3.9	17.5	8.6%
6	14:16:44	14:17:14	30	349.8	-20.3	370.1	13.7	2.3	16.0	4.3%
7	14:18:55	14:19:20	25	403.9	-4.2	408.2	12.2	2.1	14.3	3.5%
8	14:21:49	14:22:14	25	269.1	-11.6	280.6	13.0	2.7	15.7	5.6%
9	14:24:13	14:24:38	25	283.0	-14.3	297.4	11.9	2.4	14.3	4.8%
10	14:39:36	14:40:01	25	286.9	-13.1	300.0	14.2	2.6	16.8	5.6%
11	14:42:46	14:43:11	25	191.9	-21.7	213.6	11.3	2.3	13.5	6.3%
12	14:44:53	14:45:18	25	273.5	-11.5	285.0	11.4	2.5	13.9	4.9%
13	14:47:21	14:47:46	25	302.6	-21.9	324.5	17.4	2.5	19.9	6.1%
14	14:49:40	14:50:05	25	206.2	-15.1	221.2	10.2	2.8	12.9	5.9%
15	14:52:05	14:52:30	25	211.7	-22.1	233.8	9.9	2.2	12.1	5.2%
16	14:54:17	14:54:42	25	346.2	-15.0	361.2	12.3	2.2	14.5	4.0%
17	14:56:45	14:57:05	20	308.3	3.8	304.5	15.4	2.5	17.9	5.9%

) TNO Public 46/78

To be continued with Table 4.2: NH<sub>3</sub> concentration error estimation for measured NH<sub>3</sub> net plume time windows on October 2<sup>nd</sup>, 2024.

Plume No.	Start time (UTC)	End time (UTC)	Duration (s)	Total calibrated NH₃ (ppb)	Total baseline (ppb)	Integrated net_NH <sub>3</sub> (ppb)	Net_plume_uncertaint y (ppb)	t Baseline_uncertaint y (ppb)	Cumulative uncertainty (ppb)	Relative error (%)
18	14:59:09	14:59:34	25	293.8	-14.7	308.4	10.4	2.0	12.5	4.0%
19	15:01:22	15:01:47	25	133.5	-11.0	144.4	6.6	2.3	8.9	6.2%
20	15:03:48	15:04:13	25	177.2	-16.4	193.6	6.9	2.6	9.5	4.9%
21	15:06:11	15:06:36	25	138.5	-26.7	165.2	7.5	2.3	9.8	5.9%
Avg.			25.2 0.4	255 15	-14 2	269 15	11.7 0.6	2.6 0.1	14.3 0.6	5.5% 0.3%

Table 4.3: Error decomposition for each measured net NH<sub>3</sub> plume time windows on October 2<sup>nd</sup>, 2024.

Plume No	o. Start time (UTC)	End time (UTC)	Raw signal error (%)	Slope error (%)	Intercept error (%)	Temp error (%)	Poly RMSE error (%)	VSL error (%)	Baseline error (%)
1	14:03:09	14:03:34	87.4	0.1	1.2	0.0	0.6	2.4	8.4
2	14:05:56	14:06:21	90.8	0.1	1.6	0.0	0.8	3.5	3.2
3	14:08:24	14:08:49	92.6	0.0	0.8	0.0	0.5	2.3	3.6
4	14:11:14	14:11:39	83.4	0.1	2.3	0.0	1.1	4.7	8.3
5	14:13:56	14:14:26	88.5	0.0	1.3	0.0	0.4	1.7	8.1
6	14:16:44	14:17:14	90.4	0.1	1.3	0.0	1.0	4.3	2.8
7	14:18:55	14:19:20	88.2	0.1	1.4	0.0	1.4	5.9	3.0
8	14:21:49	14:22:14	89.5	0.1	1.2	0.0	0.9	3.9	4.4
9	14:24:13	14:24:38	89.7	0.1	1.5	0.0	0.9	3.7	4.1
10	14:39:36	14:40:01	91.8	0.1	1.0	0.0	0.7	3.1	3.3

) TNO Public 47/78

To be continued with Table 4.4: Error decomposition (in percentage) for each measured net  $NH_3$  plume time windows on October  $2^{nd}$ , 2024.

Plume No	. Start time (UTC)	End time (UTC)	Raw signal error (%)	Slope error (%)	Intercept error (%)	Temp error (%)	Poly RMSE error (%)	VSL error (%)	Baseline error (%)
11	14:42:46	14:43:11	91.2	0.1	1.6	0.0	0.6	2.5	4.0
12	14:44:53	14:45:18	89.0	0.1	1.6	0.0	0.9	3.7	4.7
13	14:47:21	14:47:46	93.3	0.1	0.7	0.0	0.7	3.0	2.1
14	14:49:40	14:50:05	85.6	0.1	2.0	0.0	0.9	4.0	7.4
15	14:52:05	14:52:30	88.5	0.1	2.2	0.0	0.8	3.3	5.1
16	14:54:17	14:54:42	88.0	0.1	1.4	0.0	1.4	5.9	3.1
17	14:56:45	14:57:05	92.4	0.1	0.7	0.0	0.8	3.4	2.7
18	14:59:09	14:59:34	88.5	0.1	2.0	0.0	1.1	4.6	3.8
19	15:01:22	15:01:47	78.8	0.1	4.9	0.0	0.7	3.2	12.4
20	15:03:48	15:04:13	76.3	0.1	4.5	0.0	0.9	3.8	14.4
21	15:06:11	15:06:36	82.7	0.1	3.8	0.0	0.7	3.0	9.7
Avg.			87.9	0.1	1.9	0.0	0.8	3.6	5.7
SE			1.0	0.0	0.3	0.0	0.1	0.2	0.7

) TNO Public 48/78

# 4.4 Remote measurements uncertainty calculations (A.2.3.7)

The dairy farm emitted  $CH_4$  and  $NH_3$  is estimated by the tracer modelling method (in short, TDM method), using the measurement data on Oct  $2^{nd}$ , 2024 with 21 plumes. Its uncertainty is mostly related to the instruments calibration, sensitivity, linearity, and drifts. The  $CH_4$  and  $NH_3$  emission estimates are listed in Table 4.2 and individual  $CH_4$ ,  $N_2O$ , and  $NH_3$  plume figures are shown in the Appendix B.

# 4.4.1 Error propagation for NH₃ and CH₄ emissions measured in a single day for a single livestock farm

Before conducting the emission uncertainty estimation using the TDM method, we first estimated the emissions from individual plumes of  $NH_3$  and  $CH_4$  generated by this dairy farm. The equations below were used to calculate the emission rates for  $NH_3$  and  $CH_4$ , respectively.

$$Q_{\text{NH}_3} = Q_{\text{N}_2\text{O}} \cdot \frac{M_{\text{NH}_3}}{M_{\text{N}_2\text{O}}} \cdot \frac{\int S_{\text{NH}_3}}{\int S_{\text{N}_2\text{O}}}$$
 Equation 4.10

$$Q_{\text{CH}_4} = Q_{\text{N}_2\text{O}} \cdot \frac{M_{\text{CH}_4}}{M_{\text{N}_2\text{O}}} \cdot \frac{\int S_{\text{CH}_4}}{\int S_{\text{N}_2\text{O}}}$$
 Equation 4.11

Where:

- $Q_{\text{NH}_3}$ ,  $Q_{\text{CH}_4}$  are estimated NH<sub>3</sub> and CH<sub>4</sub> emission rate, respectively;
- $Q_{N_2O}$  is known tracer (N<sub>2</sub>O) emission rate;
- *M* is molar mass of each gas (constant);
- $\int S$  is integrated concentration signal (area under curve for plume) for each gas.

The errors in these emission rates are primarily related to two sources:

#### ) TNO Public

- 1. The uncertainty in the tracer emission rate  $Q_{N_2O}$ , which can result from flow control and weighing accuracy (roughly estimated to be  $\pm 2\%$ ).
- 2. The integrated signals of NH<sub>3</sub>, CH<sub>4</sub> and N<sub>2</sub>O ( $\int S$ ) are subject to uncertainty due to instrument noise, calibration results, signal drifting.

Additionally, the definition of plume start and end times can indirectly affect the final error ratio, and also the method used for background subtraction.

Here, we assume all errors are independent and the relative error  $\sigma_{Q_{NH_3}}$  and  $\sigma_{Q_{CH_4}}$  in  $Q_{NH_3}$  and  $Q_{CH_4}$  for each individual NH<sub>3</sub> and CH<sub>4</sub> plume traverse can be given using the following equations below:

$$\sigma_{Q_{NH_3}} = Q_{NH_3} \cdot \sqrt{(\frac{\sigma_{Q_{N_2O}}}{Q_{N_2O}})^2 + (\frac{\sigma_{\int S_{NH_3}}}{\int S_{NH_3}})^2 + (\frac{\sigma_{\int S_{N_2O}}}{\int S_{N_2O}})^2}$$
 Equation 4.12

$$\sigma_{Q_{CH_4}} = Q_{CH_4} \cdot \sqrt{(\frac{\sigma_{Q_{N_2O}}}{Q_{N_2O}})^2 + (\frac{\sigma_{\int S_{CH_4}}}{\int S_{CH_4}})^2 + (\frac{\sigma_{\int S_{N_2O}}}{\int S_{N_2O}})^2}$$
 Equation 4.13

Since we have the individual emission estimations for  $Qi_{NH_3}$  or  $Qi_{CH_4}$  and their individual uncertainty  $\sigma_i$  as well. All plumes represent measurements of the same source under similar conditions, and a statistically sound estimate of the average emission rate and its total uncertainty can be best estimated using weighted mean and the uncertainty of weighted mean in below. This method gives more weight to more precise plumes (with lower  $\sigma_i$ ).

$$\hat{Q}_{\text{\tiny Weighted}} = \frac{\sum_{l=1}^{n} (\frac{Q_l}{\sigma_l^2})}{\sum_{l=1}^{n} (\frac{1}{\sigma_l^2})}$$
 Equation 4.14

$$\sigma_{\hat{Q}} = \sqrt{\frac{1}{\sum_{i=1}^{n}(\frac{1}{\sigma_{i}^{2}})}}$$
 Equation 4.15

The error estimates per plume are listed in Table 4.3. In the end, the weighted mean of NH $_3$  and CH $_4$  emissions are (0.067  $\pm$  0.001) g/s and (0.620  $\pm$  0.009) g/s, with rather small uncertainty as the relative error for NH $_3$  and CH $_4$  estimated emissions were about 1.8% and 1.5%. Consequently, the remotely measured emissions ratio of NH $_3$ :CH $_4$  for this single-day cattle farm observation was 0.110  $\pm$  0.004.

) TNO Public

Table 4.5: Total uncertainty estimation for tracer-based  $NH_3$  and  $CH_4$  emissions from a dairy farm (based on 21 plume measurements collected on October  $2^{nd}$ , 2024)

Plume No.	NH₃ emission (g/s)	Abs.NH₃ error (g/s)	NH₃ relative error (%)	CH <sub>4</sub> emission (g/s)	Abs. CH <sub>4</sub> error (g/s)	CH <sub>4</sub> relative error (%)
1	0.046	0.004	7%	0.51	0.03	5%
2	0.076	0.006	8%	0.72	0.05	7%
3	0.069	0.006	8%	0.62	0.03	5%
4	0.055	0.003	6%	0.53	0.03	5%
5	0.078	0.009	10%	0.60	0.05	8%
6	0.093	0.007	7%	0.78	0.05	6%
7	0.134	0.011	7%	1.23	0.08	7%
8	0.188	0.029	14%	1.57	0.22	14%
9	0.134	0.014	10%	1.07	0.10	9%
10	0.131	0.015	10%	1.07	0.10	9%
11	0.065	0.006	9%	0.80	0.06	7%
12	0.100	0.009	8%	0.95	0.07	7%
13	0.140	0.016	10%	1.09	0.10	9%
14	0.086	0.009	9%	0.80	0.06	8%
15	0.070	0.006	8%	0.80	0.05	6%
16	0.090	0.006	7%	0.94	0.05	6%
17	0.068	0.005	7%	0.74	0.04	5%
18	0.069	0.005	6%	0.59	0.03	5%
19	0.038	0.003	7%	0.47	0.03	6%
20	0.059	0.005	7%	0.47	0.03	6%
21	0.068	0.008	10%	0.52	0.05	9%
Unweighted mear	0.089			0.803		
Weighted mean	0.069	0.001		0.623	0.009	

# 5 Summary (input A2.2.7 & A2.3.8)

# 5.1 Input for D3 (A.2.2.7): calibration results

### 5.1.1 Calibration setup and concentration ranges

Calibration ranges were tailored to each instrument's typical application, with mobile HT covering higher NH<sub>3</sub> concentrations and flux and closed-path systems targeting lower levels.

In Table 5.1 the test parameters and conditions of the different calibration runs that were performed are given. The range of calibration parameters was selected based on the applications of the different instruments. The mobile HT is typically used for mobile measurements in or near livestock barns, where  $\rm NH_3$  concentrations can exceed 1 ppm. Therefore, a higher calibration range was applied to this system. In contrast, the flux HT systems, both from TNO and UKCEH, are primarily used at larger distances from emission sources, for example in nature reserves, where the instrument captures lower  $\rm NH_3$  concentrations. These analyzers are therefore calibrated in a lower range of concentrations. The same holds for the two QC-TILDAS closed-path systems.

The VSL RGM system has proved it well-suited for calibration of the newly developed openpath ammonia instrument HT8700E both indoor and outdoor, especially fit for low concentration range calibration, as the manufacturer calibration value were calibrated using the NH₃ permeation tubes <sup>9</sup>, with minimum 100 ppb value and its uncertainty is 15 % of each calibration range (Wang et al., 2021).

) TNO Public 52/78

<sup>&</sup>lt;sup>9</sup> https://kin-tek.com/common-disposable-tube-compounds

Table 5.1: The overview information of the TNO calibrated open- and closed-path ammonia analyzers during quantiAGREMI campaign in year 2024.

Calibration period	Calibrated ammonia analyzer	Measurement purpose	Calibration location	Calibration range(ppb)	RH range (%)	Ambient temperature range (°C)
	HT8700E-1	Mobile, source	Indoor,			
19–23 Sept	(TNO, open-path)	emission	TNO Petten lab	0 – 1260	5 – 55	21 – 25
	HT8700E-2	One-site, deposition	Indoor,			
24-26 Sept	(TNO, open-path)	flux	TNO Petten lab	0-200	0-60	20 – 23
	HT8700E-1	Mobile, source	outdoor,			
	(TNO, open-path)	emission	livestock farm	0 – 200	0	13 – 16
	HT8700		outdoor,			
00 04 Oct	(UKCEH, open-path)	Fluxes	livestock farm	0 – 100	0-35	8 – 19
02–04 Oct.	QC-TILDAS		outdoor,			
	(UKCEH, closed-path)	Fluxes	livestock farm	0 – 150*corr.	0	23 (inner constant)
	QC-TILDAS		outdoor,			
	(vTI, closed-path)	Fluxes	livestock farm	0 - 150*corr.	0	25 (inner constant)
	HT8700E-1	Mobile, source	outdoor,			
04-07 Oct.	(TNO, open-path)	emission	TNO Petten	0 – 750	0 & 35	8 – 16

) TNO Public 53/78

#### 5.1.2 Indoor and outdoor calibration results

#### 1. TNO mobile HT indoor and outdoor calibration comparison

The mobile HT exhibited a highly linear response ( $R^2 \approx 1$ ) across indoor and outdoor calibrations, with relative humidity affecting offsets only at higher concentrations while slopes remained stable.

A series of indoor calibration tests (Figure 2.3) was conducted using 3-hour concentration steps. At the highest RH level (50–55%), NH $_3$  concentrations of 0, 28.5, 72, 142, 285, 710, and 1262 ppb were applied in both upward and downward step changes, with subsets repeated at lower RH levels. Throughout the tests, laboratory temperature remained ~24 °C and the flow rate was held constant at 3.5 L min $^{-1}$ .

At the outdoor tests (Figure 3.4),  $NH_3$  concentrations of 20, 50, 100, 200, 500, and 750 ppb were supplied to the same HT mounted on the truck under both dry and semi-dry conditions (RH  $\approx$  33%). The calibration conducted at the farm was too short and covered only two concentration levels, which is insufficient for regression analysis; therefore, those data are not included here.

Table 5.2: Results of the regression analysis of TNO mobile HT for the indoor test humidity conditions were too unstable to compare. For the outdoor tests, a comparison of dry and semi-dry conditions could be made.

	Slope	Std. error slope	Offset	Std. error offset	R <sup>2</sup>
Indoor test, all data (RH ≈ 10-55%)	0.445	0.001	8.55	0.59	0.998
Indoor test, VSL < 200 ppb (mixed RH)	0.505	0.002	0.16	0.12	0.999
Outdoor test, all data (RH ≈ 0 & 33%)	0.483	0.002	-2.12	0.67	0.997
Outdoor test, dry (RH ≈ 0%)	0.492	0.002	-2.35	0.64	0.998
Outdoor test, semi-dry (RH ≈ 33%)	0.474	0.003	-1.93	1.11	0.996
Outdoor test, VSL < 200 ppb (dry)	0.499	0.004	-3.23	0.55	0.997

Table 5.2 shows that the mobile HT exhibits a linear response before and after the drives ( $R^2 \approx 1$ ), independent of indoor or outdoor calibration. For concentrations below 200 ppb, relative humidity has little effect on NH<sub>3</sub> measurements, though offsets differ between indoor and outdoor conditions, likely due to temperature effects.

#### 2. Stabilization and relative humidity effects

High relative humidity can affect calibration slope and offset at elevated NH<sub>3</sub> concentrations, though stabilization and low-concentration measurements remain largely unaffected.

Table 5.2 indicates a potential negative effect of high relative humidity on calibration slope and offset, though at high NH<sub>3</sub> concentrations this is obscured by system stabilization. For concentrations below 200 ppb, RH has little to no impact, and zero values remain stable (Figure 2.3). Stabilization effects are more pronounced at higher concentrations and under wetter conditions, likely due to the large volume and surface area of the calibration cell.

Because the HT laser path is enclosed in a glass cell during calibration, the instrument behaves effectively as a closed-path system. After an initial stabilization period, likely due to saturation

) TNO Public 54/78

of tubing and cell surfaces,  $NH_3$  concentrations at elevated RH (up to 200 ppb) approached values observed under dry conditions. Since the HT normally operates as an open-path instrument without a glass cell, RH-dependent effects observed at concentrations  $\geq$  200 ppb in the closed-cell tests may not occur in the field. Therefore, high-concentration RH corrections should not be applied to field data unless validated under representative open-path conditions (e.g., against the RIVM open-path Mini-DOAS).

#### 3. Temperature dependence

A combined temperature correction effectively compensated for measurement drift, improving the accuracy of mobile HT NH<sub>3</sub> calibration.

The outdoor calibration series of the mobile HT was followed by an additional 24 hours temperature dependence check at a fixed concentration level of 50 ppb at dry conditions (RH  $\approx$  0%). A drift in the measured concentration values was observed, which seems related to temperature (Figure 3.7). To compensate for this, we implemented a combined correction approach: first, a linear regression was applied using the reference NH $_3$  measurements provided by VSL; second, we introduced a second-order polynomial correction based on the HT's water circular temperature or internal temperature sensor, which reliably tracks ambient air temperature. This correction method significantly improved the accuracy of the NH $_3$  measurements under varying environmental conditions.

During the mobile HT outdoor calibration period, the HT ambient temperature, internal temperature, and water circular temperature were shifted. It was observed that both the slope and offset of the calibration are most affected by the HT water circular temperature. After applying the temperature correction shown in Figure 3.7c across each VSL calibration range, the new calibrated line's slope and offset for are much closer to the indoor calibration equation than before, especially reduced the differences in offset (Figure 3.9). A comparison results with and without temperature correction are clearly showed in Table 3.3.

#### 4. TNO Flux HT indoor calibration

The TNO flux HT showed excellent linearity across humidity levels, with a consistent offset likely caused by transport, while slope stability confirms its suitability for flux measurements.

Each calibration point for the TNO flux HT was maintained for 1.5 h at a constant flow rate of  $3 \text{ L min}^{-1}$ . The instrument exhibited an excellent linear response across all humidity levels, with  $R^2 = 1.0$  for both combined and individual RH conditions (Table 2.3 and Figure 2.9). However, there is a clear large offset of about 31 ppb being observed through all datasets.

Similar to the mobile HT indoor calibration, the flux HT showed that increasing RH led to decreases in both slope and offset, consistent with a closed-cell stabilization effect. A precalibration performed with the mini-DOAS at Loobos over one year (Melman, Wintjen, et al., 2025) showed a much smaller offset (~7 ppb). The large shift observed here likely resulted from mechanical stress during transport. Nevertheless, as the slope remained stable, the instrument remains suitable for flux measurements.

#### 5. Field calibration of the NH₃ instruments of UKCEH and vTI

) TNO Public 55/78

The UKCEH flux HT and two QCL systems exhibited linear responses during field calibrations, though the HT showed higher noise and RH-dependent slope and offset changes, and the QCLs systematically underestimated concentrations.

The UKCEH flux HT calibration was performed overnight outside the Dutch dairy farm using  $NH_3$  concentrations of 0–100 ppb under dry and 20–30 % RH conditions. Each step lasted 60–90 min, with temperatures between 13.5 and 17.5 °C (i.e. lower than during the TNO mobile HT measurement). The UKCEH HT system showed higher noise and instability than the two TNO HT units (Figure 3.11) at their higher calibration period temperatures. Similar to the two TNO HT units, both slope and offset for the UKCHE system deceased when RH was increased.

Field calibration of the UKCEH QCL (TILDAS) was conducted under northerly winds (6–8 m s $^{-1}$ ) and background NH $_3$  levels of 2–3 ppb (as monitored by the RIVM mini-DOAS). To meet the 13 L min $^{-1}$  flow demand, equal parts of VSL RGM calibration gas and ambient air were mixed, halving the expected response.

The vTI QCL (TILDAS) was calibrated directly afterwards using the same VSL concentrations under the same dry conditions, but at a reduced flow rate (5.8 L min<sup>-1</sup>). Both laser systems stabilized within ~15 min and showed linear responses up to 150 ppb, but systematically underestimated the applied concentrations by ~30 %, a discrepancy that is to be further investigated with the manufacturer. The overview results can be seen in Figure 3.4.

# 5.2 Input for D4 (A.2.3.8): TDM uncertainties

Overall, mobile tracer measurements successfully quantified bulk NH<sub>3</sub> and CH<sub>4</sub> emissions, while uncertainties were mainly influenced by instrument calibration, environmental conditions, and plume averaging strategies.

We applied and evaluated advanced remote measurement techniques to quantify ammonia ( $NH_3$ ) and methane ( $CH_4$ ) emissions from a livestock dairy farm in the Netherlands during the quantiAGREMI field campaign of WP3.

The core methodology was the Tracer Dispersion Method (TDM), which involves releasing a known quantity of tracer gas (nitrous oxide,  $N_2O$ ) and determining emission rates of the target gases by comparing their dispersion patterns with that of the tracer. This approach was implemented during two campaign days at the dairy farm; however, only the results from the first day are included in the report. Short-term wind direction shifts (5–10 min) are a key source of variation in emission estimates (Fredenslund et al., 2019). Emission rates and downwind concentrations also vary with meteorological factors such as wind speed, temperature, inversion height, and solar radiation.

Mobile measurement studies show that multiple downwind transects significantly reduce uncertainty, as relative error decreases exponentially with the number of detected plumes (Hensen et al., 2019). Around six plumes provide an optimal balance between accuracy and effort. Consistent with other findings (Luetschwager et al., 2021; Maazalahi et al., 2023), plume variability between transects can increase uncertainty, but averaging multiple passes mitigates this.

Errors in measured and calibrated concentrations of  $NH_3$ ,  $CH_4$ , and  $N_2O$  were quantified using standard error propagation methods. The QCL was field-calibrated using two ICOS-traceable gas standards representing high and low  $CH_4$  and  $N_2O$  concentrations. Uncertainties in the  $CH_4$  and  $N_2O$  measurements mainly stemmed from the accuracy with which the calibration

) TNO Public 56/78

gas concentration was measured, instrument handling, and regression fitting. Total absolute uncertainties were ~4.4 ppb for CH<sub>4</sub> and ~1.5 ppb for N<sub>2</sub>O (0.2 – 0.4% relative error). During plume measurements, relative uncertainties averaged ( $\pm$  SE) 1.0  $\pm$  0.1% for CH<sub>4</sub> and 6.7  $\pm$  0.5% for N<sub>2</sub>O. These uncertainties were subsequently used to quantify the propagation of total NH<sub>3</sub> and CH<sub>4</sub> emission errors using standard methods.

Ammonia (NH<sub>3</sub>) concentrations were measured using the TNO mobile HT system, pre- and post-calibrated by VSL. Plume analysis and uncertainty propagation involved integrating baseline-corrected NH<sub>3</sub> concentrations over time, with the baseline defined by linear regression between plume start and end points. NH<sub>3</sub> plumes were baseline-corrected, VSL-calibrated, and temperature-adjusted before uncertainty propagation analysis. Total relative errors averaged  $\sim$ 5.5  $\pm$  0.3 %, mainly driven by instrument noise ( $\sim$ 88% of total error), while baseline and calibration factors contributed less than 6%. This confirms that signal noise was the dominant source of uncertainty in the NH<sub>3</sub> plume measurements.

A common approach for estimating overall emissions is the calculation of unweighted mean values. Based on 21 plumes, the unweighted means were  $0.096\pm0.009~g~s^{-1}$  for NH $_3$  and  $0.80\pm0.062~g~s^{-1}$  for CH $_4$ , with relative errors of 7.8% and 9.1%, respectively. In contrast, applying individual plume error propagation yielded weighted mean emission rates, where a greater weight was assigned to larger plumes with lower associated uncertainty. The weighted estimates were  $0.069\pm0.001~g~s^{-1}$  for NH $_3$  and  $0.62\pm0.01~g~s^{-1}$  for CH $_4$ , with substantially lower relative errors of 2% and 1%, respectively. Regardless of the averaging method, the NH $_3$ -to-CH $_4$  emission ratio was consistently determined as  $0.110\pm0.004$  on the day with reliable data. For comparison, indoor daily measurements conducted by WUR reported similar emission values of  $0.075~g~s^{-1}$  for NH $_3$  and  $0.68~g~s^{-1}$  for CH $_4$ .

Our findings highlight both the robustness of the applied tracer method and the need for further refinements in measurement practices. In particular,  $NH_3$  calibration needs to be improved under varying temperature and high-humidity conditions. Further, the range of  $N_2O$  and  $CH_4$  calibration gas concentrations needs to be expanded to enhance reliability across diverse field settings.

Lastly, the remote measurement approach used here captures the bulk plume (Gillespie et al., 2023; Mønster et al., 2014) from all emission sources within the observed area. When the goal is to assess the contribution from a specific livestock farm, it will be necessary to separate individual sources. To achieve such separation, proper placement of the  $N_2O$  tracer and careful selection of wind direction and driving routes are essential. Additionally,  $NH_3:CH_4$  emission ratios (which differ between source types) may be used to distinguish different  $NH_3$  plumes, while information on farm activities such as manure spreading, etc. are needed as well. However, if the goal is merely to evaluate the overall emission impact on the surrounding environment, then the total combined emissions are the relevant measure.

) TNO Public 57/78

# 6 Recommendations for NH3 analyzer calibration and emission estimation

# 6.1 Open-path analyzer (HT8700) calibration

Proper calibration of HT8700 open-path analyzers is essential for accurate measurements. Users should note the following:

- Relative humidity (RH) impacts cannot be fully addressed using the glass-cell system. In-situ instrument comparisons are likely the most reliable strategy, despite the higher labor and cost requirements.
- When using the conventional permeator method, quality control is critical. This includes careful monitoring of oven temperature, flow rate, storage conditions, zero gas standard and periodic checks of the permeation tube weight to improve emission rate corrections.
- Stabilization time is critical during calibration. For HT cell size, a minimum stabilization period of 1.5 hours under dry conditions and at least 3 hours under humid conditions in the moderate calibration range (10 ppb to 1ppm) is recommended if VSL system is applied. If permeator method is applied that depends on the flow rate, the lower concentration range would take more time to reach final stabilization.
- Calibration should be performed whenever the instrument is relocated, transported, or subjected to mechanical stress, as these factors may cause offset drift.
- Temperature effects are a major concern under field conditions despite mostly on the
  offset. The most effective correction over the full temperature range can be achieved
  using a VSL system in a climate chamber. Alternatively, applying a temperaturecontrolled cooling pump during field campaigns may help reduce temperature-related
  drift.

# 6.2 Closed-path analyzer (QCL) calibration

For QCL systems, the following considerations are important:

- System delay time and internal cell filter changes are critical parameters. Users should conduct regular quality checks throughout the campaign period.
- A temperature-controlled environment is crucial for achieving a robust and valid calibration. Inlet lines should be kept as short as possible and using an passive-activation system is recommended. The latter will minimize adsorption effects of NH<sub>3</sub> at tube walls.

) TNO Public 58/78

- Cell pressure should be monitored in order to observe pump performance and act accordingly if obstacles hinder air-flow.
- Whenever the instrument is relocated, transported, or subjected to mechanical stress, an alignment of the mirrors may be considered which has an influence on the calibration results.
- As long as the system is maintained in a well-conditioned environment, relative humidity and temperature appear to have minimal impact on measurements.

## 6.3 VSL RGM system adaptation

VSL RGM system is most suitable for indoor calibration due to its weight and limited portability. Key recommendations are the RH range and flow rate should be enhanced to support a broader range of users, including QCL operators (demand of high flow rate) directly do the calibration.

# 6.4 Reducing TDM uncertainty in livestock farm emission measurements

To improve the accuracy of emissions measurements at livestock farms:

- Multiple measurements are required, as deposition can reduce NH<sub>3</sub> signals if measurements are taken too far from the source. Current methods do not fully correct for deposition effects, warranting further research.
- While N<sub>2</sub>O is commonly used as a tracer gas for the TDM measurement, C<sub>2</sub>H<sub>6</sub> may be a better option for agricultural sources due to its minimal emission from livestock in rural areas, least toxicity, and cost-effectiveness.
- GHG gases measured by QCL, signal drifts/offsets should be checked before and after each measurement campaign to ensure data reliability.

TNO Public 59/78

# 7 References

- Chen, H., Vinković, K., Sun, C., Peters, W., Hensen, A., van der Gon, H., van Zanten, M., van den Bulk, P., Velzeboer, I., & van der Zee, T. (2025). A novel approach to rapidly tracking whole-farm methane emissions. *Environmental Research Letters, 20*(3), 034016. <a href="https://doi.org/10.1088/1748-9326/adb1f6">https://doi.org/10.1088/1748-9326/adb1f6</a>
- Fehsenfeld, F. C., Apel, E. C., Dickinson, R. E., & et al. (2002). Results from an informal intercomparison of ammonia measurement techniques. *Journal of Geophysical Research: Atmospheres*, 107 (D15). https://doi.org/10.1029/2001JD001327
- Fredenslund, A. M., Rees-White, T. C., Beaven, R. P., Delre, A., Finlayson, A., Helmore, J., Allen, G., & Scheutz, C. (2019). Validation and error assessment of the mobile tracer gas dispersion method for measurement of fugitive emissions from area sources. *Waste Management*, 83, 68–78. https://doi.org/10.1016/j.wasman.2018.10.036
- Gillespie, L. D., Ars, S., Williams, J. P., Klotz, L., Feng, T., Gu, S., Kandapath, M., Mann, A., Raczkowski, M., Kang, M., Vogel, F., & Wunch, D. (2023). A Modified Gaussian Plume Model for Mobile in situ Greenhouse Gas Measurements. *Atmospheric Measurement Techniques* (Preprint), 2040(September), 1–26. https://amt.copernicus.org/preprints/amt-2023-193/
- Hensen, A., Loubet, B., Mosquera, J., Van Den Bulk, W. C. M., Erisman, J. W., Dämmgen, U., Milford, C., Löpmeier, F. J., Cellier, P., Mikuška, P., & Sutton, M. A. (2009). Estimation of NH3 emissions from a naturally ventilated livestock farm using local-scale atmospheric dispersion modelling. *Biogeosciences*, 6(12), 2847–2860. <a href="https://doi.org/10.5194/bg-6-2847-2009">https://doi.org/10.5194/bg-6-2847-2009</a>
- Hensen, A., Velzeboer, I., Frumau, K. F. A., van den Bulk, W. C. M., & van Dinther, D. (2019). Methane emission measurements of offshore oil and gas platforms: TNO Report R10895 (Report No. R10895). Petten, The Netherlands: TNO. https://publications.tno.nl/publication/34634946/XYcOP9/TNO-2019-R10895.pdf
- Jordan, A., & Damak, F. (2024). *ICOS Central Analytical Laboratories Flask and Calibration Laboratory (FCL) quality control report 2024*. ICOS ERIC. <a href="https://meta.icos-cp.eu/objects/JHg2gKn0ffLv83qdLx4BkE5r">https://meta.icos-cp.eu/objects/JHg2gKn0ffLv83qdLx4BkE5r</a>
- Lemes, Y. M., Häni, C., Kamp, J. N., & Feilberg, A. (2023). Evaluation of open- and closed-path sampling systems for the determination of emission rates of NH<sub>3</sub> and CH<sub>4</sub> with inverse dispersion modeling. *Atmospheric Measurement Techniques*, 16, 1295–1309. <a href="https://doi.org/10.5194/amt-16-1295-2023">https://doi.org/10.5194/amt-16-1295-2023</a>
- Luetschwager, E., von Fischer, J. C., & Weller, Z. D. (2021). Characterizing detection probabilities of advanced mobile leak surveys: Implications for sampling effort and leak size estimation in natural gas distribution systems. *Elementa: Science of the Anthropocene*, *9*(1), Article 00143. <a href="https://doi.org/10.1525/elementa.2020.00143">https://doi.org/10.1525/elementa.2020.00143</a>
- Maazallahi, H., Delre, A., Scheutz, C., Fredenslund, A. M., Schwietzke, S., Denier van der Gon, H., & Röckmann, T. (2023). Intercomparison of detection and quantification methods for methane emissions from the natural gas distribution network in Hamburg, Germany. *Atmospheric Measurement Techniques, 16*, 5051–5073. <a href="https://doi.org/10.5194/amt-16-5051-2023">https://doi.org/10.5194/amt-16-5051-2023</a>
- Macé, T., et al. (2022). Air pollution monitoring: Development of ammonia (NH<sub>3</sub>) dynamic

) TNO Public 60/78

- reference gas mixtures at nanomoles per mole levels to improve the lack of traceability of measurements. *Atmospheric Measurement Techniques*, 15, 2703–2718. <a href="https://doi.org/10.5194/amt-15-2703-2022">https://doi.org/10.5194/amt-15-2703-2022</a>
- Melman, E. A., Wintjen, P., Zhang, J., & Rutledge-Jonker, S., Hensen, A., Felter, K. M., van der Molen, M., Snellen, H., de Boer, J., Eijkelboom, M., Haaima, M., van der Hoff, R., van Mansom, H., Voorneveld, M., Vilà-Guerau de Arellano, J., Wichink Kruit, R. J., & van Zanten, M. C. (2025, November 12). On the efficiency of biosphere– atmosphere ammonia exchange processes over a Scots pine forest and its link to ecosystem activity (Preprint). SSRN. <a href="https://ssrn.com/abstract=5737184">https://dx.doi.org/10.2139/ssrn.5737184</a>
- Metrology, J. C. F. G. I. (2008). Evaluation of measurement data Guide to the expression of uncertainty in measurement. *International Organization for Standardization Geneva ISBN*, 50 (September), 134. <a href="http://www.bipm.org/en/publications/guides/gum.html">http://www.bipm.org/en/publications/guides/gum.html</a>
- Miller, D. J., Sun, K., Tao, L., Khan, M. A., & Zondlo, M. A. (2014). Open-path, quantum cascade-laser-based sensor for high-resolution atmospheric ammonia measurements. *Atmospheric Measurement Techniques*, 7(1), 81-93. https://doi.org/10.5194/amt-7-81-2014
- Mønster, J. G., Samuelsson, J., Kjeldsen, P., Rella, C. W., & Scheutz, C. (2014). Quantifying methane emission from fugitive sources by combining tracer release and downwind measurements A sensitivity analysis based on multiple field surveys. *Waste Management*, 34(8), 1416–1428. <a href="https://doi.org/10.1016/j.wasman.2014.03.025">https://doi.org/10.1016/j.wasman.2014.03.025</a>
- Nair, A. A., & Yu, F. (2020). Quantification of Atmospheric Ammonia Concentrations: A Review of Its Measurement and Modeling. *Atmosphere*, 11(10), 1092. https://doi.org/10.3390/atmos11101092
- Norman, M., Spirig, C., Wolff, V., et al. (2008). Ambient gaseous ammonia: Evaluation of continuous measurement methods. *NYSERDA Report*.
- Núñez, M. (2013). *Mass balances for continuous stirred tank reactors (CSTRs)* [Lecture notes]. Department of Chemical Engineering, University of California, Santa Barbara.
- Physical Chemistry. (1961). *In Journal of the Franklin Institute* (Vol. 272, Issue 4). https://doi.org/10.1016/0016-0032(61)90576-2
- Pogány, A., Balslev-Harder, D., Braban, C. F., Cassidy, N., Ebert, V., Ferracci, V., Hieta, T., Leuenberger, D., Lüttschwager, N., Martin, N. A., Pascale, C., Tiebe, C., Twigg, M. M., Vaittinen, O., van Wijk, J., Wirtz, K., & Niederhauser, B. (2016). A metrological approach to improve accuracy and reliability of ammonia measurements in ambient air.

  \*Measurement Science and Technology, 27(11), 115012. https://doi.org/10.1088/0957-0233/27/11/115012
- Pogány, A., Lüttschwager, N. O. B., Banik, G. D., Persijn, S., de Boed, E. J. J., Sutour, C., Macé, T., Nwaboh, J. A., Werhahn, O., & Ebert, V. (2025). Towards an optical gas standard for ammonia measurements in air at ambient levels. *Journal of Quantitative Spectroscopy and Radiative Transfer*, 347(March). https://doi.org/10.1016/j.jasrt.2025.109643
- Pollack, I. B., Lindaas, J., Roscioli, J. R., Agnese, M., Permar, W., Hu, L., & Fischer, E. V. (2019). Evaluation of ambient ammonia measurements from a research aircraft using a closed-path QC-TILDAS operated with active continuous passivation. *Atmospheric Measurement Techniques*, 12, 3717–3742. https://doi.org/10.5194/amt-12-3717-2019
- Sasakawa, M., Tsuda, N., Machida, T., Arshinov, M., Davydov, D., Fofonov, A., & Belan, B. (2025). Revised methodology for CO<sub>2</sub> and CH<sub>4</sub> measurements at remote sites using a working standard-gas-saving system. *Atmospheric Measurement Techniques*, *18*(8), 1717–1730. <a href="https://doi.org/10.5194/amt-18-1717-2025">https://doi.org/10.5194/amt-18-1717-2025</a>

) TNO Public 61/78

- Sintermann, J., Dietrich, K., Häni, C., Bell, M., Jocher, M., & Neftel, A. (2016). A miniDOAS instrument optimised for ammonia field measurements. *Atmospheric Measurement Techniques*, *9*(6), 2721–2734. https://doi.org/10.5194/amt-9-2721-2016
- Swart, D., Zhang, J., Van Der Graaf, S., Rutledge-Jonker, S., Hensen, A., Berkhout, S., Wintjen, P., Van Der Hoff, R., Haaima, M., Frumau, A., Van Den Bulk, P., Schulte, R., Van Zanten, M., & Van Goethem, T. (2023). Field comparison of two novel open-path instruments that measure dry deposition and emission of ammonia using flux-gradient and eddy covariance methods. *Atmospheric Measurement Techniques*, *16*(2), 529–546. <a href="https://doi.org/10.5194/amt-16-529-2023">https://doi.org/10.5194/amt-16-529-2023</a>
- Twigg, M. M., Braban, C. F., Famulari, D., et al. (2022). Intercomparison of in situ measurements of ambient NH<sub>3</sub>: instrument performance and application under field conditions. *Atmospheric Measurement Techniques*, *15*, 6755–6771. https://doi.org/10.5194/amt-15-6755-2022
- van der Zee, T. C., Bannink, A., van Bruggen, C., Groenestein, C. M., Huijsmans, J. F. M., Lagerwerf, L. A., Luesink, H. H., & Velthof, G. L. (2022). *Methodology for the calculation of emissions from agriculture: Calculations for methane, ammonia, nitrous oxide, nitrogen oxides, non-methane volatile organic compounds, fine particles and carbon dioxide emissions using the National Emission Model for Agriculture (NEMA)* (RIVM Report No. 2022-0002). National Institute for Public Health and the Environment. <a href="https://doi.org/10.21945/RIVM-2022-0002">https://doi.org/10.21945/RIVM-2022-0002</a>
- Vechi, N. T., Mellqvist, J., & Scheutz, C. (2022). Quantification of methane emissions from cattle farms using the tracer gas dispersion method. Agriculture, *Ecosystems & Environment*, 330, 107885. https://doi.org/10.1016/j.agee.2022.107885
- Wang, K., Kang, P., LU, Y., Zheng, X., Liu, M., Lin, T. J., Butterbach-Bahl, K., & Wang, Y. (2021). An open-path ammonia analyzer for eddy covariance flux measurement. *Agricultural and Forest Meteorology*, 308–309(March), 108570. <a href="https://doi.org/10.1016/j.agrformet.2021.108570">https://doi.org/10.1016/j.agrformet.2021.108570</a>

) TNO Public 62/78

# 8 Acknowledgement

The author(s) would like to thank for Euramet sponsoring the project and the collaborators, e.g. UKCEH, vTI, and VSL. And we also thank for the reviewers: Dr. Stefan Persijn from VSL Delft and Dr. Pascal Wintjen from TNO Petten, for their careful reading of the manuscript and for providing constructive comments and suggestions, which have greatly improved the clarity and quality of this report.

Ondertekening

TNO EMSA, Petten, 17 november 2025

Namens Research Manager van EMSA Marieke van Milligen,

Peter Petiet, Deputy Research Manager EMSA (Environmental, Modelling, Sensing & Analysis)

) TNO Public 63/78

# Appendix A

# **TNO Tasks in quantiAGREMI**

The tasks of TNO in quantiAGREMI are summarized in the table below.

Task 2.1	Technical installation of remote measurements set-up
A 2.1.5	Remote measurement techniques that evaluate diffuse source systems like farms or field are already in use. Here, TNO will work on the improvement of remote NH3 measurements, by evaluating and combining high-end open path instruments and closed path (laser-based spectroscopy) instruments. In addition, remote NH3 measurements with sensors will be included, if a promising NH3 sensor is available at that time.
Task 2.2	Laboratory testing
A. 2.2.1	Develop a measurement protocol for determining metrological performances such as linearity, repeatability, zero reading and cross-sensitivities for determining uncertainty of newly developed sensors from A2.1.2 - A2.1.4 and sensors to be used in field measurements, using RGMs of WP1 and specifications from A1.1.1. This includes properties like amount fraction ranges and composition of the test gas mixtures.
A 2.2.5	TNO with the support of VSL will improve the remote NH3 measurements to lower their uncertainty defined in A1.1.1 and include mobile open path NH3 measurements. Tests with special designed inlet systems will optimize by <1 second step response the commercial closed path analyzers (e.g. Aerodyne, MIRO, Picarro). The improvement of the technique will be tested using a high dilution RGM from A1.1.4 and the tests will be linked to A3.2.4 taking place in Switzerland.
A 2.2.6	The uncertainty budget of the remote NH3 measurement techniques will be estimated from the tests in A2.2.5.
A 2.2.7	TNO, WR and Vaisala, will write an evaluation report based on the results of the testing, calibration and validation measurements for new and existing sensors. The report will be submitted to EURAMET as D3: 'Evaluation report based on the results of the testing, calibration and validation measurements for new and existing sensors for a better estimation of livestock emissions.'
Task 2.3	Field testing
A 2.3.2	Based on A1.3.1-A1.3.6 and A1.4.3, LUKE, WR, TNO, and INRAE with support from VTT, PTB, UKCEH, KIT, VSL, IMTelecom, Senseair, GASERA, and Vaisala will develop a measurement plan for the campaigns in Finland and the Netherlands.
A 2.3.6	TNO, VSL and WR will perform mobile measurements and remote stationary measurements of CH4, NH3 and N2O. This type of testing is valuable for quick testing of emissions for enforcement policies of the future. The main challenges for remote measurements are the low concentrations and varying meteorological conditions that play a role in repeatability and background corrections. By comparison with the reference measurements and the controlled tests of A2.3.5, a more accurate estimate of the uncertainty in the remote measurements will be made. Also, the sensors from A2.2.2, A2.2.3 and A2.2.4 will be tested in combination with the remote mobile and stationary measurements, which allows the testing of their performance in different concentration ranges defined in A1.1.1.
A 2.3.7	INRAE, LUKE, TNO, WR, VSL, and VTT in collaboration with IMTelecom, Senseair, GASERA, and Vaisala will analyze, compare and interpret the collected results from A2.3.3 - A2.3.6 field tests. Methods and models developed in described in D2 (A1.5.7) will be used, evaluated and improved. Consistency of concentrations measurement will be analyzed based on biological, physical and chemical influencing factors. Emissions will be calculated and compared to N and C mass balance (A1.5.3) deficit and existing EF. The main contributions to the uncertainty will be identified as key indicators. VSL will assist in the data analysis and propagation of uncertainties for the used models.

) TNO Public 64/78

#### A 2.3.8

Using input from A2.3.3-A2.3.7, VTT, VSL, LUKE, WR, TNO, INRAE and IMTelecom will write a summary report based on the identified key-indicators and the improved emission models for increasing the representativeness of the emission estimations and determine their uncertainty. The report will also include the developed farm-monitoring systems for evaluating the efficiency of reduction measures, as well as the relevant farmers' management tools.

VTT, VSL, LUKE, WR, TNO, INRAE and IMTelecom will review the summary report and send it to the coordinator. Once the report has been agreed by the consortium, the coordinator on behalf of VTT, VSL, LUKE, WR, TNO, INRAE and IMTelecom will submit it to EURAMET as D4: 'Summary report on the identified key-indicators and the improved emission models for increasing the representativeness of the emission estimations and determine their uncertainty. The report will also include the developed farm-monitoring systems for evaluating the efficiency of reduction measures, as well as the relevant farmers' management tools'.

) TNO Public 65/78

## Appendix B

# CH<sub>4</sub>, N<sub>2</sub>O and NH<sub>3</sub> Plume Transects

Tracer method results for two tracer release periods.

First two panels: 8 plumes time slot tracer release period 1 (14:00-14:25 UCT, Oct  $2^{nd}$ , 2024); Second four panels: 12 plumes time slot tracer release period 2 (14:35-15:10 UTC). Each panel pair shows: (1) individual CH<sub>4</sub>, NH<sub>3</sub>, and N<sub>2</sub>O enhanced concentrations above the background; (2) the correlation between individual time-step and cumulative enhanced CH<sub>4</sub>, NH<sub>3</sub>, and N<sub>2</sub>O value ratios per net plume (after the background removal).

) TNO Public 66/78

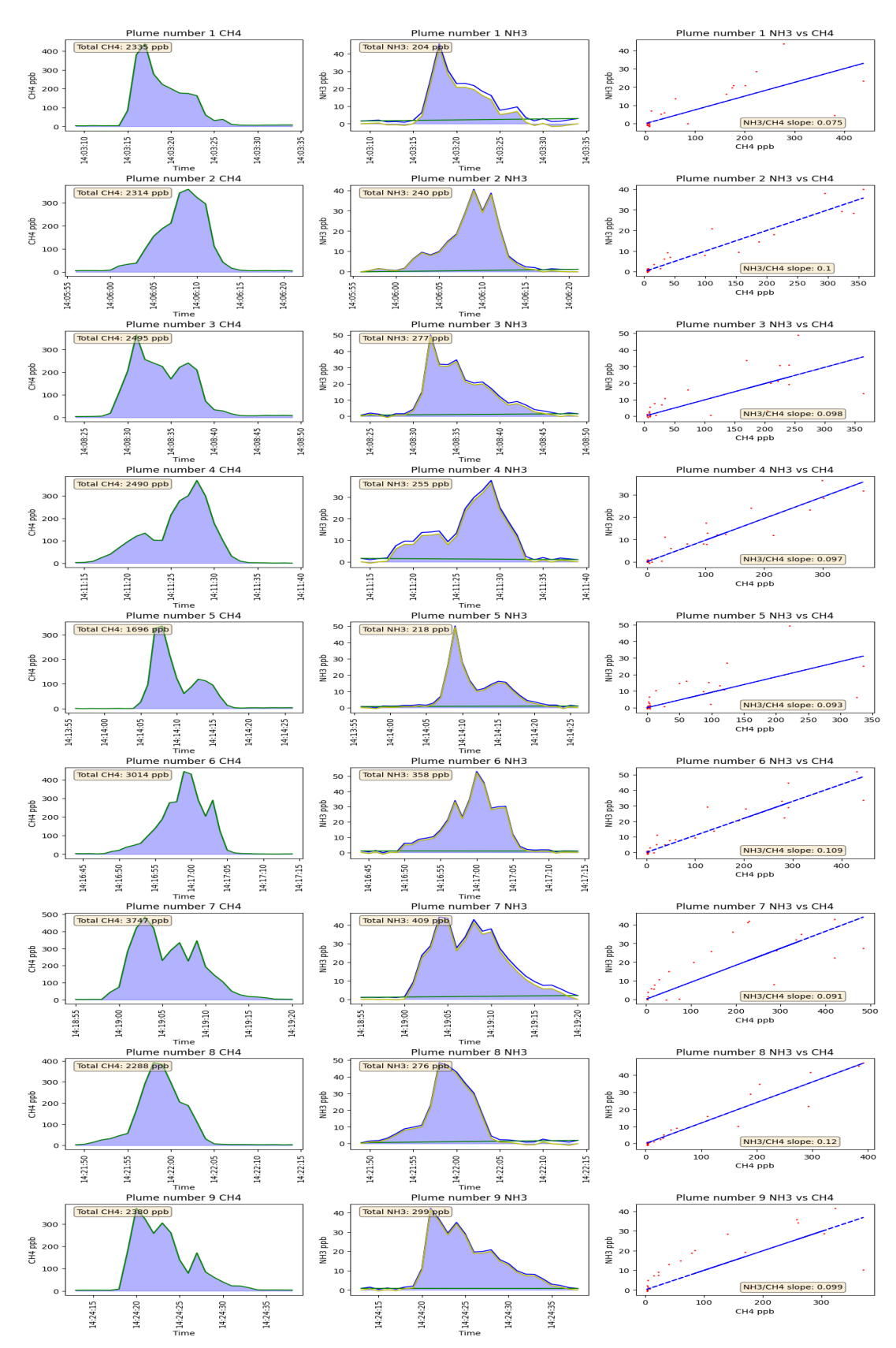


Figure S1. Nine measured CH₄ and NH₃ enhanced plumes above the background during the 1st tracer release (14:00–14:25 UTC) and NH₃:CH₄ linear regression slope of each plume window.

) TNO Public 67/78

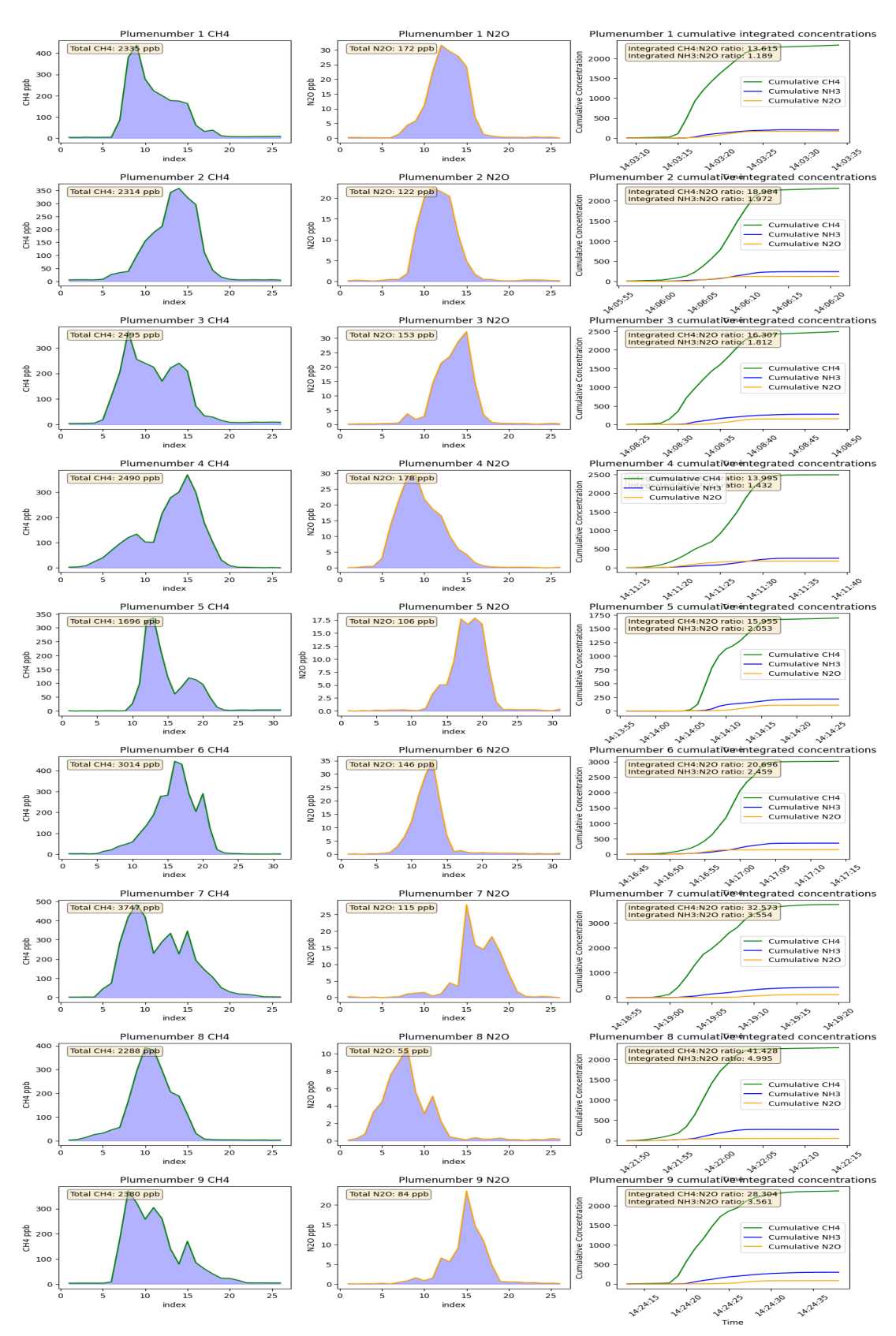


Figure S2. Nine measured  $CH_4$  and  $N_2O$  tracer enhanced plumes above the background during the 1st tracer release (14:00–14:25 UTC) and cumulative  $CH_4$ :  $N_2O$  and  $NH_3$ :  $N_2O$  ratios of each plume window.

) TNO Public 68/78

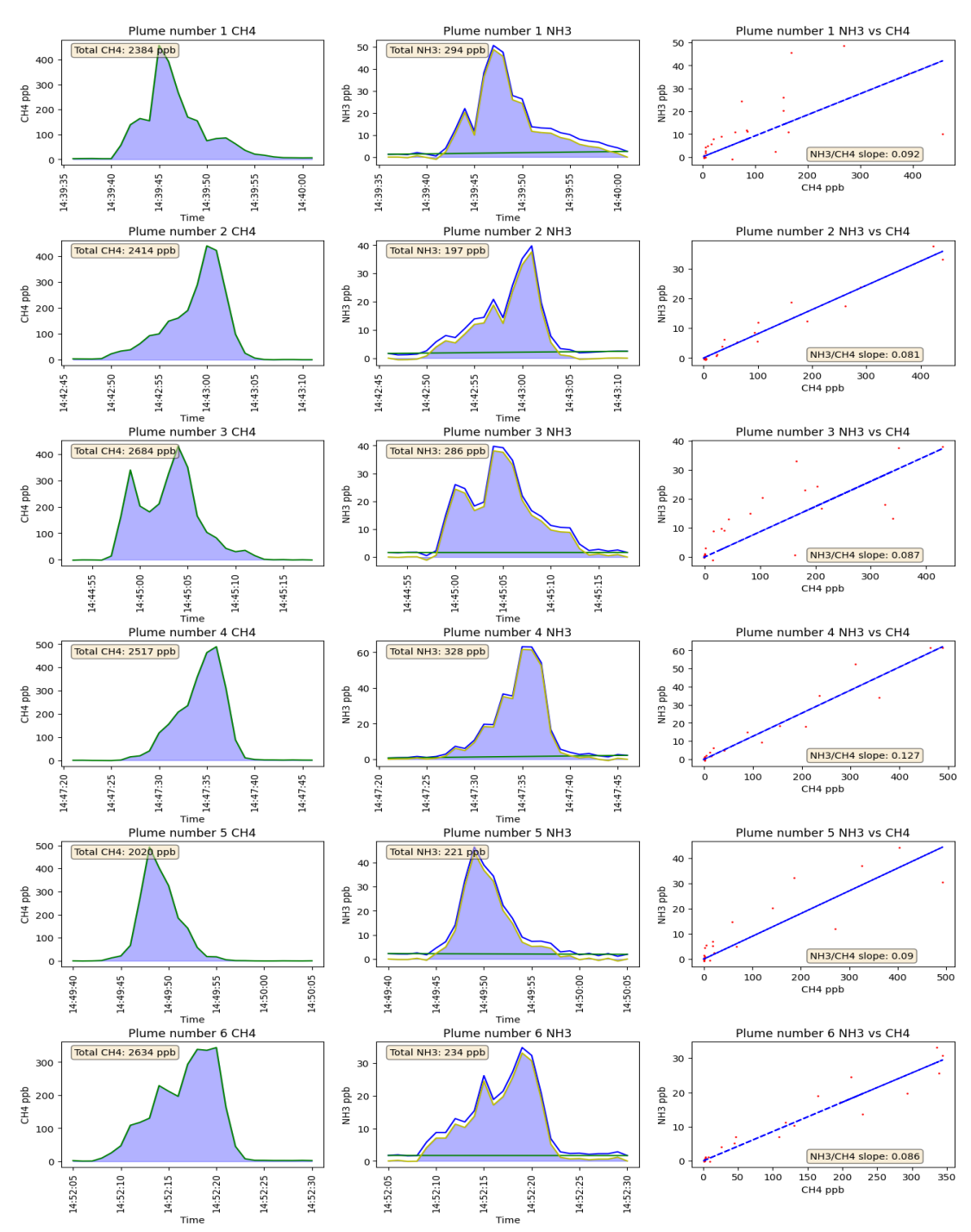


Figure S3. The first six measured CH<sub>4</sub> and NH<sub>3</sub> enhanced plumes above the background during the 2<sup>nd</sup> tracer release (14:39–14:53 UTC), and NH<sub>3</sub>:CH<sub>4</sub> linear regression slope of each plume window.

) TNO Public 69/78

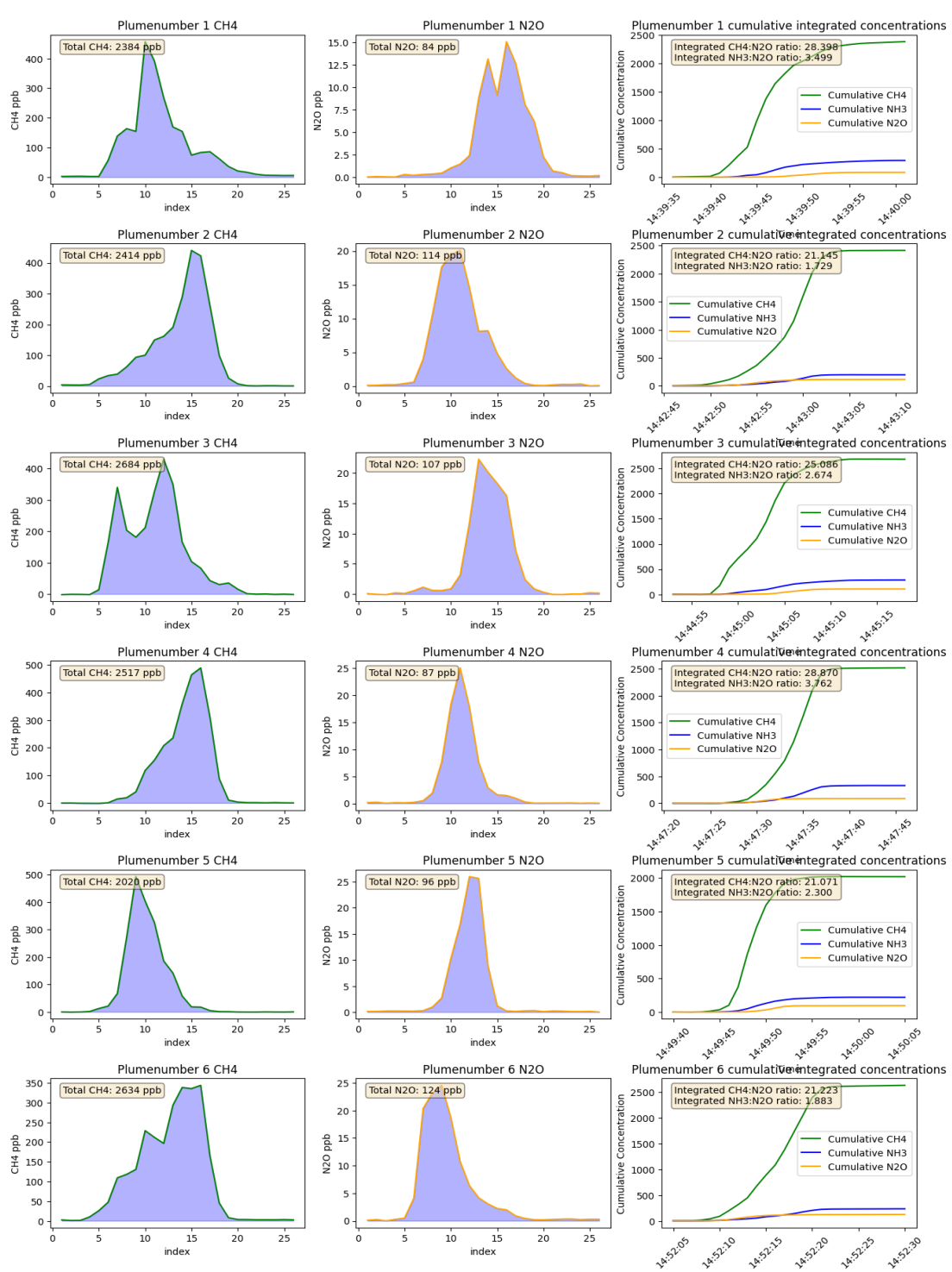


Figure S4. The first six measured  $CH_4$  and  $N_2O$  tracer enhanced plumes above the background during the  $2^{nd}$  tracer release (14:39–14:53 UTC), and cumulative  $CH_4$ :  $N_2O$  ratio and cumulative  $NH_3$ :  $N_2O$  ratio of each plume window.

TNO Public 70/78

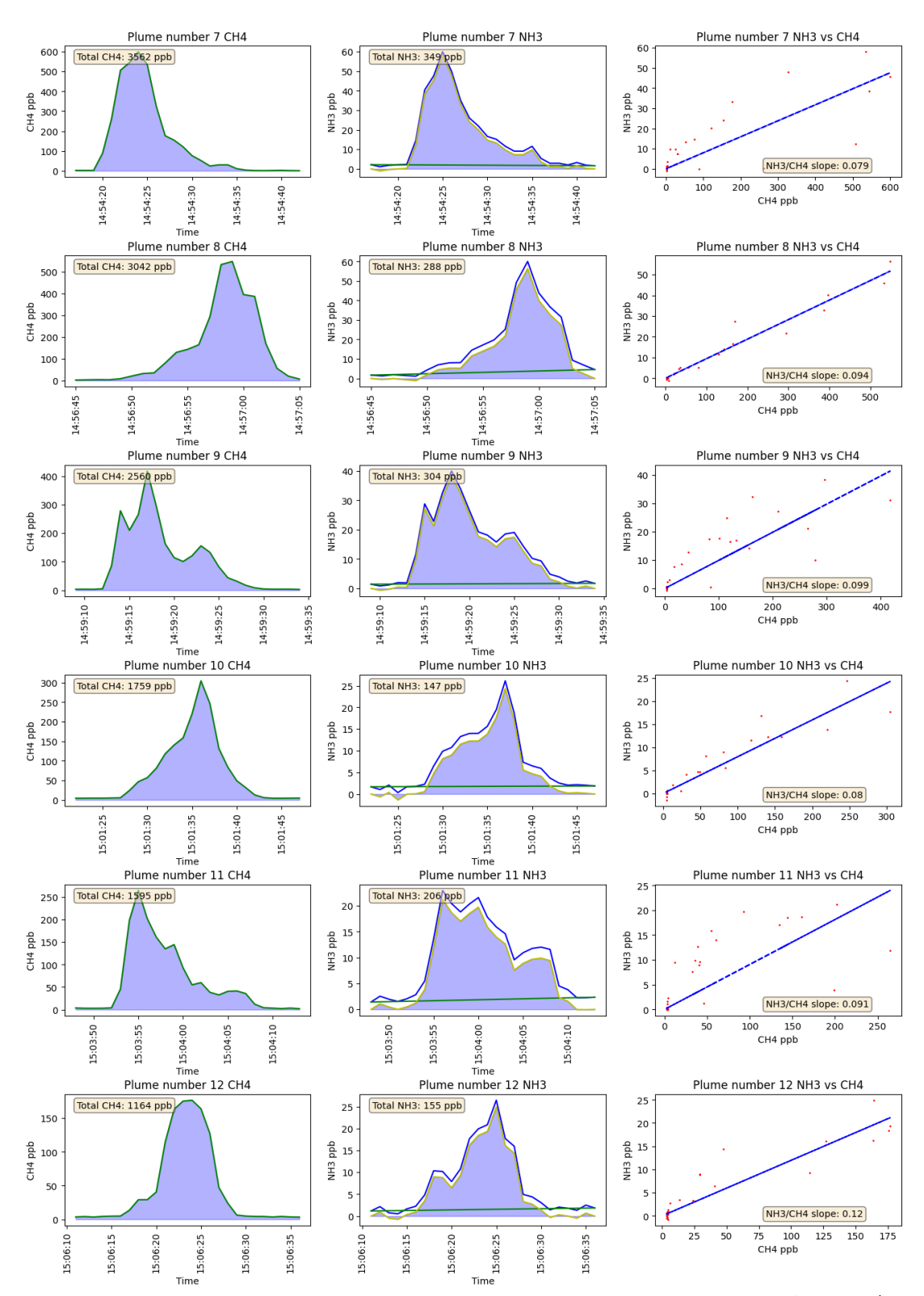


Figure S5. The other 6 measured CH<sub>4</sub> and NH<sub>3</sub> enhanced plumes above the background during the 2<sup>nd</sup> tracer release (14:54–15:07 UTC), and NH<sub>3</sub>:CH<sub>4</sub> linear regression slope of each plume window.

TNO Public 71/78

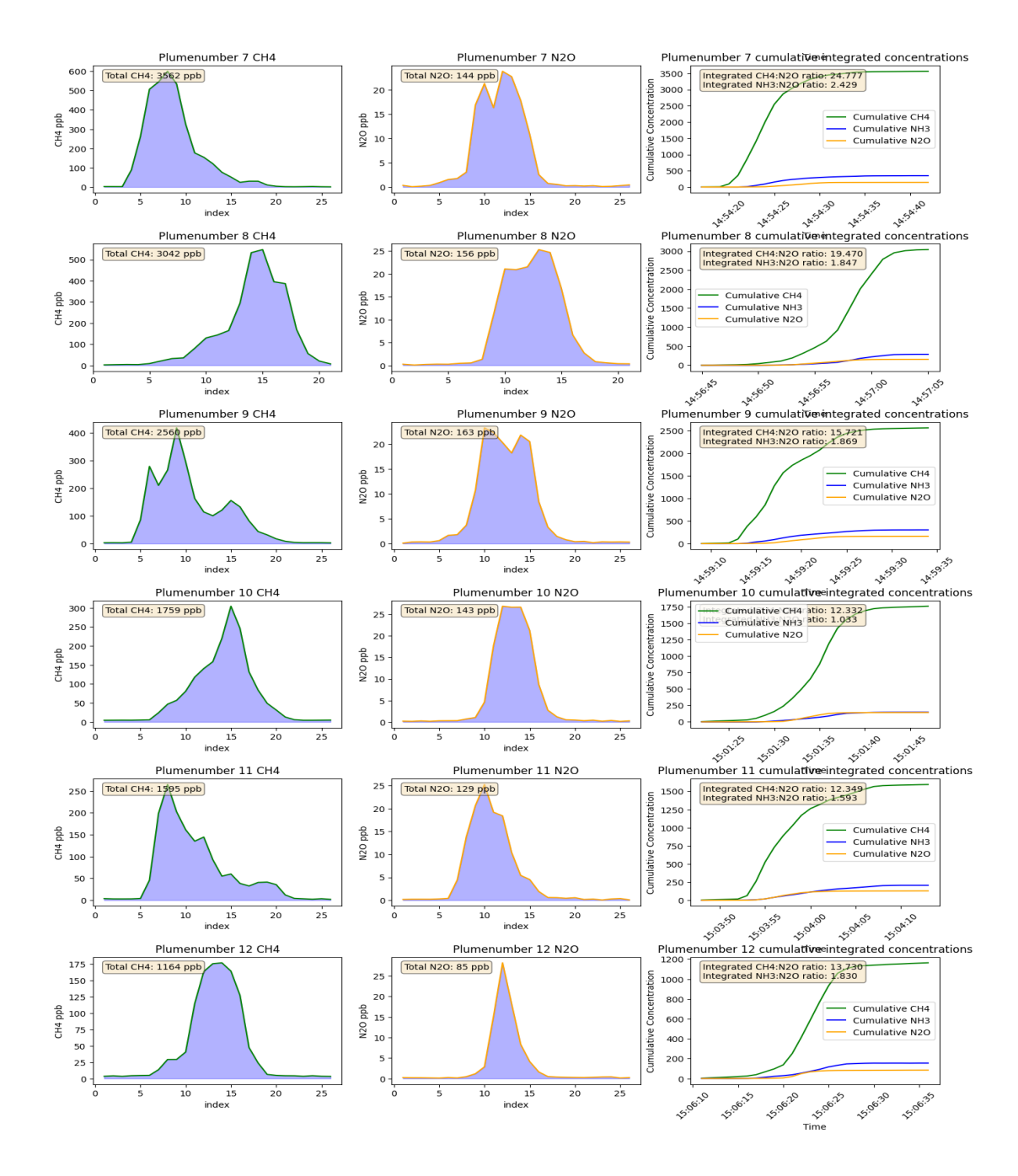
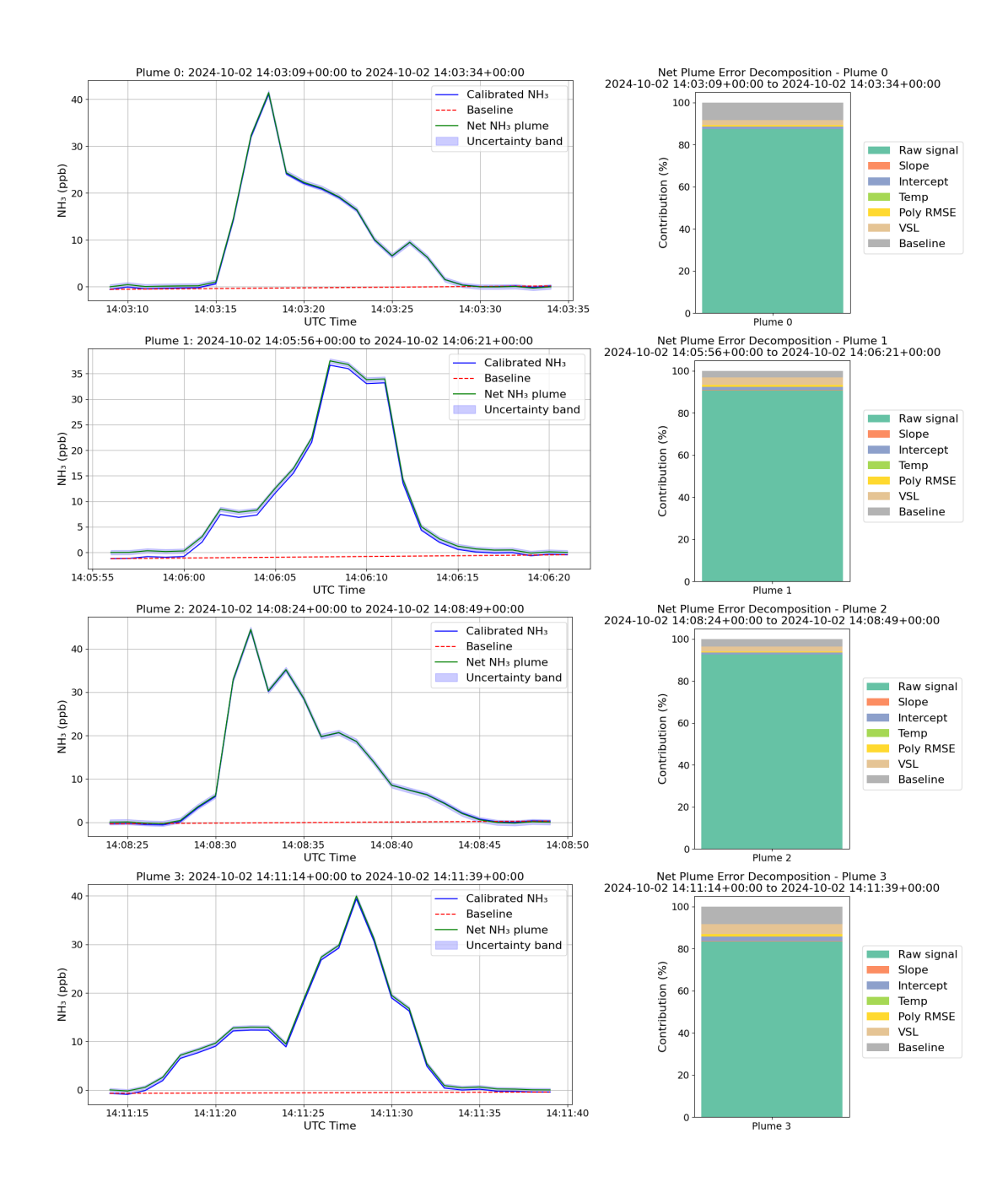


Figure S6. The other 6 measured CH<sub>4</sub> and  $N_2O$  tracer enhanced plumes above the background during the  $2^{nd}$  tracer release (14:54–15:07 UTC), and cumulative CH<sub>4</sub>:  $N_2O$  ratio and cumulative NH<sub>3</sub>:  $N_2O$  ratio of each plume window.

TNO Public 72/78

# Appendix C

# **Net NH3 plume and its uncertainty**



) TNO Public 73/78

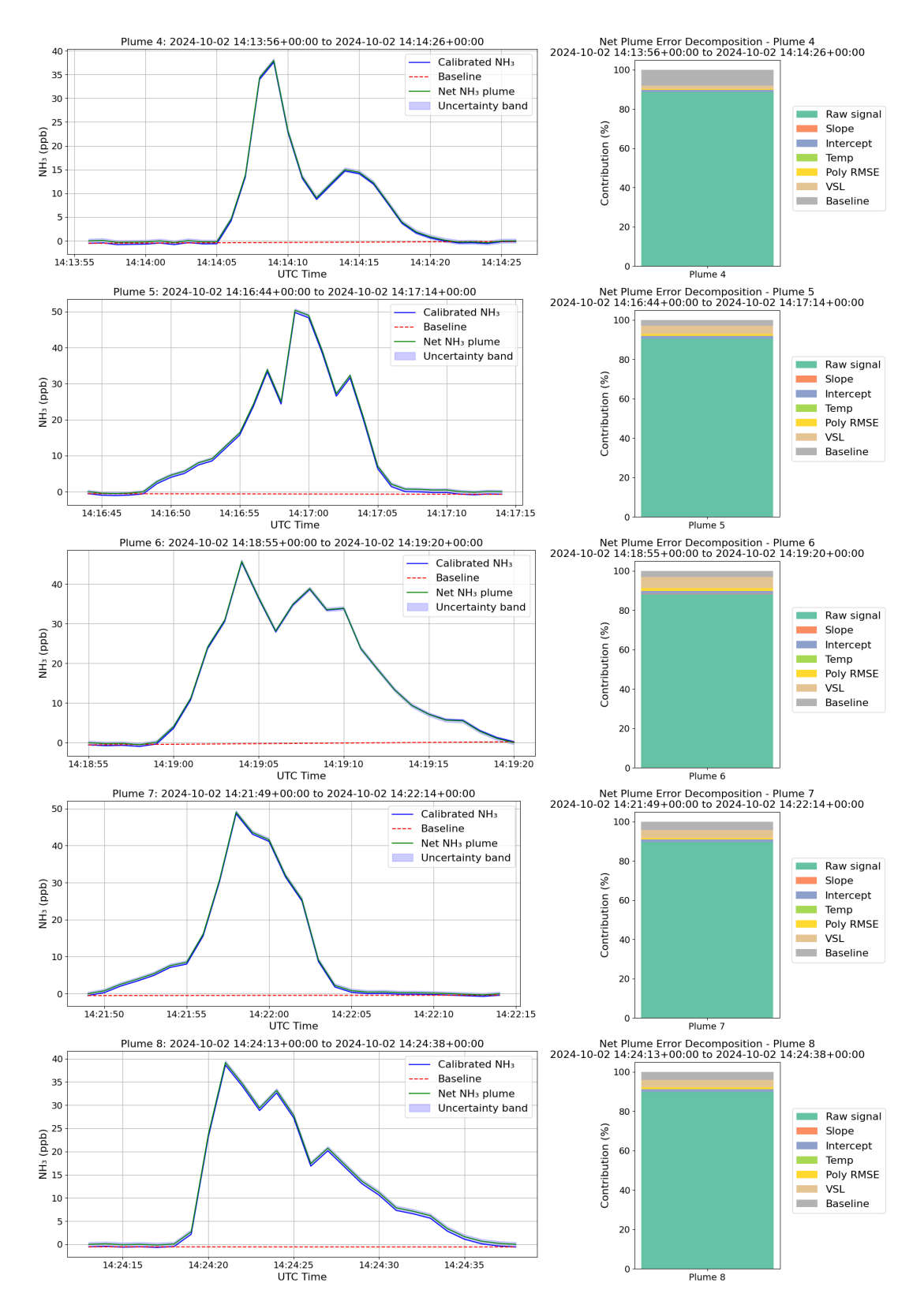
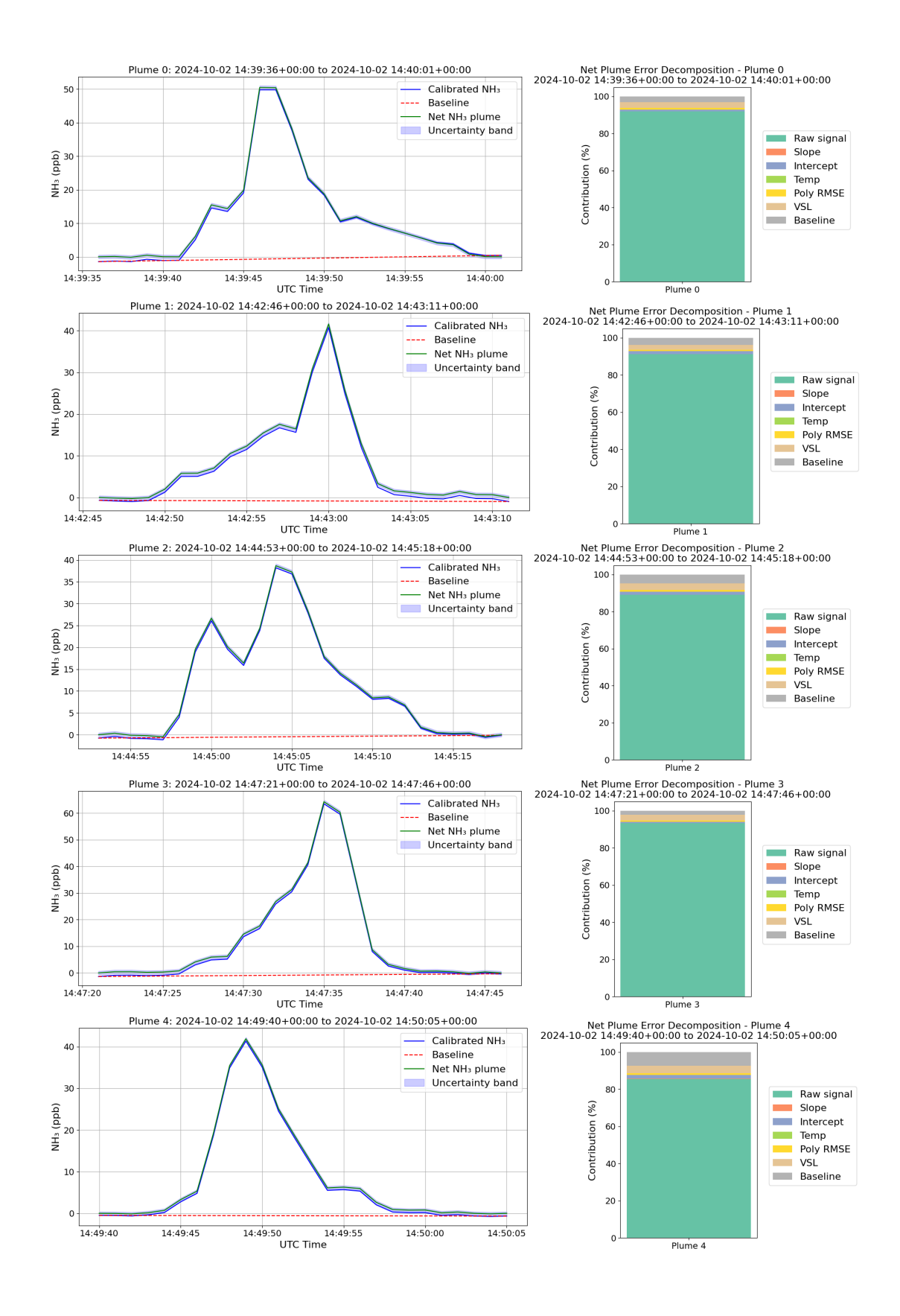
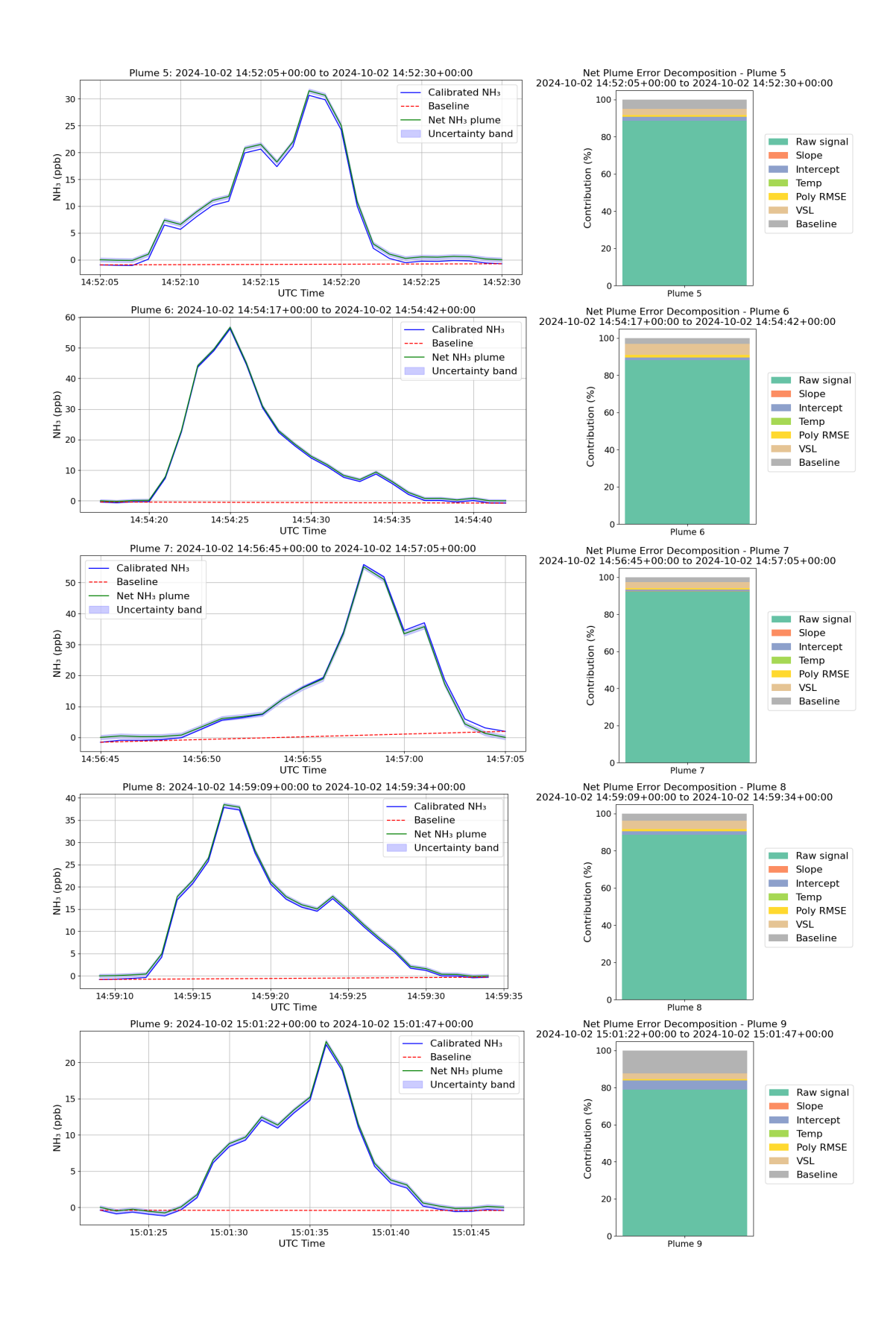


Figure S7. The nine measured NH₃ net plumes and their uncertainty bands in the left; and individual error decomposition per net plume in the right during the 1<sup>st</sup> tracer release period (14:00–14:25 UTC, October 2<sup>nd</sup>, 2024).

TNO Public 74/78



) TNO Public 75/78



TNO Public 76/78



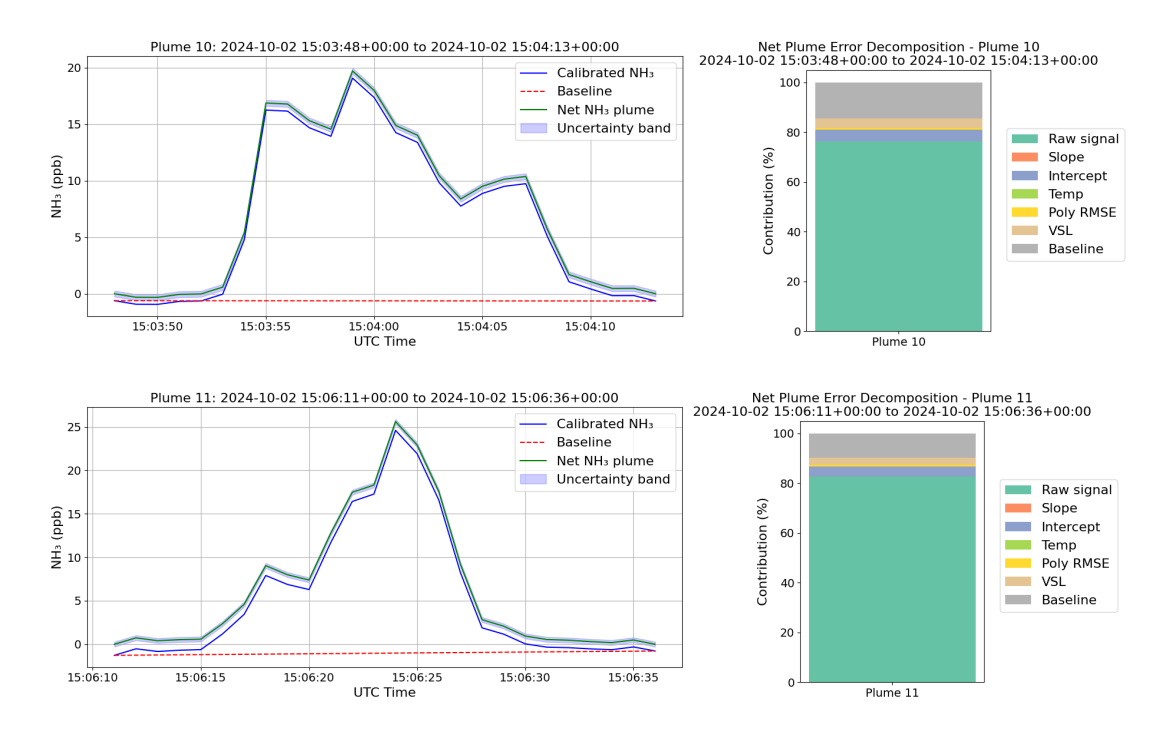


Figure S8. The twelve measured NH₃ net plumes and their uncertainty bands in the left; and individual error decomposition per net plume in the right during the 2<sup>nd</sup> tracer release period (14:39–15:07 UTC, October 2<sup>nd</sup>, 2024).

TNO Public 77/78



www.tno.nl